A Comparative Study of Site Response in Western Washington Using Earthquake Data

by

Ruhollah Keshvardoost Jobaneh

A submitted to the Graduate Faculty of
Auburn University
in partial fulfillment of the
requirements for the Degree of
Master of Science

Auburn, Alabama
December 13, 2014

Keywords: Site response, amplification,
earthquake hazard, Seattle, Washington State

Approved by

Lorraine W. Wolf, Chair, Professor of Geophysics
Ming-Kuo Lee, Professor of Geology
Ashraf Uddin, Professor of Geology

Abstract

Broadband and strong motion seismic data from three moderate to large earthquakes were used to determine site response characteristics in the Seattle and Tacoma, Washington, area. The three earthquakes chosen for analysis were the 2012 M_w 6.1 Vancouver Island earthquake, the 2012 M_w 7.8 Queen Charlotte Island earthquake, and the 2014 6.6 M_w Vancouver Island earthquake. Resonant frequencies and relative amplification of ground motions were determined using Fourier spectral rations of velocity and acceleration records from three-component seismic stations within and adjacent to the Seattle and Tacoma basins. Recordings from the sites were selected based on their signal to noise ratios. Both the Standard Spectral Ratio (SSR) and the Horizontal-to-Vertical Spectral Ratio (HVSR) methods were used in the analysis and results from each were compared. Although 56% of the sites exhibited consistent results between the two methods, other sites varied considerably. Sites that had acceptable recordings from more than one of the earthquakes were compared. Using the results, several factors postulated to influence site response were examined for this study. These included depth to bedrock and age/type of geologic material. Although the scope of this study is limited, results of the analysis suggest that sites located on the Pleistocene continental glacial drift tend to have high amplification at 1-1.5 Hz by both HVSR and SSR results. Acceleration data from the Seattle Liquefaction Array (SLA) were also used to determine the site response in different depths. The spectra and the SSRs from this station indicate

consistent frequency characteristics of the near-surface amplification among the earthquakes. The depth of the sediments to the bedrock along with the age and the type of the geologic units are investigated as the two major factors involved in the SSR and the HVSR results.

Dedication

This thesis is dedicated to my loving parents for their endless love, support, and encouragement.

Acknowledgments

The author would like to thank Drs. Andy Frassetto, John Taber, and Chad Trabant from IRIS for their help and support with acquiring and analysis of the data. My appreciation is also extended to Dr. Charlotte Rowe from Los Alamos National Laboratory (LANL) for her expertise, time, and guidance. Thanks to Drs. Thomas Pratt and Arthur Frankel from Geological Society of America (GSA) for their contribution to this research. I would also like to appreciate my committee member Dr. Ming-Kuo Lee for his support, contribution and knowledge. My sincere appreciation goes to my advisor and the head of my committee, Dr. Lorraine Wolf. This accomplishment would not be possible without her dedication, patience, knowledge, intelligence, and support. I would also like to thanks to my other committee member Dr. Ashraf Uddin for his help and support both academically and spiritually. To all other Geology and Geography faculty, staff and colleagues goes my gratitude for making this department such a wonderful place to study and enjoy the life at the same time. My deepest gratitude goes to my parents for their love, dedication, and support throughout this work.

Table of Contents

List of Figures

List of Tables

List of Abbreviations

IRIS	Incorporated Research Institution for Seismology
HVSR	Horizontal to Vertical Spectral Ratio
SSR	Standard Spectral Ratio
CSZ	Cascadia Subduction Zone
GSA	Geological Society of America

Introduction

The Cascadia Subduction Zone (CSZ) megathrust stretches from northern Vancouver Island to California and separates the subducting Juan de Fuca plate from the overriding North America plate (Fig. 1). This subduction zone produced the January 26, 1700, Cascadia earthquake, with an estimated moment magnitude of 8.7-9.2 (Atwater et al., 2005). Several other significant earthquakes have occurred in the western part of Washington in the past century. The April 13, 1949, 7.1 M_w Olympia earthquake, the April 29, 1965, 6.7 M_w Olympia earthquake and the February 28, 2001, 6.8 Mw Nisqually earthquake on which occurred very close to the epicenter of 1949 event, are among the most important. Smaller magnitude earthquakes happen frequently (almost once a month) (Barnett et al., 2009).

Situated above the CSZ, the Seattle and Tacoma metropolitan areas in the Puget Lowland of western Washington are at risk from earthquake related damage. These seismically active areas overlie sedimentary basins and are home to over 3.5 million people. Since sedimentary basins affect seismic waves and often increase the level of earthquake damage, it is crucial to gain a better understanding of earthquake waves as they travel through basin sediments.

Site characteristics, such as fundamental period and wave amplification, are influenced by sediment type, location, and thickness of sedimentary units, and can affect

ground shaking at a given location. Ground motions experienced at a site are a function of the earthquake source, the wave path, and the characteristics (e.g., sediment type, local geology, depth to bedrock) of the site itself. Much research by seismologists and engineers has focused on understanding and predicting these site characteristics for estimating seismic hazard in areas where the potential for large earthquakes exists. The site effect can be represented by an empirical transfer function that captures the influence of surficial geologic units on earthquake ground motions. Two common techniques used in previous studies for approximating this transfer function are the horizontal-to-vertical spectral ratios (HVSRs) and the standard spectral ratios (SSRs) (e.g., Frankel (1999, 2002, 2009), Molnar et al., (2004), Pratt (2006), Koçkar and Akgün (2012), Garcia-Fernandez and Jimenez (2012)).

The goal of this study is to determine site effects on ground motions at several locations near the urban centers of Seattle and Tacoma using broadband and strong motion data acquired for three different earthquakes: (1) the October 28, 2012, Mw 7.8 Queen Charlotte earthquake (2) the April 24, 2014, Mw 6.6 Vancouver Island earthquake, and (3) the November 8, 2012, Mw 6.1 Vancouver Island earthquake (Fig. 1). Results from this study will be compared with results from similar studies previously conducted in this area. The SSR results will also be compared to the HVSRs to investigate the consistency of the results at each method. This study will also explore the two major factors affecting the ground motion amplification in the study area.

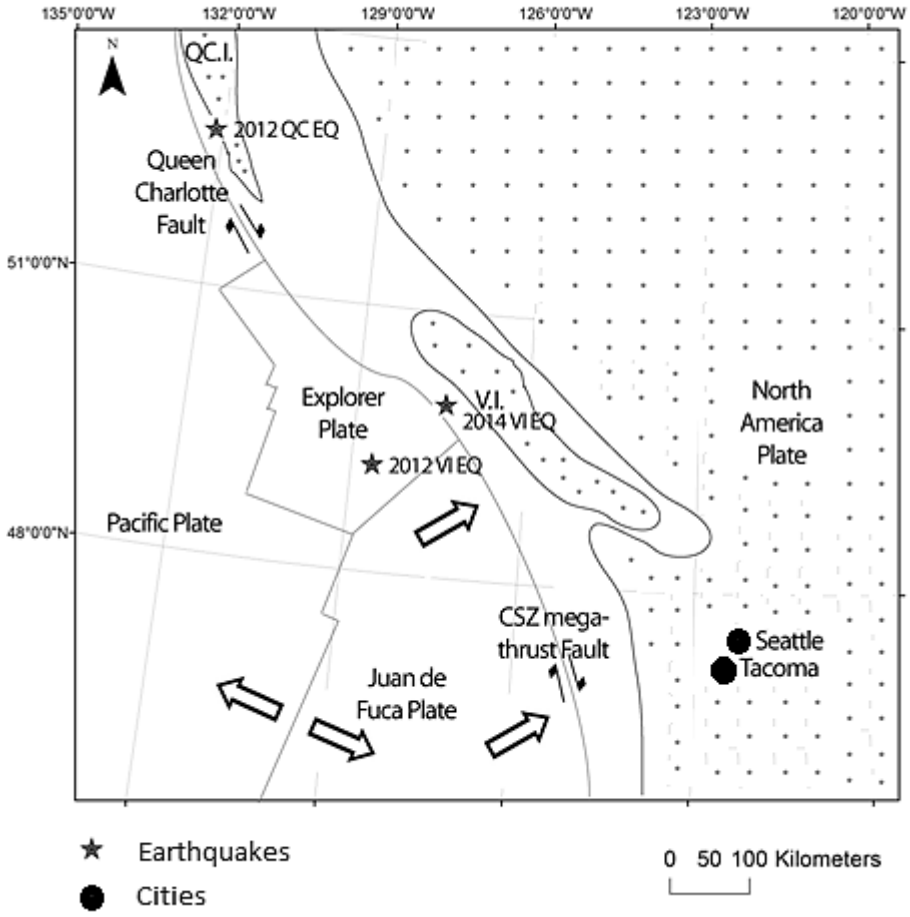

Fig. 1. Simplified tectonic map showing the epicentral locations of earthquakes used in this study. The Juan de Fuca plate and the Explorer plate are subducting under the North America plate, forming the Cascadia Subduction Zone. Stippled area indicates land.

Background and Geologic Setting

The main sources of earthquakes in the Pacific Northwest are associated with plate motions involving the Pacific, North America, and Juan de Fuca plates (Fig. 1). Strain accumulation resulting from these plate interactions is released through earthquakes within the subducting Juan de Fuca plate, along the plate interface, or in the overriding plate (Barnett et al., 2009). The Queen Charlotte fault, is an active transform fault that forms a triple junction where it intersects the Explorer plate, the Juan de Fuca plate and the North America plate, transitioning to become the CSZ.

The **M** 8.7 to 9.2 Cascadia earthquake in 1700 occurred along the CSZ and made a fault rupture estimated to be approximately 1000 km long from northern California to Vancouver Island in British Columbia with an average slip of 20 m (Atwater et al., 2005). North-south shortening resulting from oblique plate convergence (Khazaradze et al., 1999) has produced east-trending thrust faults and dextral strike-slip faults throughout the Puget Lowland fore-arc basin. Crustal faulting in this area is the main mechanism for the formation of several thick sedimentary basins (Brocher et al., 2001). Among these basins, the Seattle and Tacoma basins pose the highest level of hazard because of their proximity to large populations.

The stratigraphy of Seattle basin has been studied using surface exposures, industry boreholes, and seismic profiles tied to the boreholes by many geoscientists (Fig. 2) (Johnson et al., 1996; Brocher et al., 1998; Snelson et al., 2007; Troost and Booth, 2008). Almost 1.1 km of

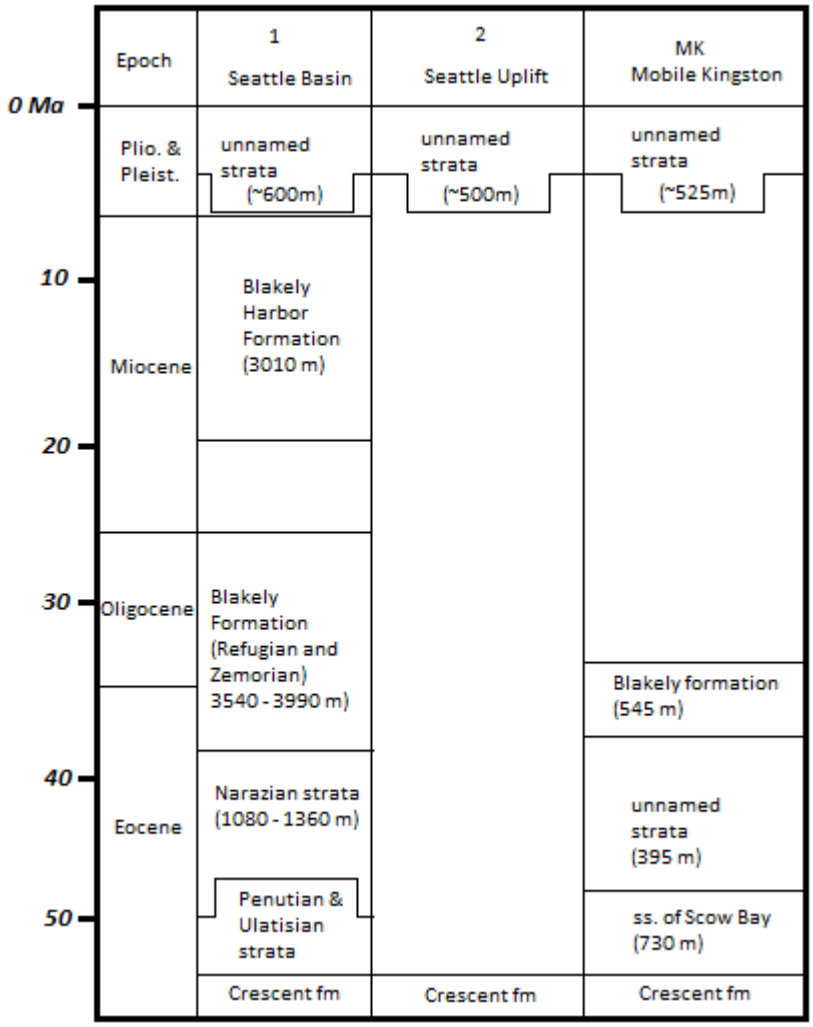

Fig. 2. Stratigraphic column for the Puget Lowland (Snelson et al., 2007).

unconsolidated Pleistocene and Holocene deposits at the top of the basin is assumed to be the main cause of amplification of seismic waves (Frankel et al., 1999, 2002; Pratt et al.,

2003). The upper part of these deposits is a temporally and spatially complex collection of glacial outwash till, lacustrine deposits, and recessional deposits that were formed when the Puget Lowland was glaciated during at least six different episodes in the Pleistocene (Booth, 1994). Well logs and seismic reflection data indicate that there are sedimentary rocks of Eocene and Miocene age below these unconsolidated Holocene deposits. The Miocene age Blakely Harbor Formation contains of siltstones, conglomerates and non-marine sandstones (Fig. 2). The conglomerate clasts are poorly sorted pebbles, cobbles, and boulders, of which about 85% are from Crescent Formation (Johnson et al., 1994, 1996). The Eocene to Oligocene Blakely Formation consists of different deep marine sequences. The Crescent Formation, which is stratigraphically below the Blakely Formation, consists of basalt and minor interbeds of siltstone, tuff, and conglomerate (Johnson et al., 1994; Jones 1996; Snelson et al., 2007).

Previous Work

Many studies have used ground motions to characterize the effects of sedimentary basins on seismic waves. Examples include Frankel (1999, 2002, and 2009), Molnar et al. (2004), Pratt et al. (2006), Ghasemi et al. (2009), and Koçkar and Akgün (2012).

Frankel (1999) analyzed seismograms from 21 earthquakes (M_L 2.0-4.9) recorded by digital seismographs situated on wide variety of geologic units and developed a new inversion procedure to estimate site response. He observed high amplifications on artificial fill, more moderate amplification for sites on stiff Pleistocene soils, and low response for rock sites. The results of his study also showed a strong 2-Hz resonance at sites with surficial layers of fill and younger alluvium.

In another study, Frankel et al. (2002) used the recordings of the M 6.8 Nisqually earthquake and its M_L 3.4 aftershock to study site response and basin effects for 35 locations in Seattle, Washington. This study used SSRs, or Fourier spectral ratios of horizontal ground motions recorded at soft sediment sites relative to a reference site. He observed that sites on artificial fill and young alluvium had the largest 1-Hz amplification for both the mainshock and aftershock.

Molnar et al. (2004) examined site responses in Victoria, British Columbia, using weak ground motion recordings of the 2001 Nisqually earthquake in Washington. They analyzed the data using both the SSR method and the HVSR method and observed a considerable variation in acceleration spectra across the city due to local site conditions. The HVSR method uses the average of the horizontal components of the shear wave divided it by the vertical component. For their reference recordings for the SSR calculations, they used stations at thin soil sites (< 3 m) having a flat-amplitude spectra at frequencies less than 10 Hz. They found that sites with thicker soils (5-10 m) showed peak amplitudes at 2-5 Hz.

Pratt et al. (2006) used SSR and HVSR methods at 47 sites in the Puget Lowland and observed significant amplification of 1.5- to 2.0-Hz shear waves within sedimentary basins. The SSR curves at thick basin sites showed peak amplification at frequencies of 3 to 6 Hz and lower amplification at frequencies above 6 Hz. They proposed that the attenuation within the basin strata is the main cause of the spectral decay at frequencies above the amplification peak.

Frankel (2009) studied the effect of basins on site response in the Puget Lowland using 3D finite-difference simulations for five earthquakes, including the M 6.8 Nisqually earthquake. His modeling suggests a dependence of amplification on the directivity of the earthquake rupture. Earthquake directivity is the focusing of wave energy along a fault in the direction of rupture. He found that S waves are focused toward the southern margin of the Seattle basin in an area \that experienced increased chimney damage from the Nisqually earthquake. Chimney damage is used as a proxy for the intensity of ground shaking (Fig. 3).

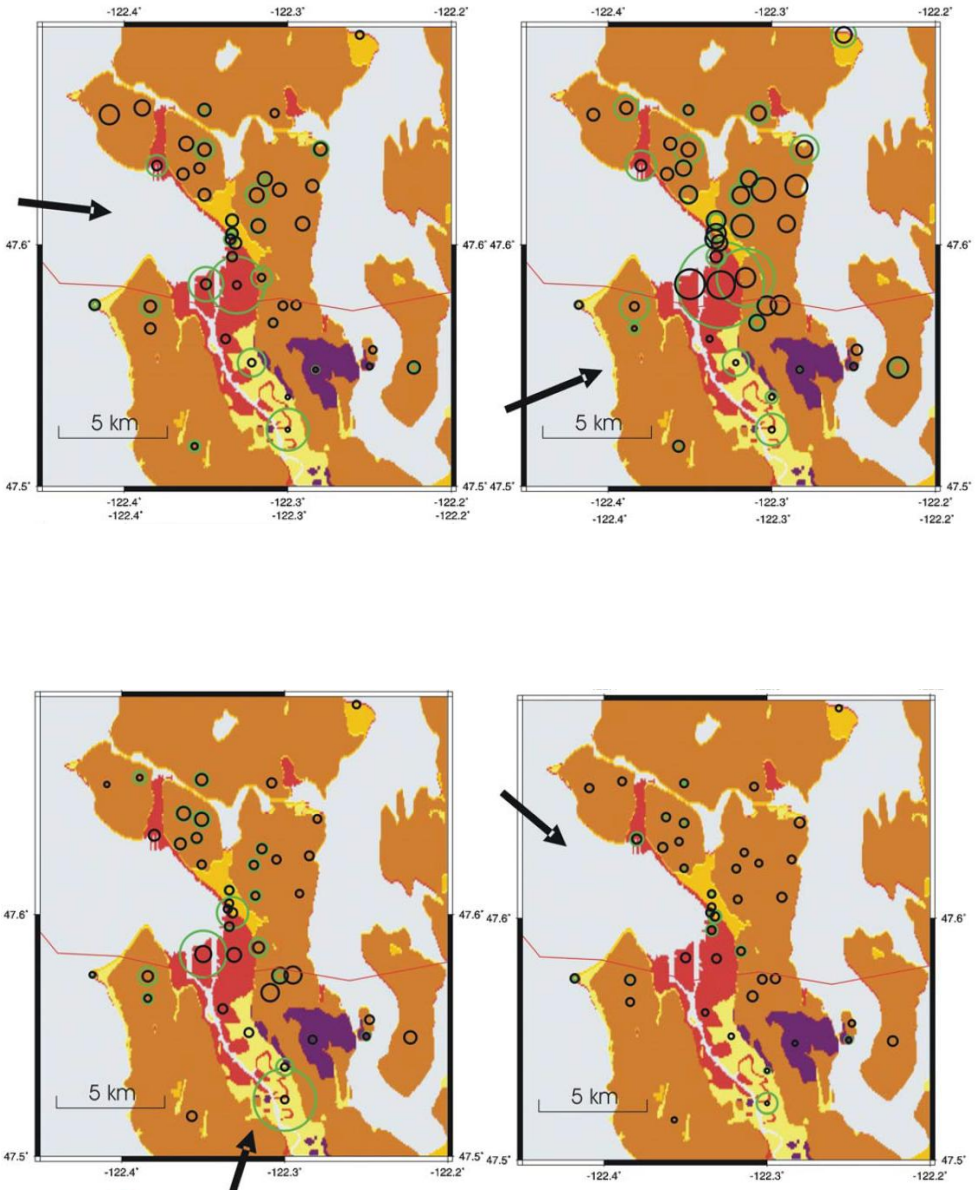

Fig. 3. Maps indicate observed (green circles) and predicted (black circles) amplification at 1 Hz for four earthquakes plotted on map of surface geology. Circle size is proportional to 1 Hz amplification. Arrows show direction of seismic wave propagation based on the location of the earthquake. Stations with no green circles did not record that particular earthquake (Frankel, 2009).

Analogues

In this section, four investigations from India, Turkey, Spain and South Africa using methods similar to those in this study are presented and serve as analogues to validate the modeling approach.

Jammu City, India

Passive seismic methods including HVSR and microtremors were used to investigate the site response at 30 station locations located in frontal part of the Himalaya Mountains, which contain soft sediments that have strong effects on recorded ground motions (Mahajan et al., 2012). Mahajan et al. (2012) used shear-wave velocities from the top 30 m l of Pleistocene and Holocene sediments overlying Lower Miocene bedrock, along with seismic data from the 20 October, 1991 (Mb 6.8) Chamilo earthquake to calculate the site response spectrum at the sites. Buildings of different heights have different resonant frequencies, making amplification in certain period ranges an important engineering concern. The response spectrum of the sites indicates a five to seven times increase in peak ground acceleration for single or two-story buildings. Fig. 4 shows amplification ratios, periods, and shear wave velocities at different sites in the N-S and NW-SE directions (Mahajan et al., 2012). The study show eight to twelve times increase in amplification at 2 to 3 Hz frequency in the central part and 1.75 to 2 Hz in peripheral parts of the city.

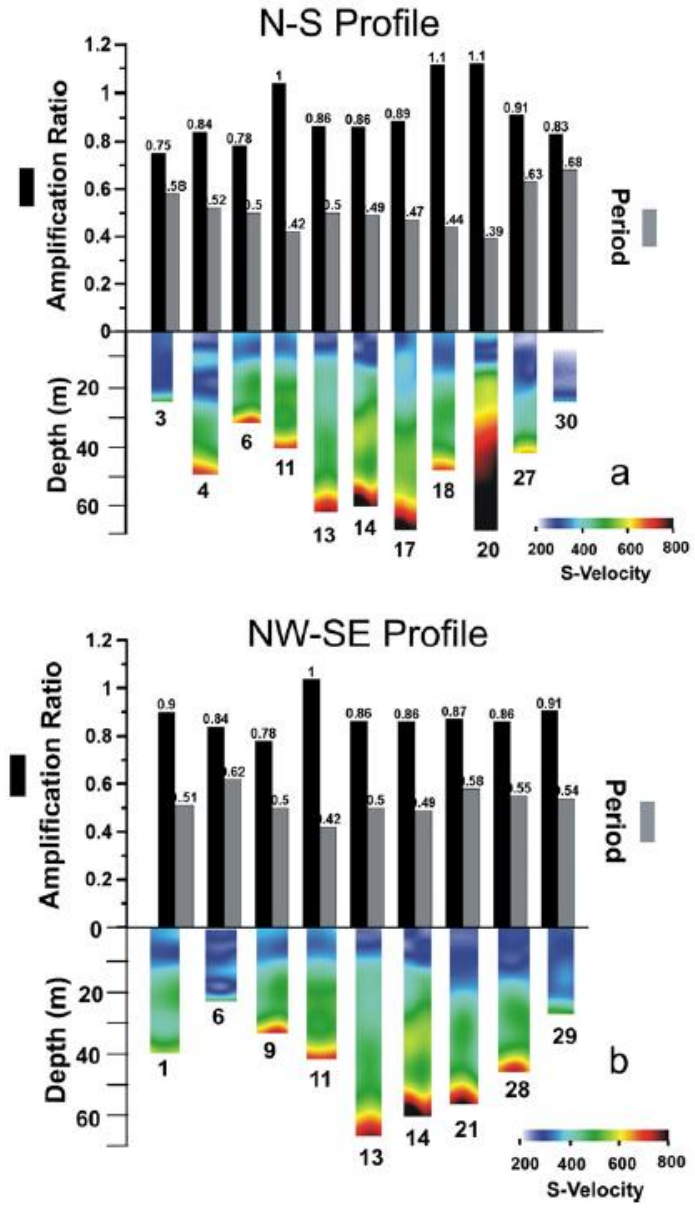

Fig. 4. Amplification ratios and corresponding shear-wave velocities for sites in Jammu city. Upper panel (a) shows results from N-S profile; lower panel (b) shows results from NW-SE profile. (From Mahajan et al., 2012).

The stations located in the central part of the city (e.g., Sites 14 and 9) show HVSR curves with clear peaks in comparison to the sites in the northwestern and southwestern

part of the town (e.g., Sites 7, 25) (Fig. 5). Broad HVSR peaks imply a low impedance contrast between basement and overlying sediments and only provide a range of amplification values. Overall, it can be concluded that HVSR can only be successful in areas with high impedance contrast (Mahajan et al., 2012).

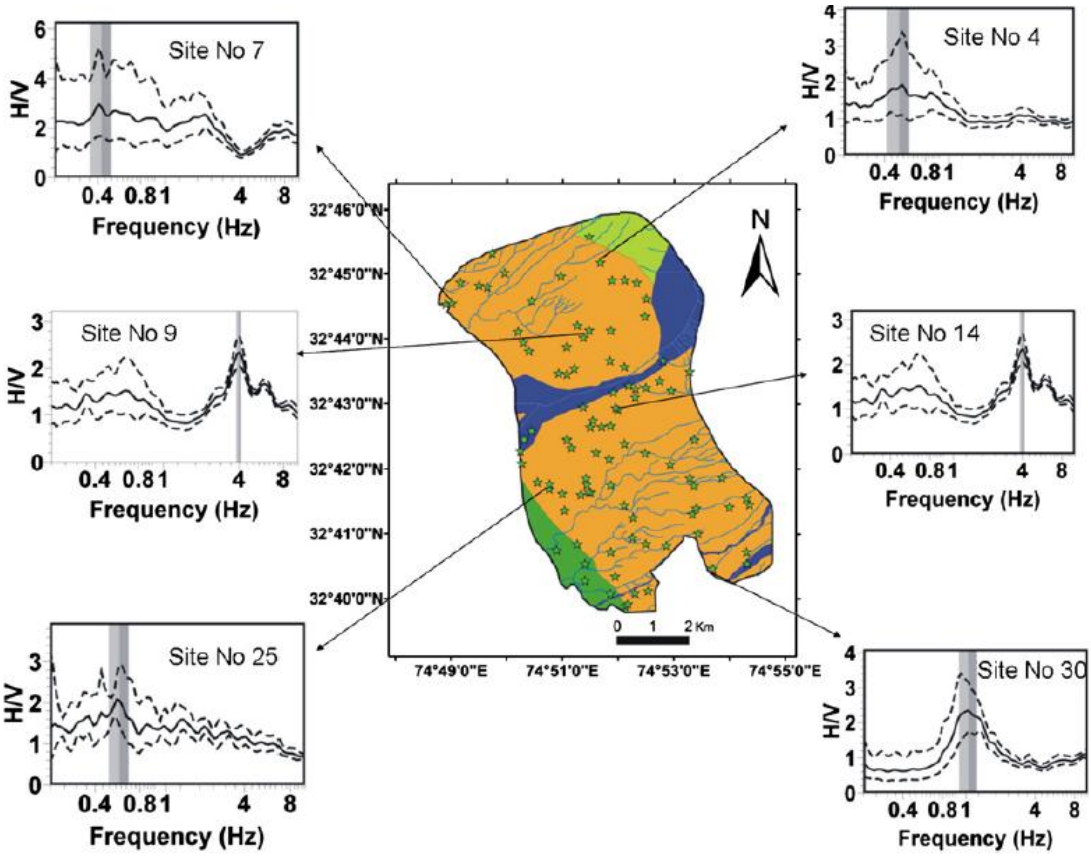

Fig. 5. HVSR curves in different part of Jammu city. Sharp peaks are associated with high impedance contrast as opposed to broad peaks that are indicative of low impedance contrast from Mahajan et al., (2012).

Ankara, Turkey

Koçkar and Akgün (2012) collected 352 microtremor measurements in the western part of the Ankara basin within the Plio-Pleistocene fluvial and Pleistocene and Holocene alluvial and terrace sediments. They used HVSRs of these measurements to calculate the fundamental periods and amplification of their sites. These measurements were correlated with the *in situ* measurements of dynamic properties of geologic information. The results from this study indicate that three main factors were involved in the site response: (1) age of the geologic formation, (2) depth of the sediments to the bedrock, and (3) non-uniform subsurface configuration. Due to the presence of low-velocity deposits near the surface, stations located at Pleistocene and Holocene sediments show high amplification at longer periods than the older Plio-Pleistocene fluvial sediments. The HVSR results further showed that the variation of the fundamental period agreed well with maximum amount of amplification at a given site. Pleistocene and Holocene sediments, which are the thicker and unconsolidated, possess low shear wave velocity and show higher amplification results at fundamental periods.

Using the HVSR results, the results of Vs30 measurements (average shear wave velocity in the upper 30 m), and geologic information, Koçkar and Akgün (2012) created a site class zonation map for the Ankara basin. The map provides a tool to assess and mitigate the potential risk from future seismic events in the study area (Fig.7).

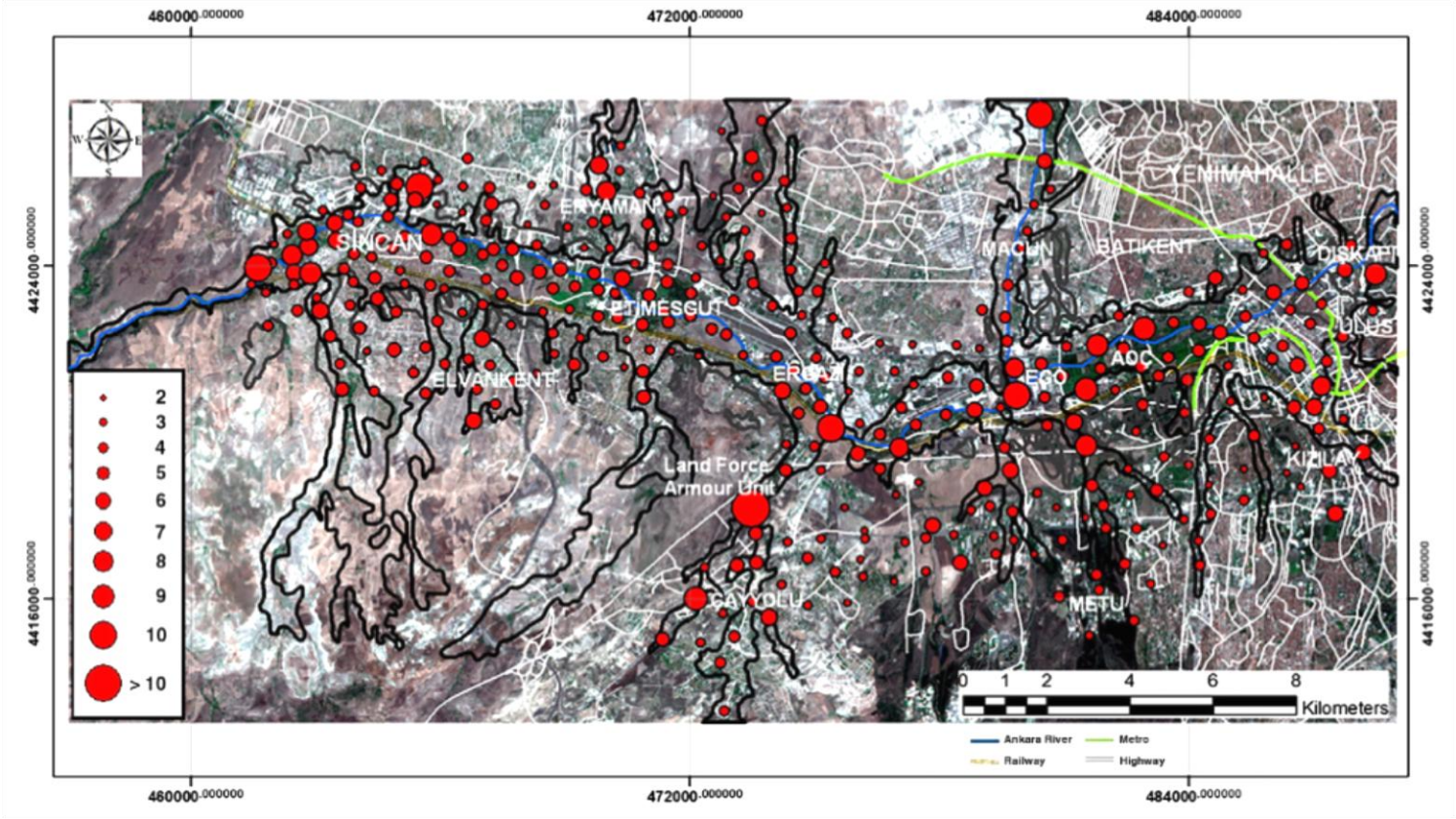

Fig. 6. Map of the regions with the maximum amplification levels from HVSR method in Ankara basin (Koçkar and Akgün, 2012).

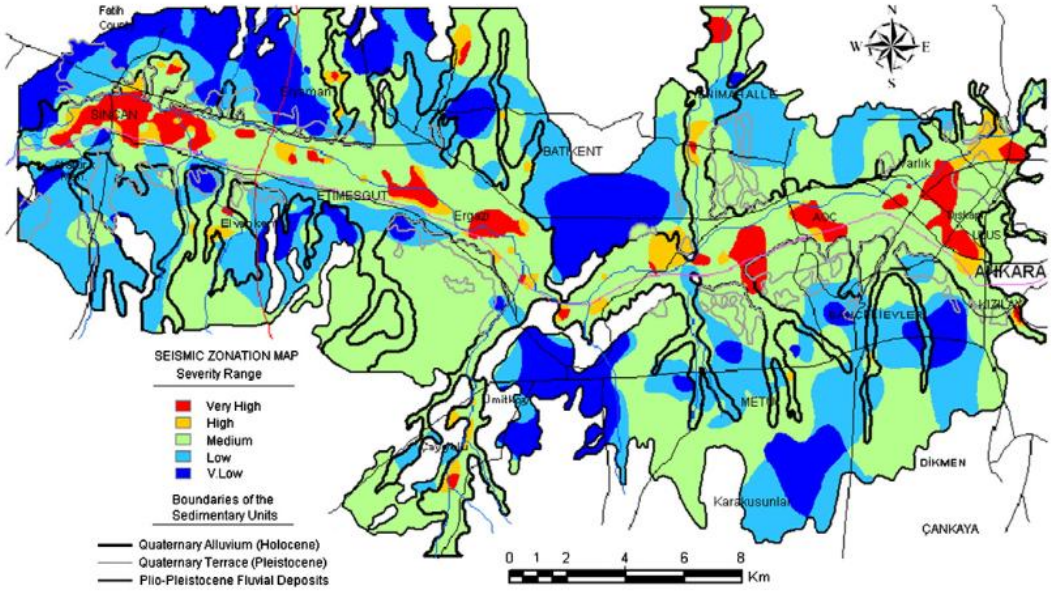

Fig. 7. Seismic zonation map for assessing the effects in the Ankara basin. The plot includes the site classification map based on average Vs30 measurements and the maps of HVSR regarding resonance periods and maximum amplifications (Koçkar and Akgün, 2012).

Vega Baja, Spain

Garcia-Fernandez and Jimenez (2012) conducted ambient noise surveys at 90 sites over the central part of the Lower Segura River basin in the Vega Baja region, located southeast of the Iberian Peninsula. This dataset, along with geological, geotechnical, and other geophysical data, was used to identify multiple peaks in some of the HVSR curves. The dataset represents different impedance contrasts at depths that were modeled to characterize the Vega Baja soils units, depth to the bedrock, and depth to the rock units. The depth to the bedrock varies in different parts of the basin from 30 m to 50 m. The average of the shear-wave velocity over the soil unit is approximately 200 m/s, and the average velocity in the top 30 m is around 300 m/s.

In Fig. 8, three examples of experimental and 1D synthetic H/V curves from their paper are shown together with three generalized models indicating the subsurface structure in Vega Baja. Model 1 sites are mainly located at the central and western part of the Lower Sengura basin and the northern border of the Hurchillo, Benejuzar and Guardamar Mountains. Model 2 sites are in the Orihuela-Callosa Ranges. Model 3 sites are located in the north, south, and east sections of the Lower Segura basin. The results of the study show a strong relationship of fundamental periods with lithological variation with sediment thickness (Garcia-Fernandez and Jimenez, 2012).

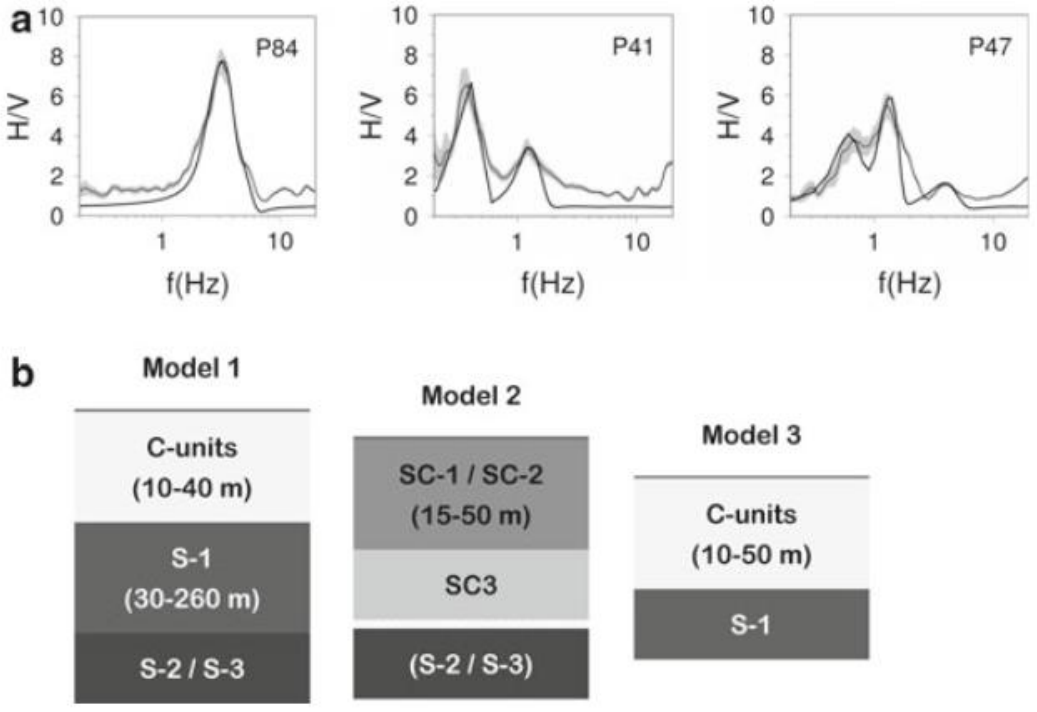

Fig. 8. (a) Examples of observed (light gray line =mean value) and 1D modeled H/V (dark gray line) values; (b) generalized 1D soil models in Vega Baja (Garcia-Fernandez and Jimenez, 2012).

Durban, South Africa

A refined version of the HVSR generated by cultural seismic noise has been used to study the seismic response of several sites in Durban area of South Africa (Fernandez and Brandt, 2000). Three components of two ambient noise samples separated by several minutes were acquired at 18 sites. Although the data samples were different in time and frequency content, the HVSR curves look very similar in most of the pairs (Fig. 9). Not only were the frequency peaks almost identical, but also the ranges of amplifications were very similar. The method used in this study is based on using a hard-rock site ("the Kloof") as a reference and comparing all the soft sites relative to the hard-rock site (Fig. 9). This comparison with a hard- rock site helps to gain a better understanding of the physical meaning of the site response. Results from this study showed that the influence of the layer system on the vertical component of motion does not exceed the value of two; therefore, it can be assumed that the majority of amplification is due to the horizontal motion.

Fig. 9 shows the HVSRs at two different times at two of the sites that are underlain with unconsolidated sediments. Fig. 9 also includes the site response at each site relative to the hard rock site, which is thought to be in direct relation to the amplification factor.

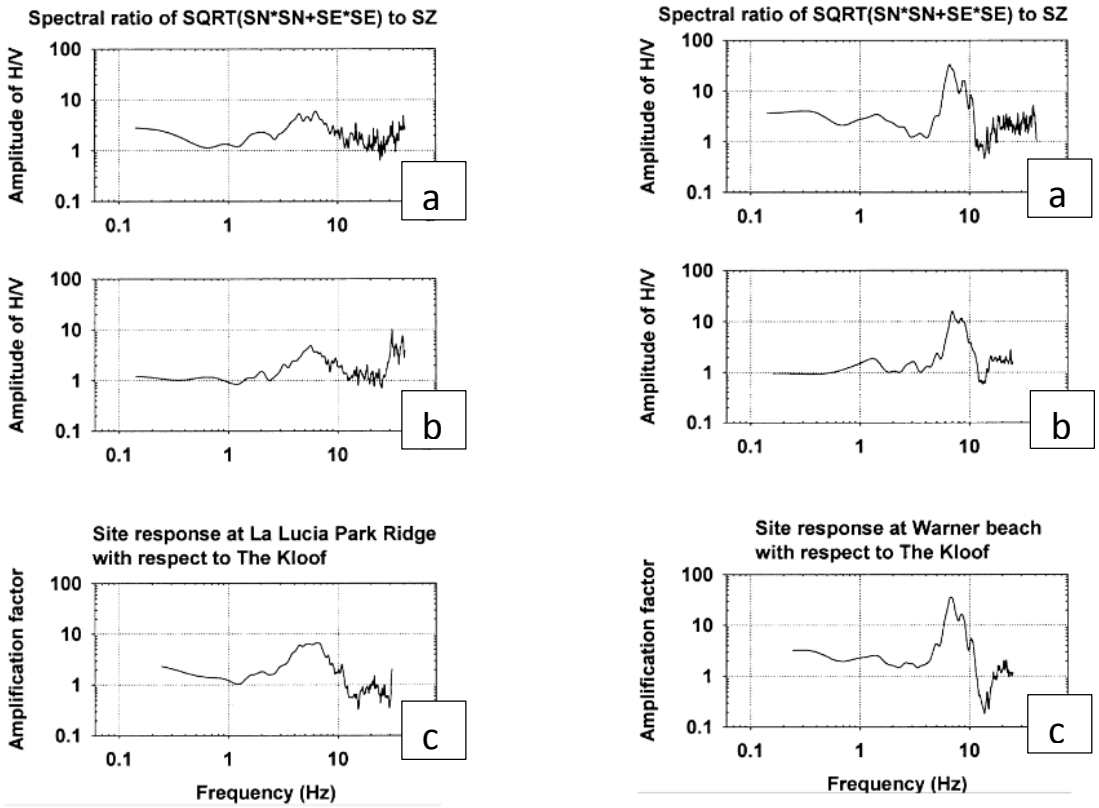

Fig. 9. Left column: two HVSRs (a and b) at La Lucia Ridge (consolidated sand). Site response (c) is with respect to hard rock site "The Kloof." Right column: two HVSRs (a and b) at Warner beach (sand). Site response (c) is again with respect to hard rock site "The Kloof" (Fernandez and Brandt, 2000).

Methodology

This section provides information about data acquisition and analysis. Data acquisition includes station selection and sources for broadband, strong motion, and other supporting data. Data analysis includes the methods used to process all the acquired seismic data. Three-component broadband data record velocity and cover a wide frequency band (0.01 to 25 Hz). Strong motion data measure acceleration and are useful for recording large-amplitude, high frequency (0 to 100 Hz) seismic waves.

Data Acquisition

Broadband data

Seismic stations used in this study are located in western Washington, most of which are within Seattle and Tacoma basins (Fig. 10). Most of the sites are underlain by thick sedimentary sequences that fill the basins; however, in a few cases the bedrock is exposed or located very close to the surface. Three-component data from 16 broadband stations of the University of Washington (UW) and Transportable Array (TA) networks were selected and the data were downloaded from the Incorporated Research Institutions for Seismology (IRIS) data center (http://service.iris.edu/irisws/timeseries/docs/1/builder) for the November 8th, 2012 Vancouver Island earthquake. All data have a 40-Hz sampling frequency with the length of 40 minutes. Ten stations having acceptable signal

to noise ratio (more than 2) were selected and cover areas with different liquefaction susceptibility (Fig. 10). The station name, network, latitude, longitude, and elevation of each station are shown in Table 1.

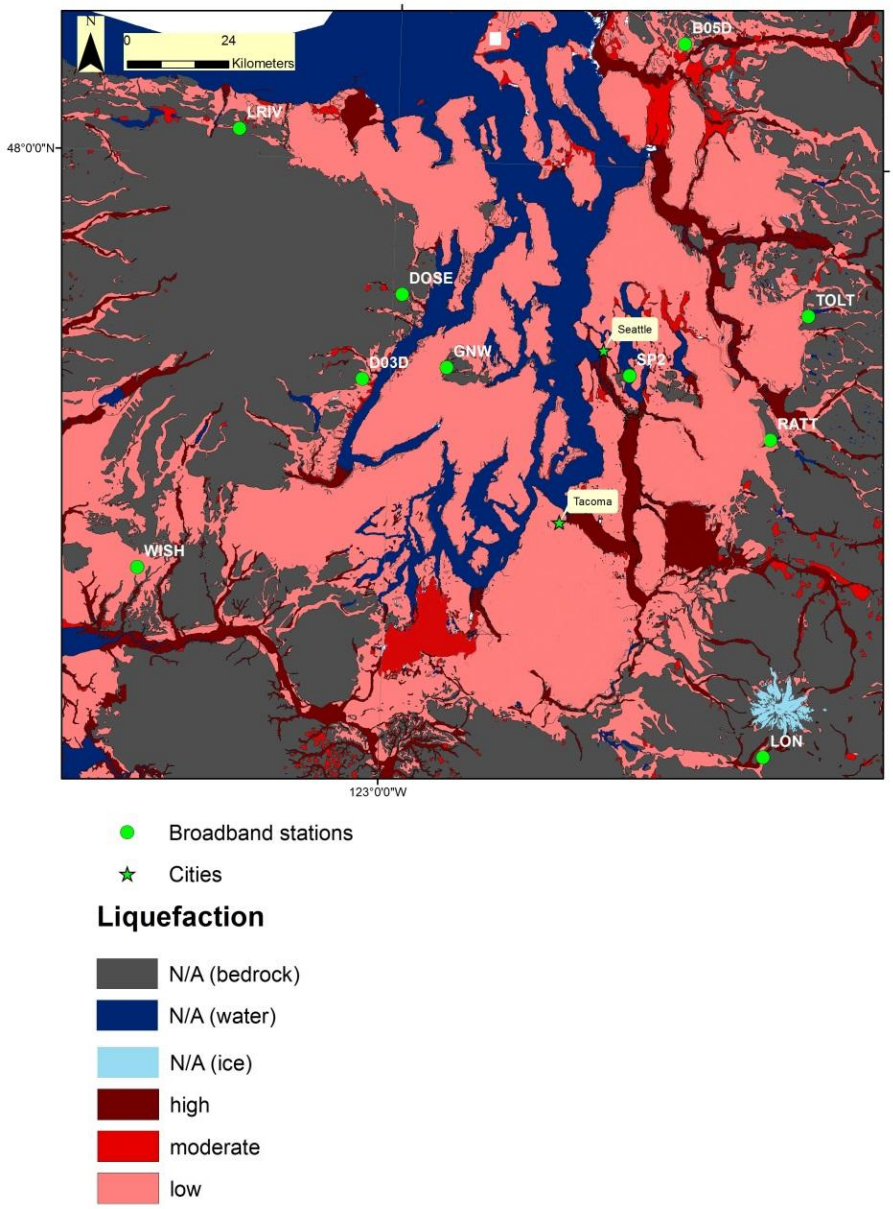

Fig. 10. Locations of ten broadband stations selected for this study overlain on liquefaction susceptibility map (Palmer et al., 2004).

Table 1. Broadband stations recorded the 2012 Vancouver Island earthquake.

Network	Station	Latitude	Longitude	Elevation(m)	Geologic Unit
TA	B05D	48.2641	-122.096	153	Pleistocene continental glacial drift
TA	D03D	47.5347	-123.089	262	Pleistocene continental glacial drift
UW	DOSE	47.7172	-122.972	53	Pleistocene continental glacial drift
UW	GNW	47.56413	-122.825	220	Paleogene and Neogene intrusive rock
UW	LON	46.7506	-121.81	853	Paleogene and Neogene fragmental volcanic rock
UW	LRIV	48.0575	-123.504	293	Pleistocene continental glacial drift
UW	RATT	47.42546	-121.803	440	Paleogene and Neogene fragmental volcanic rock
UW	SP2	47.55629	-122.249	30	Pleistocene continental glacial drift
UW	TOLT	47.69	-121.69	541	Paleogene and Neogene volcanic rock
UW	WISH	47.11698	-123.771	45	Pleistocene and Holocene alluvium

Strong motion data

Forty-seven three-component acceleration records were acquired from strong motion stations for the Mw 7.8 Queen Charlotte Island earthquake and Mw 6.6 Vancouver Island earthquake that occurred at 3:04:08 am on October 28th, 2012, and 3:10:12 am on April 24th, 2014, respectively. The IRIS URL Builder was used to download 40 minutes of data with 100-Hz sampling frequency (Fig. 11). Tables 2 and 3 list the station name, location, elevation, and geologic unit of each station used in the study.

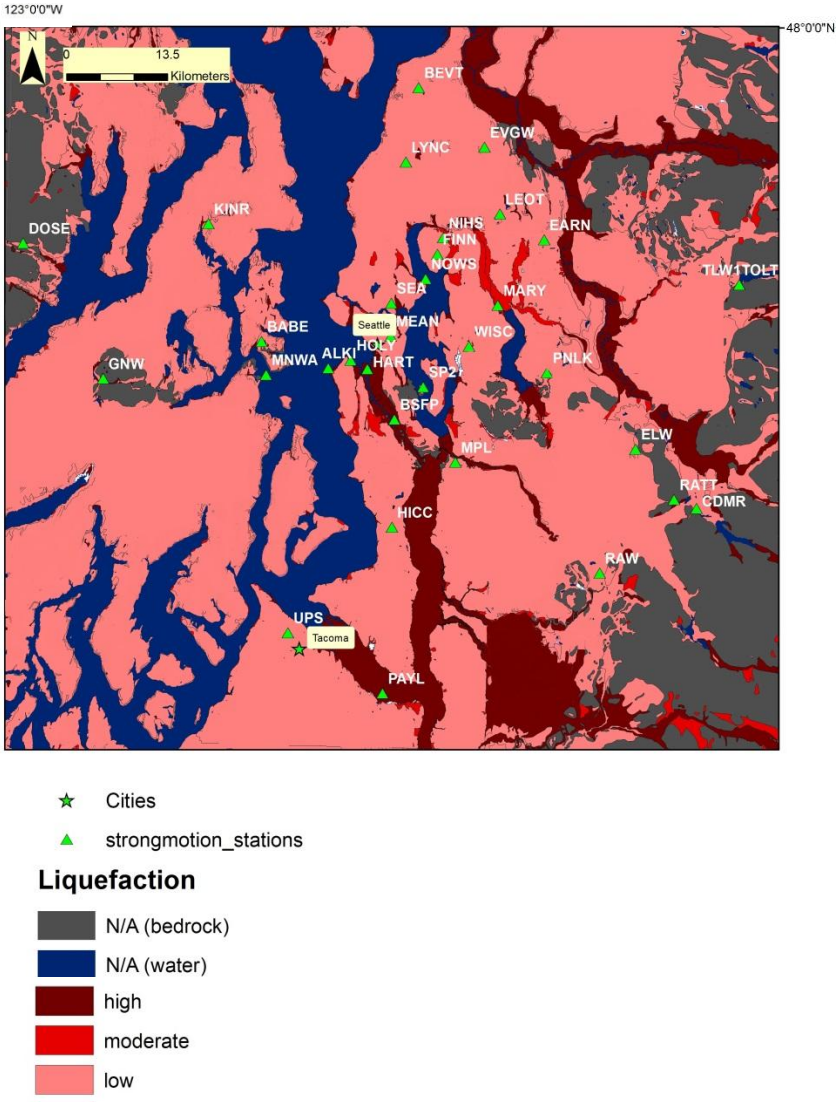

Fig. 11. Strong motion stations overlain on liquefaction map (Palmer et al., 2004).

Table 2. Strong motion stations for the 2012 Queen Charlotte earthquake.

Network	Station	Latitude	Longitude	Elevation (m)	Geologic Unit
UW	ALCT	47.65	-122.04	55	Pleistocene continental glacial drift
UW	ALKI	47.58	-122.42	1	Pleistocene and Holocene alluvium
UW	BABE	47.61	-122.54	83	Pleistocene continental glacial drift
UW	DOSE	47.72	-122.97	53	Pleistocene continental glacial drift
UW	EARN	47.74	-122.04	159	Pleistocene continental glacial drift
UW	ERW	48.45	-122.63	389	Pleistocene continental glacial drift
UW	EVCC	48.01	-122.2	0	Pleistocene continental glacial drift
UW	EVGW	47.85	-122.15	10	Pleistocene continental glacial drift
UW	FINN	47.72	-122.23	121	Pleistocene continental glacial drift
UW	HICC	47.39	-122.3	115	Pleistocene continental glacial drift
UW	LON	46.75	-121.81	853	Paleogene and Neogene fragmental volcanic rock
UW	LRIV	48.06	-123.5	293.8	Pleistocene continental glacial drift
UW	LYNC	47.83	-122.29	19	Pleistocene continental glacial drift
UW	MARY	47.66	-122.12	11	Pleistocene and Holocene alluvium
UW	MEAN	47.62	-122.31	37	Pleistocene continental glacial drift
UW	MNWA	47.57	-122.53	8	Paleocene to Miocene marine sedimentary rock
UW	NIHS	47.74	-122.22	137	Pleistocene continental glacial drift
UW	NOWS	47.69	-122.25	21	Pleistocene and Holocene alluvium
UW	PAYL	47.19	-122.31	10	Pleistocene and Holocene alluvium
UW	PNLK	47.58	-122.03	128	Pleistocene continental glacial drift
UW	RATT	47.43	-121.8	440	Paleogene and Neogene fragmental volcanic rock
UW	SP2	47.56	-122.25	30	Pleistocene continental glacial drift
UW	SQM	48.07	-123.05	45	Pleistocene continental glacial drift
UW	SVOH	48.29	-122.63	22	Pleistocene continental glacial drift
UW	SWID	48.01	-122.41	62	Pleistocene continental glacial drift
UW	TOLT	47.69	-121.69	541	Paleogene and Neogene volcanic rock
UW	WISH	47.12	-123.77	45	Pleistocene and Holocene alluvium

Table 3. Strong motion stations for the 2014 Vancouver Island earthquake.

Network	Station	Latitude	Longitude	Elevation (m)	Geologic Unit
UW	ALCT	47.65	-122.04	55	Pleistocene continental glacial drift
UW	ALKI	47.58	-122.42	1	Pleistocene and Holocene alluvium
UW	BABE	47.61	-122.54	83	Pleistocene continental glacial drift
UW	DOSE	47.72	-122.97	53	Pleistocene continental glacial drift
UW	EARN	47.74	-122.04	159	Pleistocene continental glacial drift
UW	ERW	48.45	-122.63	389	Pleistocene continental glacial drift
UW	EVCC	48.01	-122.2	0	Pleistocene continental glacial drift
UW	EVGW	47.85	-122.15	10	Pleistocene continental glacial drift
UW	FINN	47.72	-122.23	121	Pleistocene continental glacial drift
UW	HICC	47.39	-122.3	115	Pleistocene continental glacial drift
UW	LON	46.75	-121.81	853	Paleogene and Neogene fragmental volcanic rock
UW	LRIV	48.06	-123.5	293.8	Pleistocene continental glacial drift
UW	LYNC	47.83	-122.29	19	Pleistocene continental glacial drift
UW	MARY	47.66	-122.12	11	Pleistocene and Holocene alluvium
UW	MEAN	47.62	-122.31	37	Pleistocene continental glacial drift
UW	MNWA	47.57	-122.53	8	Paleocene to Miocene marine sedimentary rock
UW	NIHS	47.74	-122.22	137	Pleistocene continental glacial drift
UW	NOWS	47.69	-122.25	21	Pleistocene and Holocene alluvium

Data Analysis

There are three main factors affecting the recorded waveform of a seismic signal: the source, the path, and the site. To isolate the site response from the other two factors, we use seismic recordings from the same earthquake at stations that are approximately on the same azimuth. This eliminates the effect of the source and partially reduces the influence of path. The distances between the stations are relatively close in comparison to the source-receiver distance; however, seismic waves experience attenuation as a

function of distance and this effect is accounted for in the data processing by using an attenuation correction (discussed below).

Three-component Broadband data

After downloading the broadband data, a bandpass filter (0.2-15Hz) (Langston, [http://www.ceri.memphis.edu/people/clangstn/, accessed on 28/7/2014]) was applied to each component. A segment of data with a length of 75 seconds (3001 samples) starting before the S-wave was extracted from each waveform for each station. Then the data were demeaned, detrended, and tapered, before calculating the power spectra for each component (horizontal east (H_e), horizontal north (H_n), and vertical (V_z) (Fig. 12). MATLAB^{TM}'s power spectral density function (PSD) was used for this purpose. The spectral amplitudes were corrected for attenuation and spherical spreading using the following equation:

$$A_c\,(f) = A_o\,(f)\, r^{0.5}\, e^{\pi f t/Qs(f)} \qquad (1)$$

where $A_o\,(f)$ is observed amplitude, $A_c\,(f)$ is corrected amplitude, f is frequency, t is travel time, r is source-receiver distance, and $Q_s\,(f)$ is a frequency-dependent s-wave attenuation factor (Pratt and Brocher, 2006). The bedrock relation of $Q_s\,(f) = 380\, f^{0.39}$ (Atkinson, 1995) was utilized in the equation to correct for attenuation and spherical spreading. The source-receiver distance was estimated using the geographic coordinates of the epicenter and stations. Due to the shallow depth (<15 km) of the focal point in all the events used in this study, the source-receiver distance approximately equals the arc distance used in the correction. According to Atkinson (1995), the value of $r^{0.5}$ is

preferred to *r* for source-receiver distances of more than 230 km. To calculate the travel time, the p-wave arrival was subtracted from the exact time of the earthquake.

To calculate the HVSR, the spectra from the horizontal components (H_n and H_e) were averaged and divided by the vertical component (V_z). The results were smoothed using a MATLAB^{TM} function that uses a 20-point moving average. The data processing procedure is shown schematically in Fig. 12.

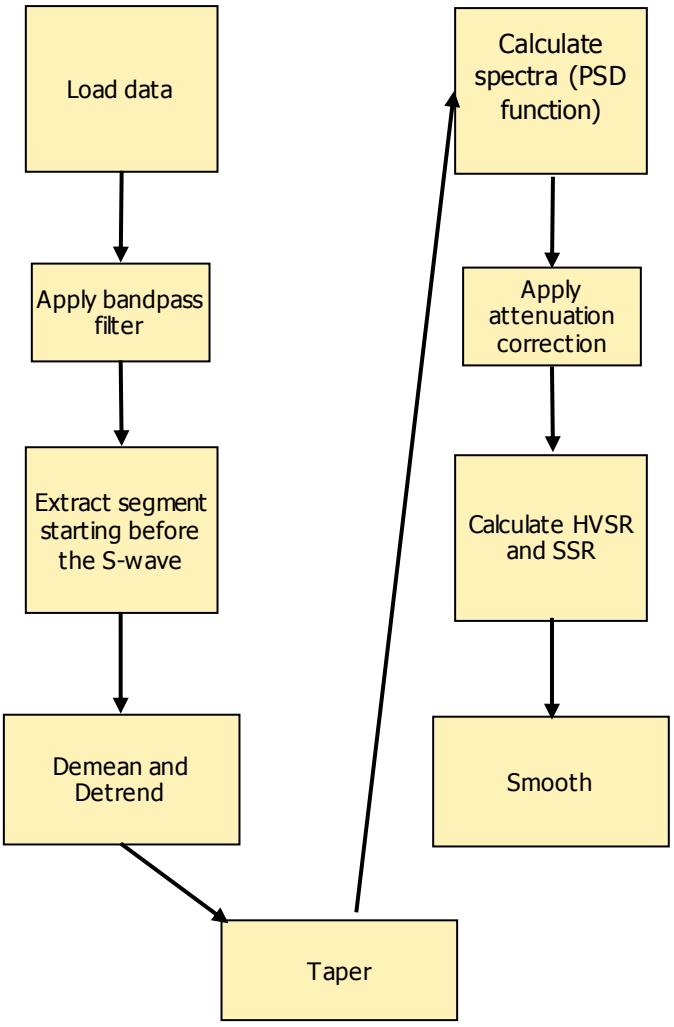

Fig. 12. Flowchart showing data processing steps for data used in this study.

Strong motion data

The processing of strong motion data was similar to that used for the broadband data. However, the bandpass filter used low- and high-end frequencies of 0.2 and 25 Hz, respectively, and the segments were 70 s (7001 samples) long (Fig. 13). A smoothing function was applied to the strong motion data using a 5-point span window.

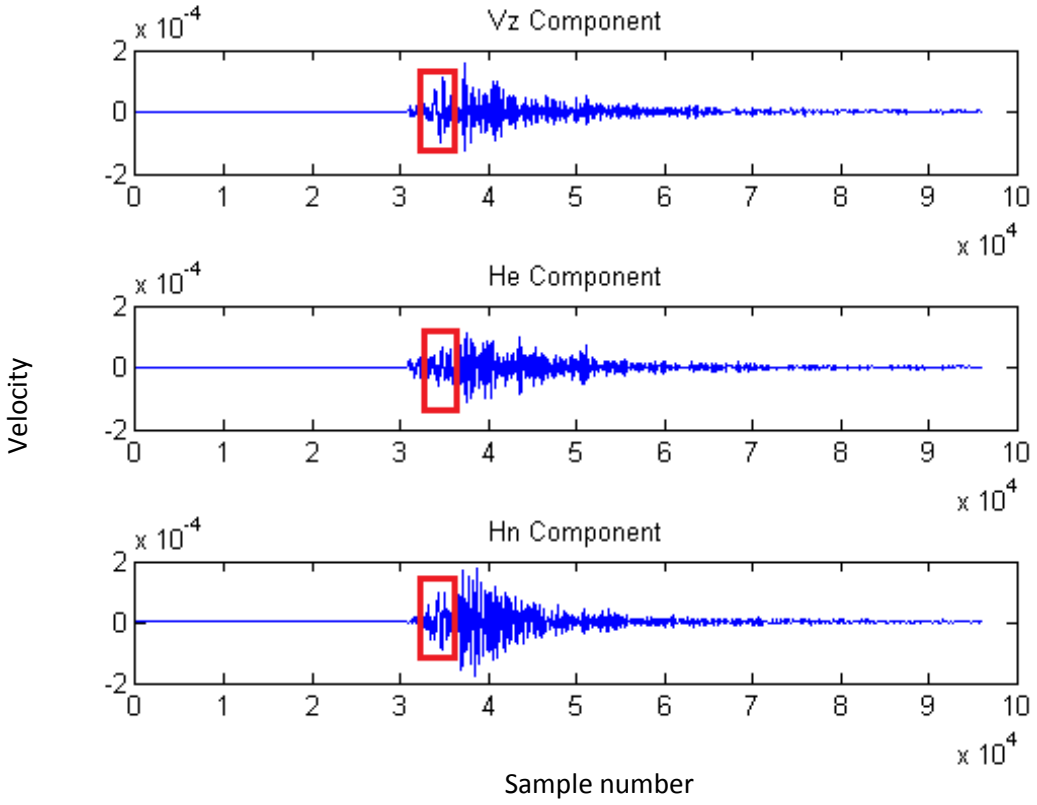

Fig. 13. Example of a 3-component broadband seismogram used in this study. The extracted data segment (red rectangle) begins shortly before the S wave and continues for 70 seconds.

Liquefaction array

One strong motion station, SLA, (also known as Seattle liquefaction array) recorded acceleration data from several depths (0 m (surface), 4.5 m, 44.9 m, and 56.4

m). The site has a high level of noise introduced by trains traveling nearby. To eliminate the train noise, a bandpass filter with the cut off frequencies of 0.02 and 25 Hz was used on each component before extracting the segment and calculating the SSRs (Fig. 14).

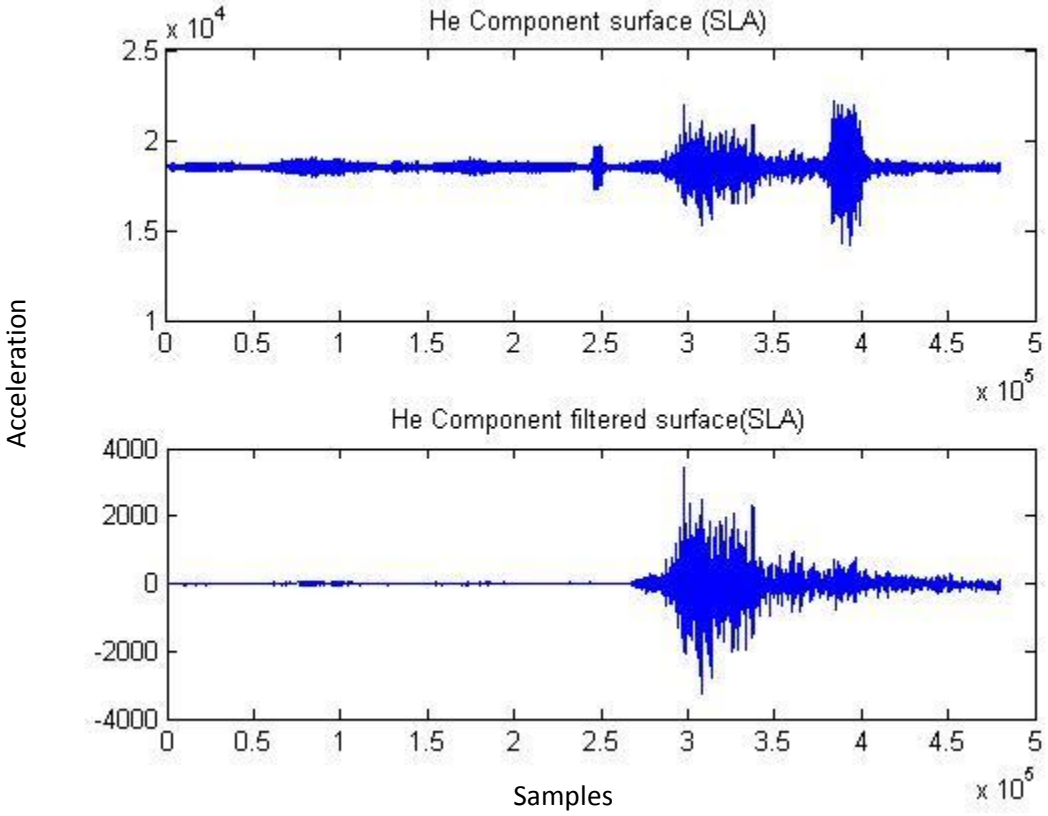

Fig. 14. Example of effect of bandpass filter on H_e component of acceleration from the liquefaction array before (upper plot) and after (lower plot) its application. High-amplitude noise (seen between 3.8 x 10 -5 and 4.0 x 10-5 on upper plot) is reduced significantly after filtering (lower plot).

Results

This chapter includes the HVSR and SSR results from the 2012 Queen Charlotte strong motion data, the 2014 Vancouver Island strong motion data, and the 2012 Vancouver Island broadband data. It also contains the results from the Seattle liquefaction array. Details for each earthquake are included in Table 4.

Table 4. Earthquakes used in the analysis.

Event number	**1**	**2**	**3**
Location	Queen Charlotte	Vancouver Island	Vancouver Island
Date	10/28/2012	4/24/2014	11/8/2012
Time	03:04:08 UTC	03:10:12 UTC	02:01:50 UTC
Latitude	52.788° N	49.8459° N	49.231° N
Longitude	132.101° W	127.444° W	128.477° W
Magnitude	MW7.8	MWW6.6	MW6.1
Depth	14.0 km	11.4 km	13.7 km
Data type	Strong motion	Strong motion	Broadband
Sampling rate	100 samples/sec	100 samples/sec	40 samples/sec

SSR Results

1. The 2012 Queen Charlotte Earthquake

Fig. 15 shows the SSR plots from the 2012 Queen Charlotte earthquake strong motion data organized by the local geologic environment of the station location. Out of the 16 stations located on Pleistocene continental glacial drift, 11 show a peak at ~1 Hz

frequency. In contrast, fundamental peak frequencies at 3 Hz are observed at DOSE and SP2 stations. Most of the stations indicate low amplification at frequencies higher than 6 Hz. Secondary peaks are also observed at 2 Hz at LRIV, LYNC, EVCC, and NIHS.

(a) Pleistocene continental glacial drift

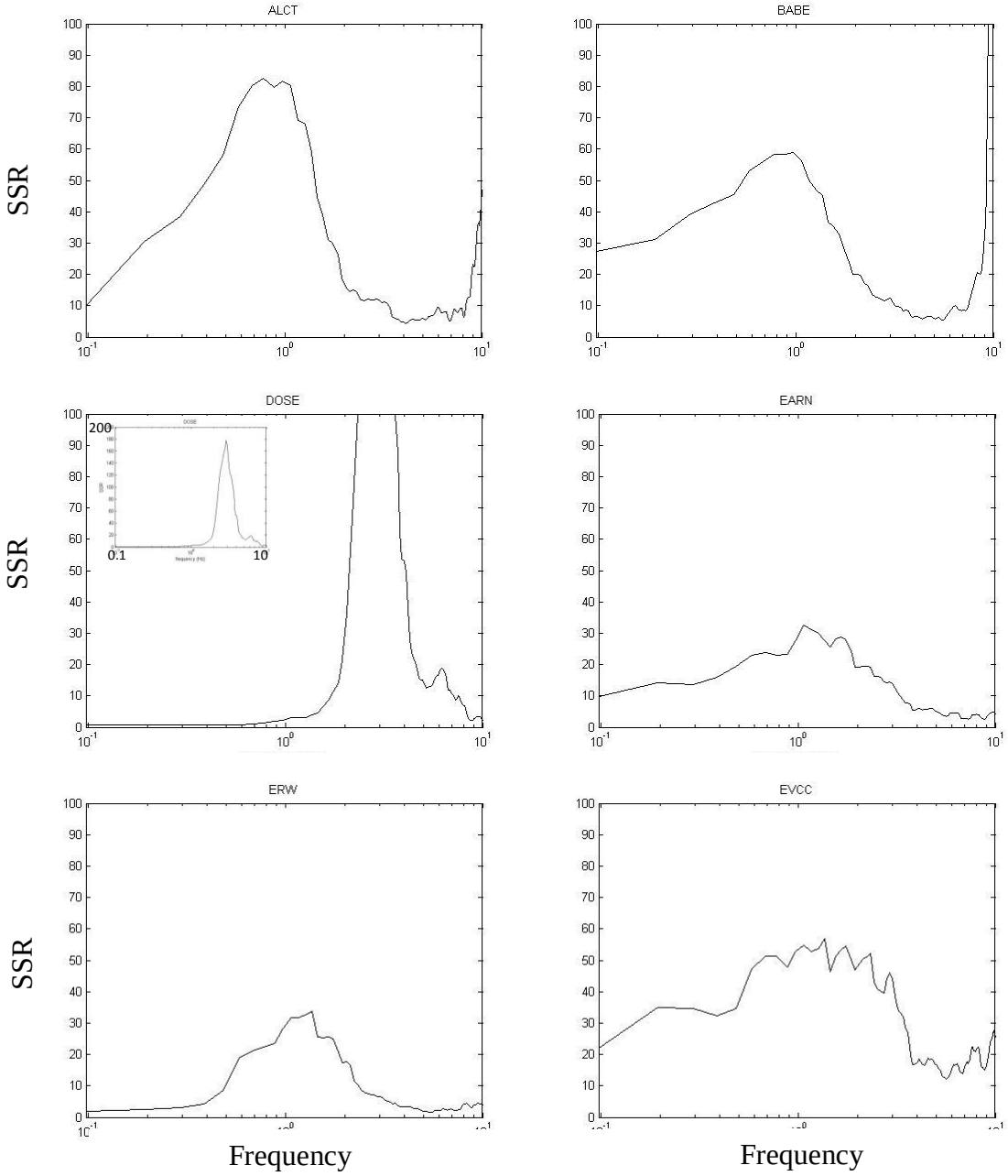

Pleistocene continental glacial drift (continued)

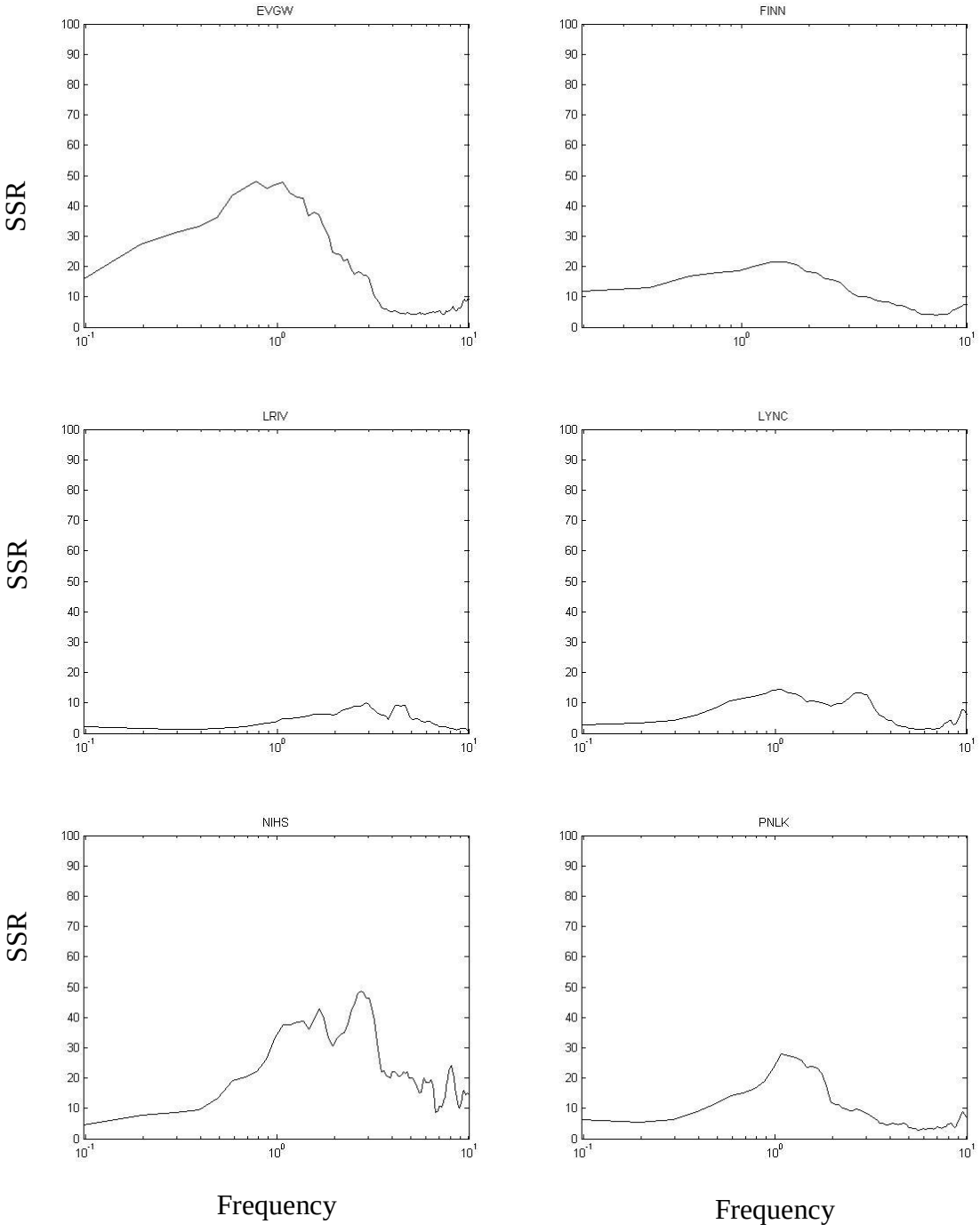

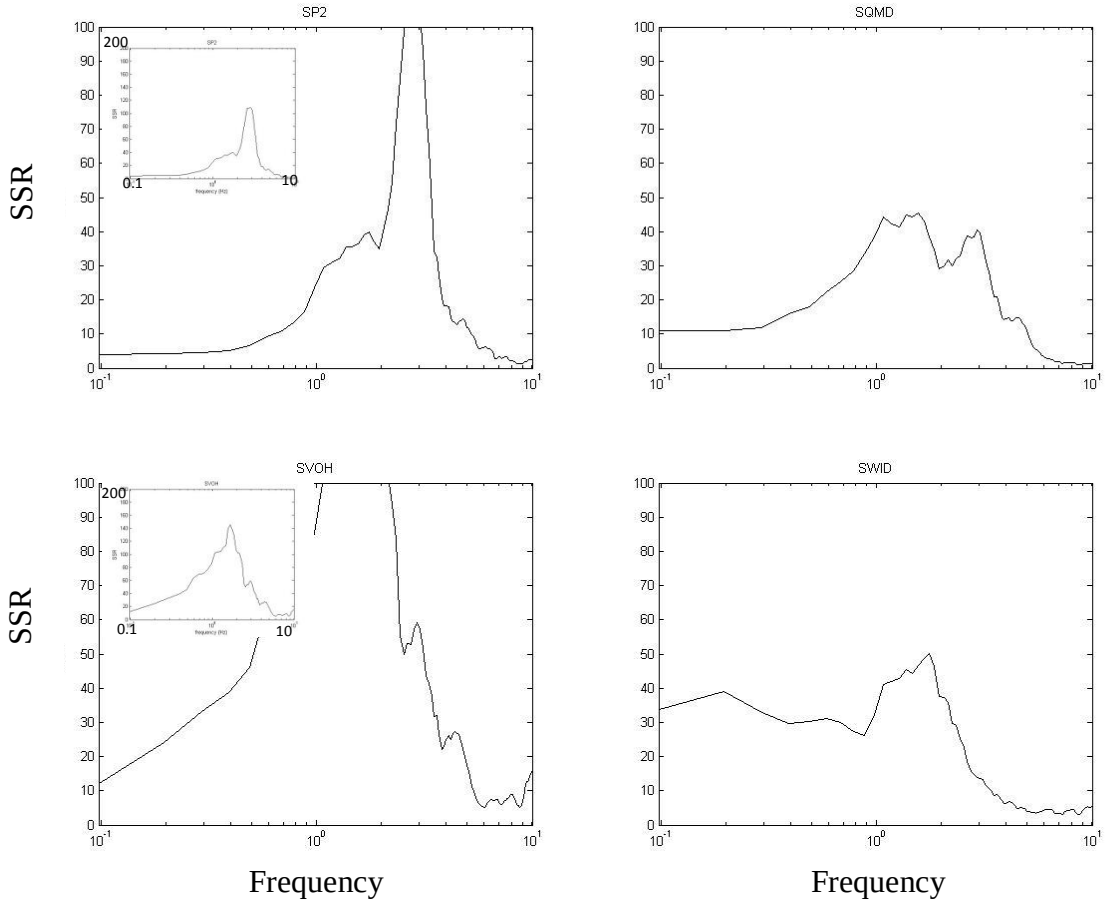

(b) Paleogene and Neogene volcanic rock

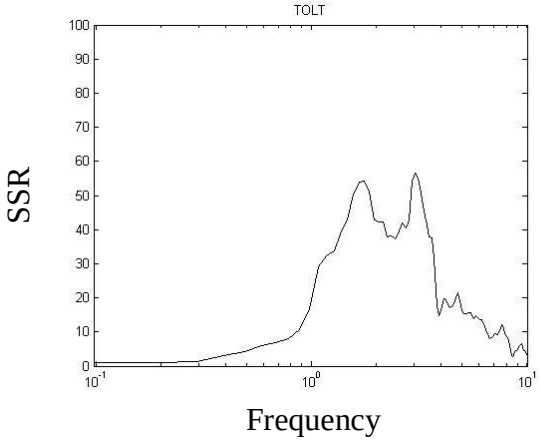

(c) Pleistocene and Holocene alluvium

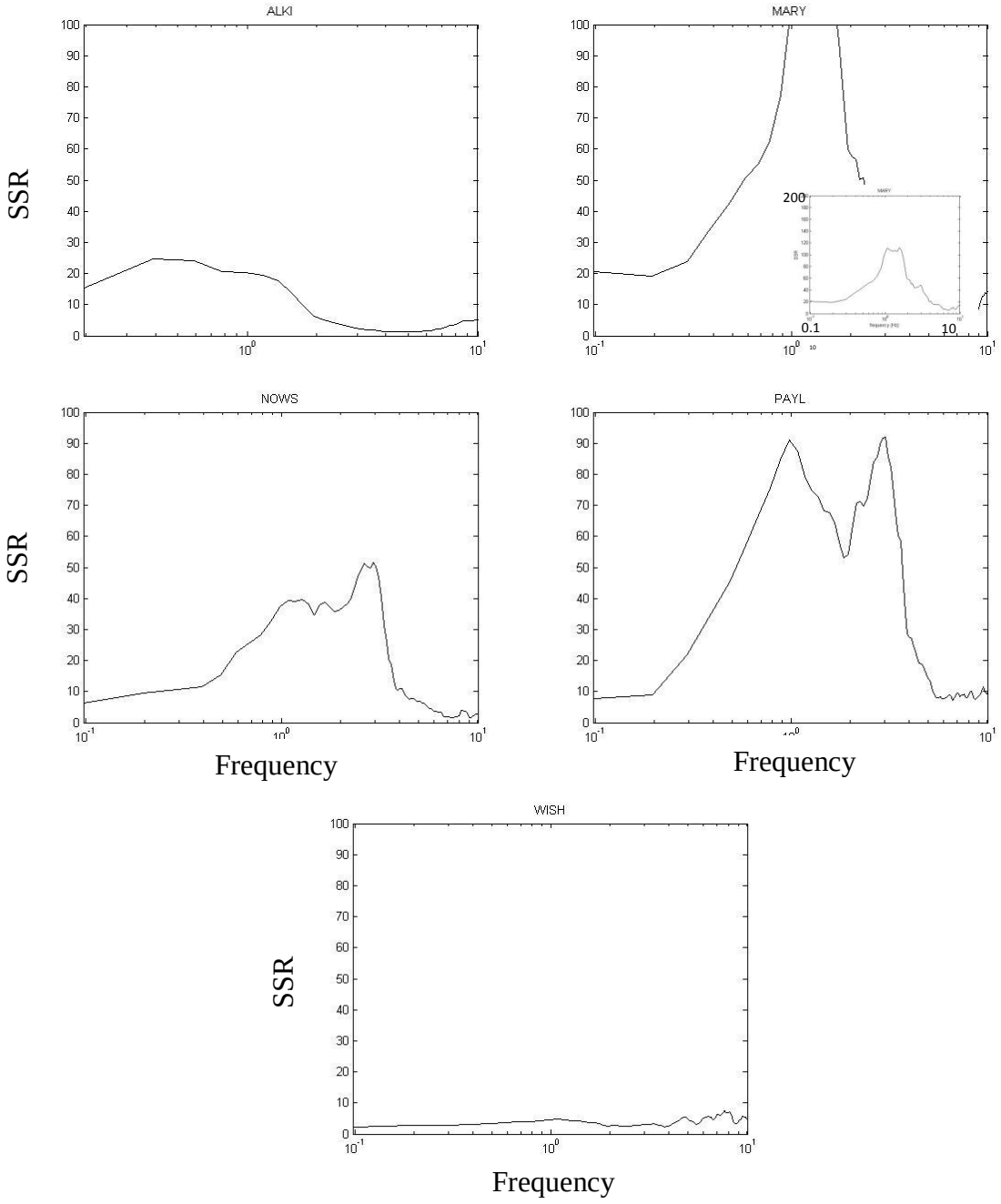

(d) Paleogene and Neogene fragmental volcanic rock and Paleocene to Miocene marine sedimentary rock

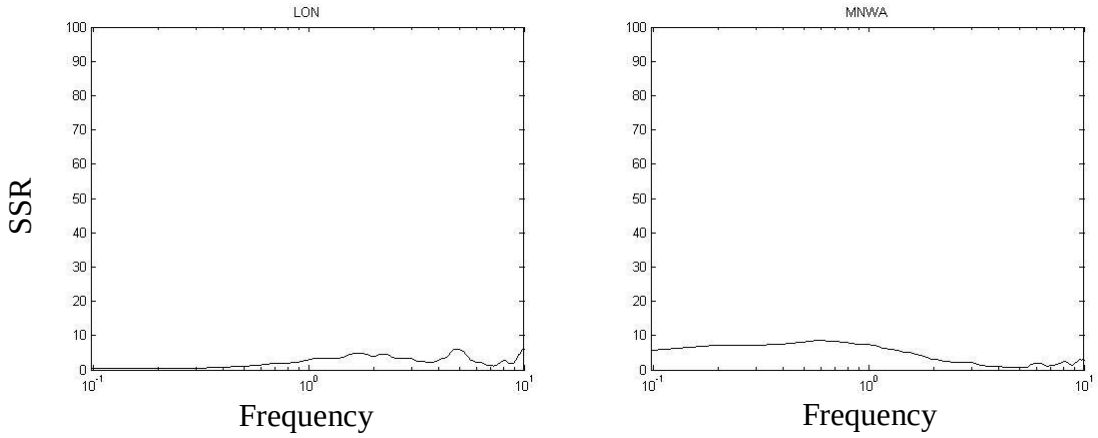

Fig. 15. SSR results from the 2012 Queen Charlotte earthquake strong motion data. Results are displayed with respect to underlying geology, as determined from Washington Department of Natural Resources (http://www.dnr.wa.gov/BusinessPermits/Pages/PubMaps.aspx) last accessed on 8/8/2014. (a) Pleistocene continental glacial drift, (b) Paleogene and Neogene volcanic rock, (c) Pleistocene and Holocene alluvium, (d) Paleogene and Neogene fragmental volcanic rock and Paleocene to Miocene marine sedimentary rock. Refer to Fig. 12 and Table 2 for station locations. The insets show the full extent of the some larger peaks.

TOLT, which is the only station located on Paleogene and Neogene volcanic rock, shows peaks at 2 and 3 Hz. Three out of five stations located on Pleistocene and Holocene alluvium have peaks at 1 and 3 Hz, with the exception of ALKI (0.4 Hz) and MARY (2 Hz). Contrary to other stations located in this type of geology, WISH indicates a flat response at all frequencies. LON and MNWA, located on Paleogene and Neogene fragmental volcanic rock and Paleocene to Miocene marine sedimentary rock, respectively, also show a flat response at all frequencies.

2. The 2014 Vancouver Island earthquake

Fig. 16 shows the SSR plots for strong motion data from the 2014 Vancouver Island earthquake organized by the local geologic environment of the station location.

(a) Pleistocene continental glacial drift

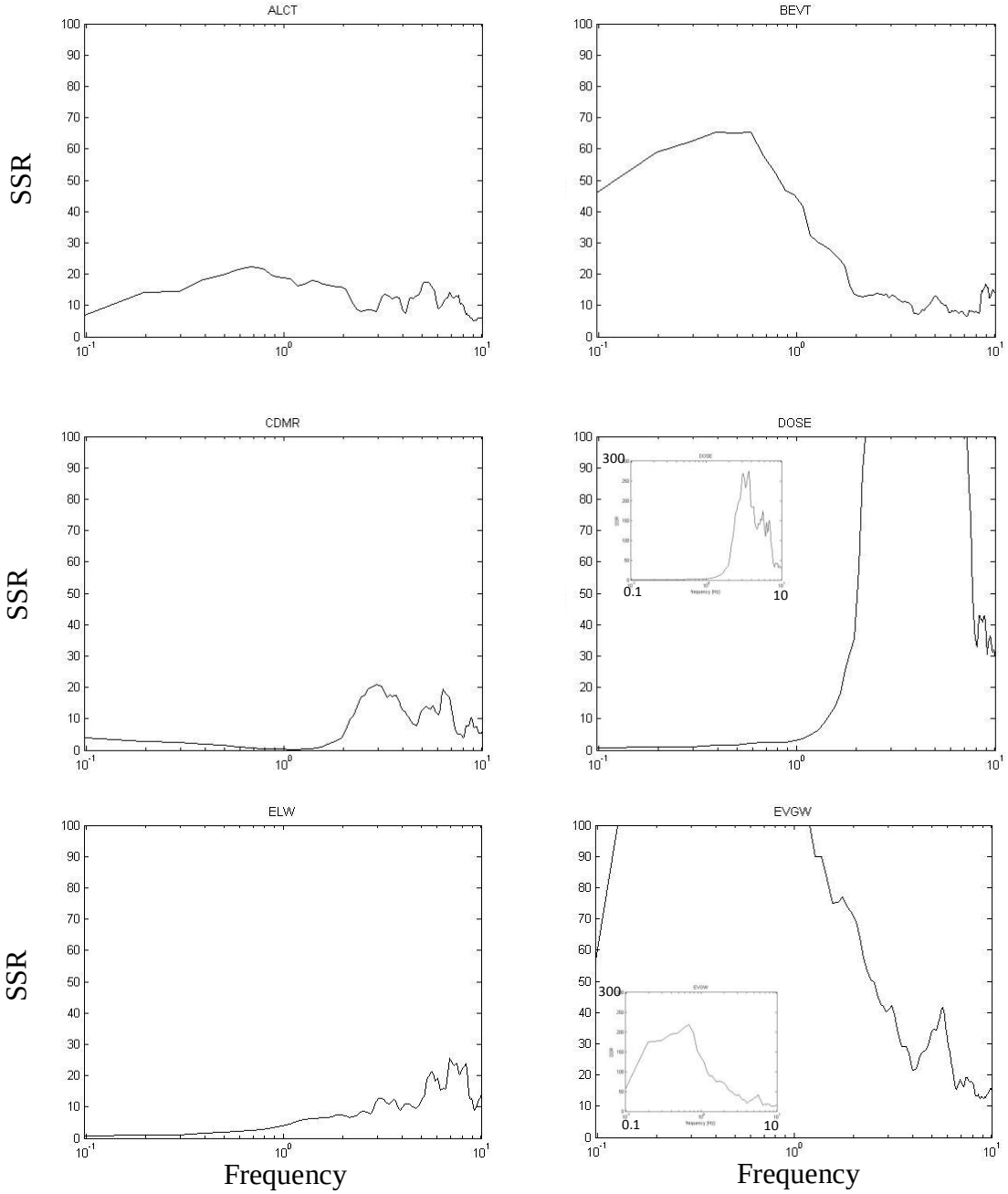

Pleistocene continental glacial drift (continued)

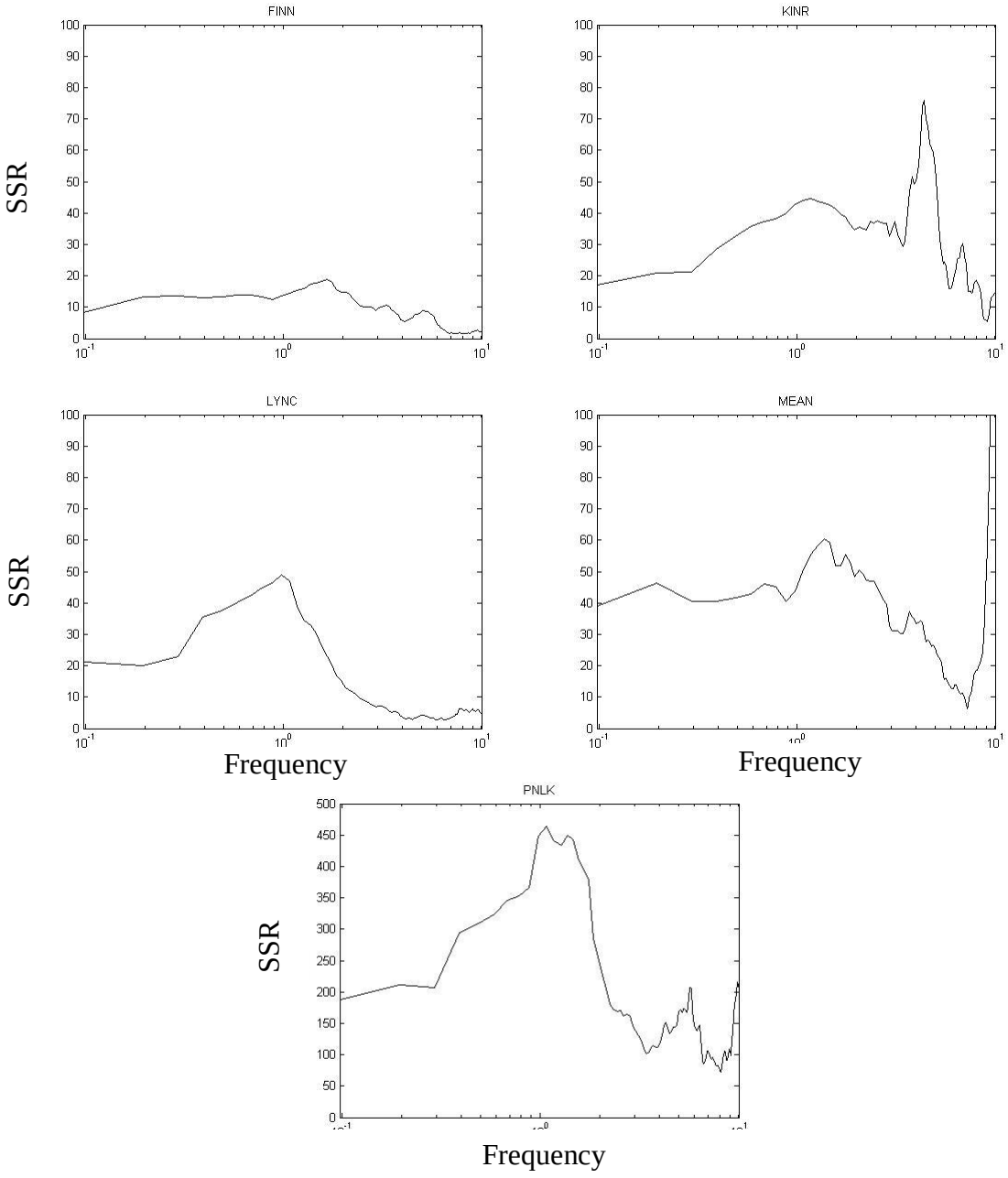

(b) Paleogene and Neogene volcanic rock

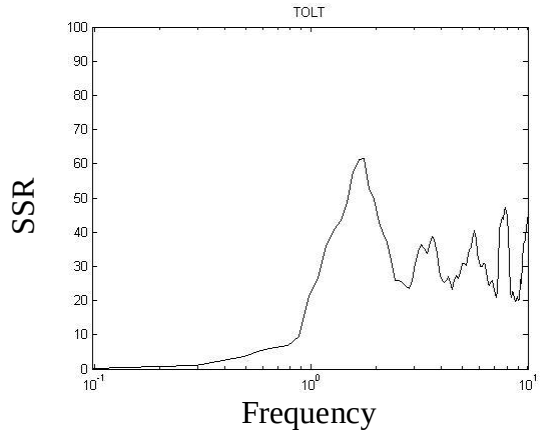

(c) Pleistocene and Holocene alluvium

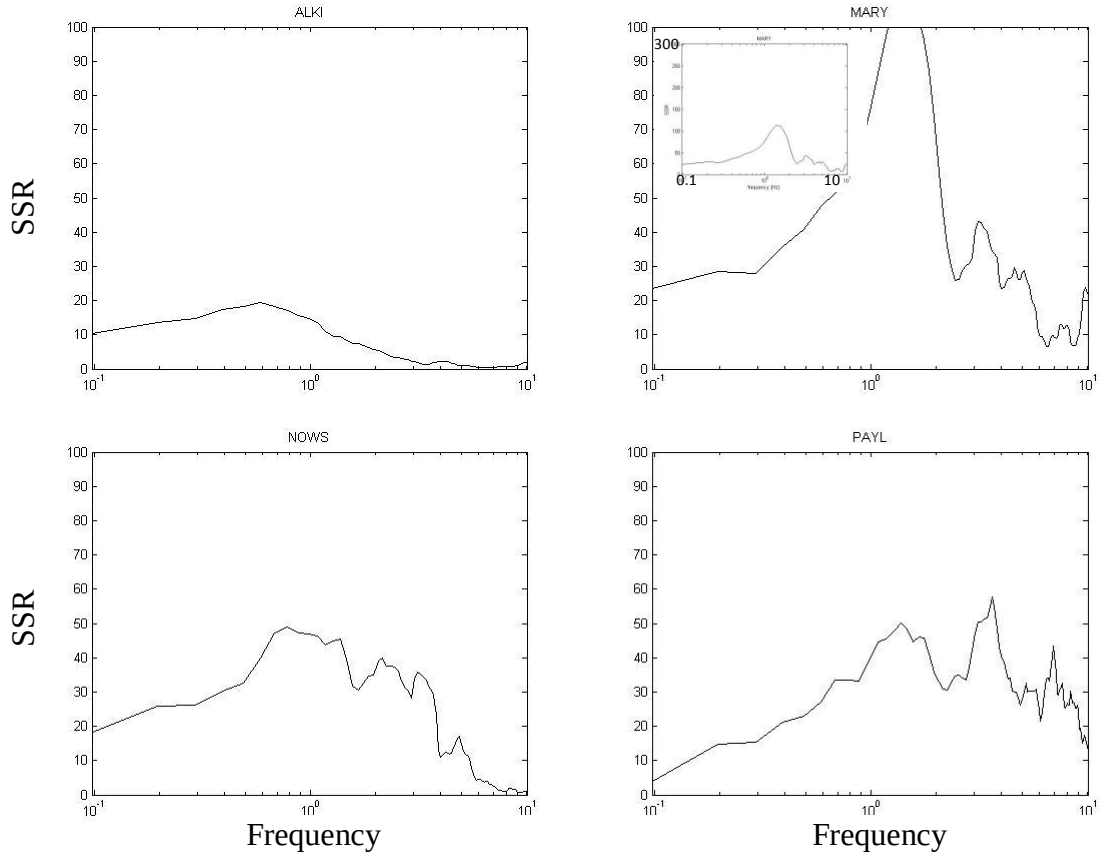

Fig. 16. The SSR results from the 2014 Vancouver Island earthquake strong motion data. Results are displayed with respect to underlying geology, as determined from Washington Department of Natural Resources (http://www.dnr.wa.gov/BusinessPermits/Pages/PubMaps.aspx) last accessed on 8/8/2014. (a) Pleistocene continental glacial drift, (b) Paleogene and Neogene volcanic rock, (c) Pleistocene and Holocene alluvium. Refer to Fig. 12 and Table 3 for station locations. The insets show the full extent of larger peaks. The station PNLK is plotted on a different scale.

For the 2014 Vancouver Island earthquake, peaks from 0.6 to 8 Hz are observed on stations located on Pleistocene continental glacial drift. Five stations out of 11 share a peak at 1 to 1.5 Hz. However, there is little consistency in the peak frequencies in terms of the site geology. DOSE shows large peaks at 3 and 5 Hz. CDMR, KINR, and ELW indicate peaks at 7 Hz. ALCT, BEVT, and EVGW have peaks at 0.7 to 0.8 Hz.

The response from TOLT (peaks at 1.5, 3, 5.5, and 7 Hz), which is located on Paleogene and Neogene volcanic rock, is quite similar to its response from the 2012 Queen Charlotte earthquake. Likewise, the responses from all stations located in Pleistocene and Holocene alluvium are similar to those from 2012 Queen Charlotte earthquake located in the same type of geology. Despite differences on SSR relative amplification values, peak frequencies at 11 stations are the same as those observed from the 2012 Queen Charlotte Island earthquake.

3. The 2012 Vancouver Island earthquake

Fig. 17 shows the SSR plots from broadband data from the 2012 Vancouver Island earthquake organized by site geology at the station location.

(a) Pleistocene continental glacial drift

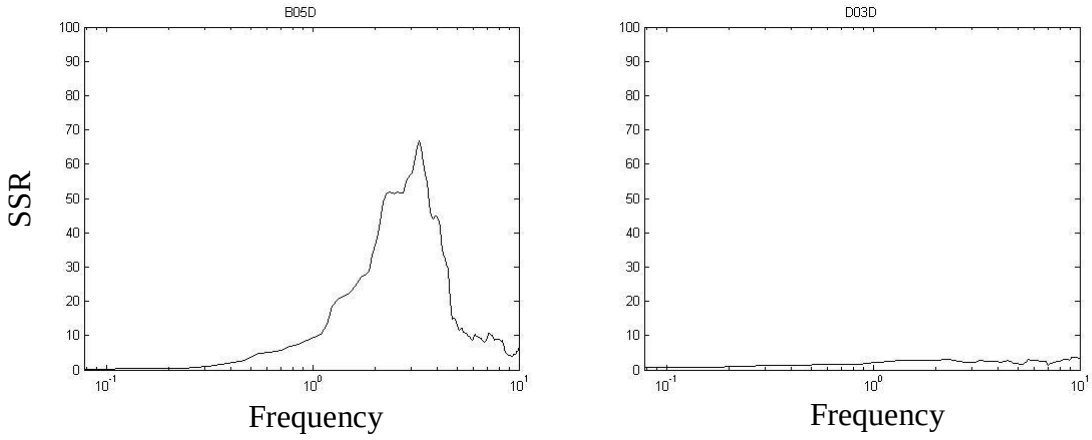

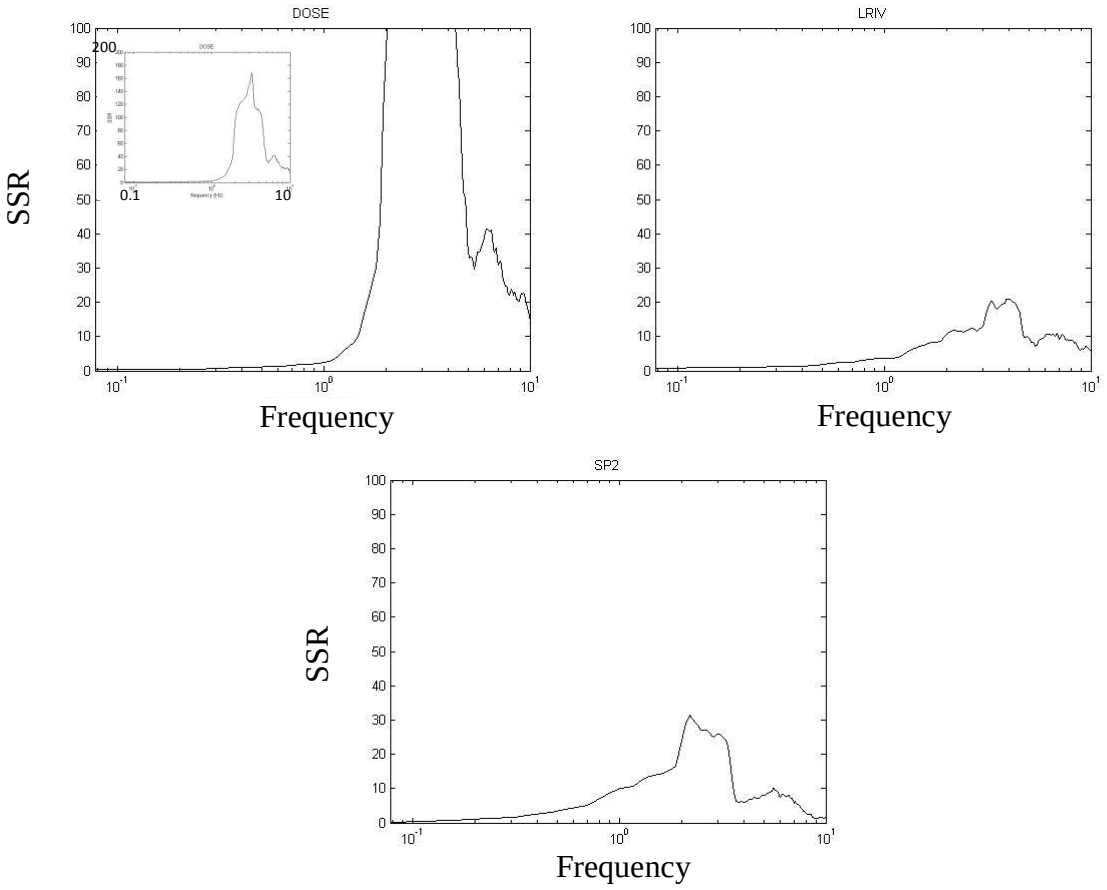

(b) Paleogene and Neogene volcanic rock

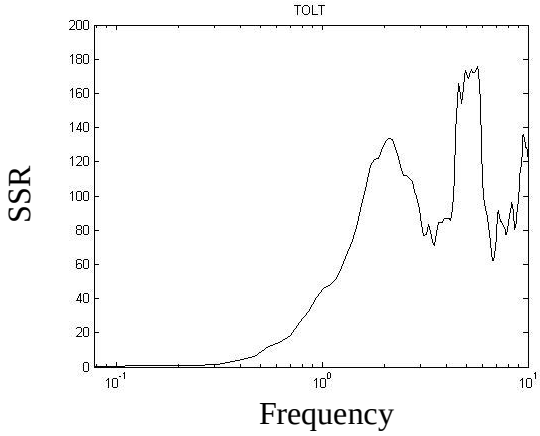

(c) Pleistocene and Holocene alluvium

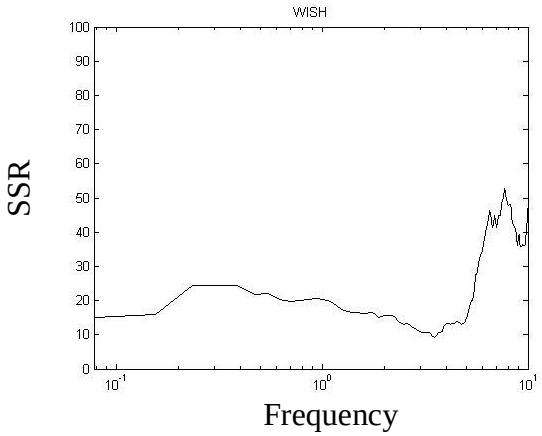

(d) Paleogene and Neogene fragmental volcanic rock

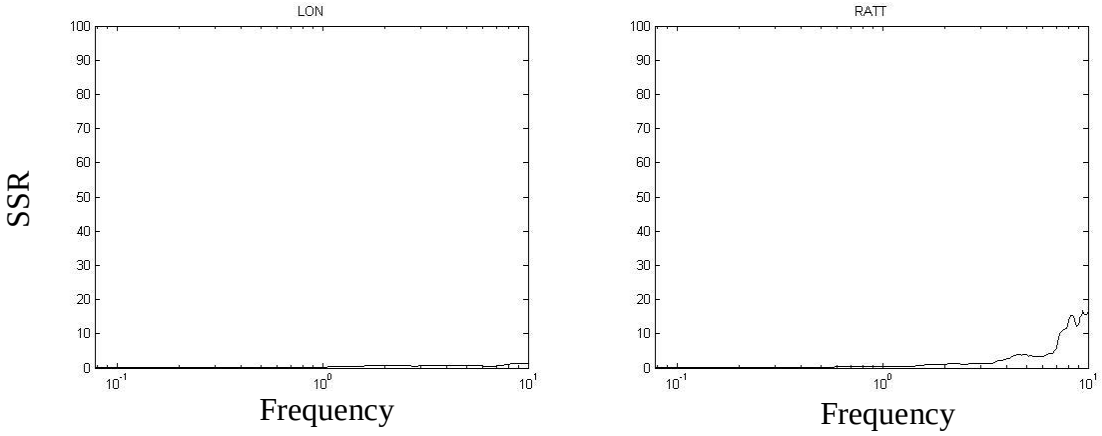

Fig. 17. SSR results from the 2012 Vancouver Island earthquake broadband data. Results are displayed with respect to underlying geology, as determined from Washington Department of Natural Resources (http://www.dnr.wa.gov/BusinessPermits/Pages/PubMaps.aspx) last accessed on 8/8/2014. (a) Pleistocene continental glacial drift, (b) Paleogene and Neogene volcanic rock, (c) Pleistocene and Holocene alluvium, (d) Paleogene and Neogene fragmental volcanic rock. Refer to Fig. 11 and Table 1 for station locations. Insets show the extent of the larger peaks

The SSR results from 2012 Vancouver Island earthquake broadband data show consistent results for stations located on the Pleistocene continental glacial drift. All of these stations show peaks at 3 Hz and a flat response at lower frequencies. TOTL show peaks at 3, 5, and 7 Hz, which is quite similar to the response from this station in the

previous earthquakes. The only station located on the Pleistocene and Holocene alluvium, WISH, shows a peak at 8 Hz. Stations located on Paleogene and Neogene fragmental volcanic rock, LON and RATT, show a relatively flat response, except for the frequencies higher than 7 Hz at station RATT.

HVSR Results

1. *The 2012 Queen Charlotte earthquake*

Fig. 18 shows the HVSR plots from strong motion data for the 2012 Queen Charlotte organized by site geology at the station location.

(a) Pleistocene continental glacial drift

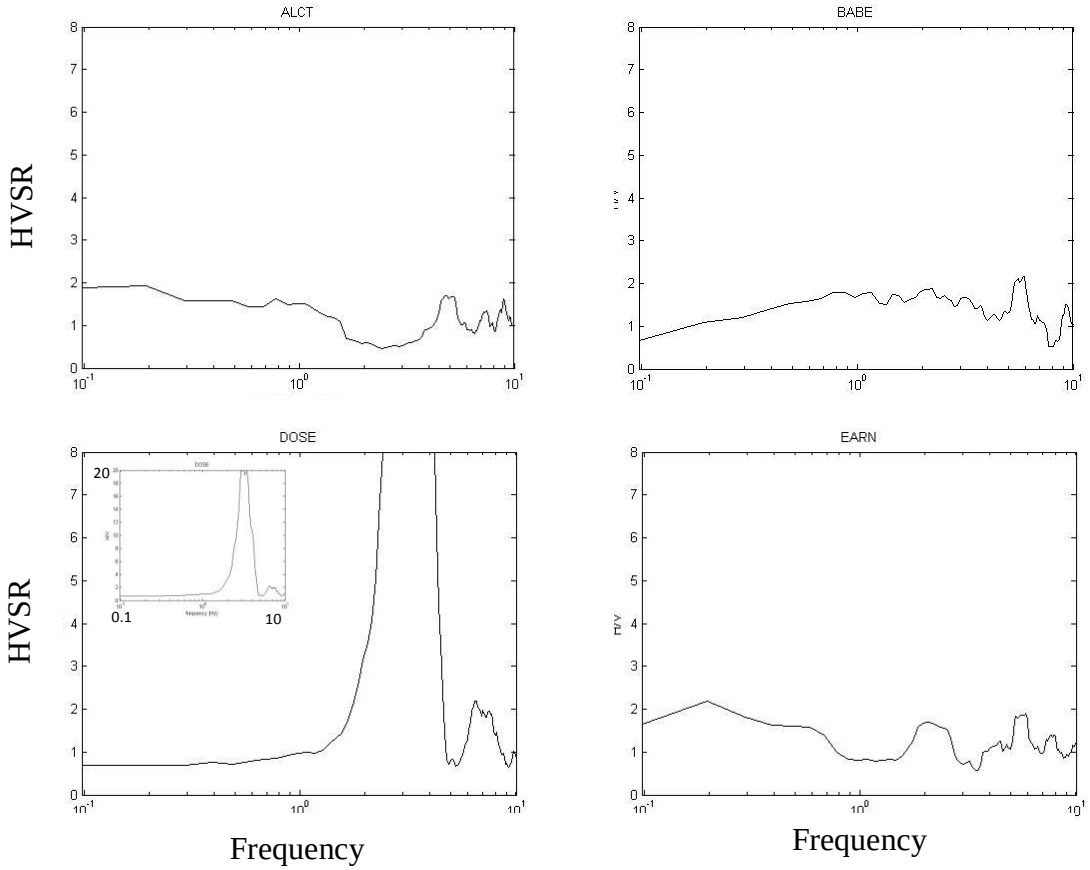

Pleistocene continental glacial drift (continued)

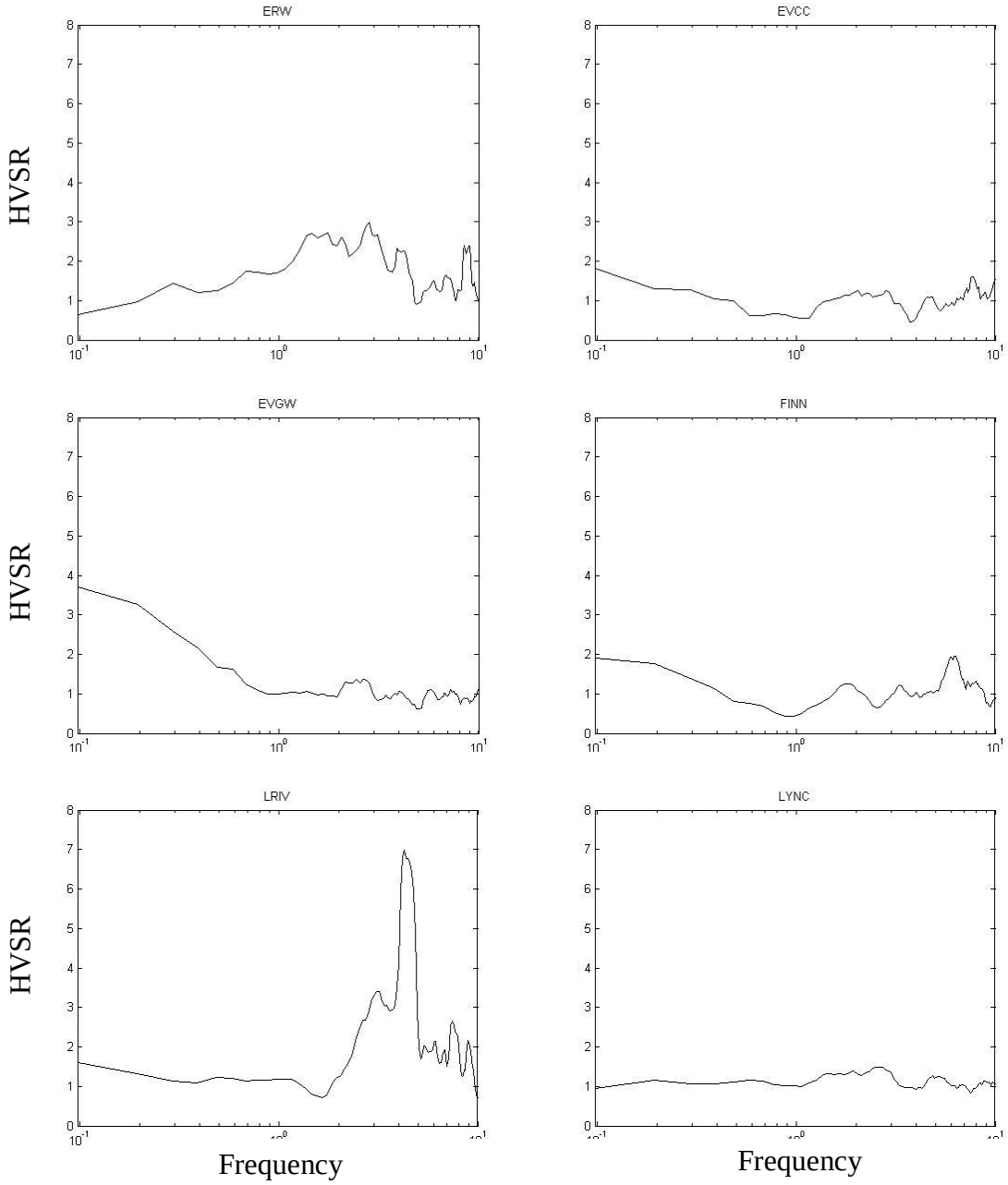

Pleistocene continental glacial drift (continued)

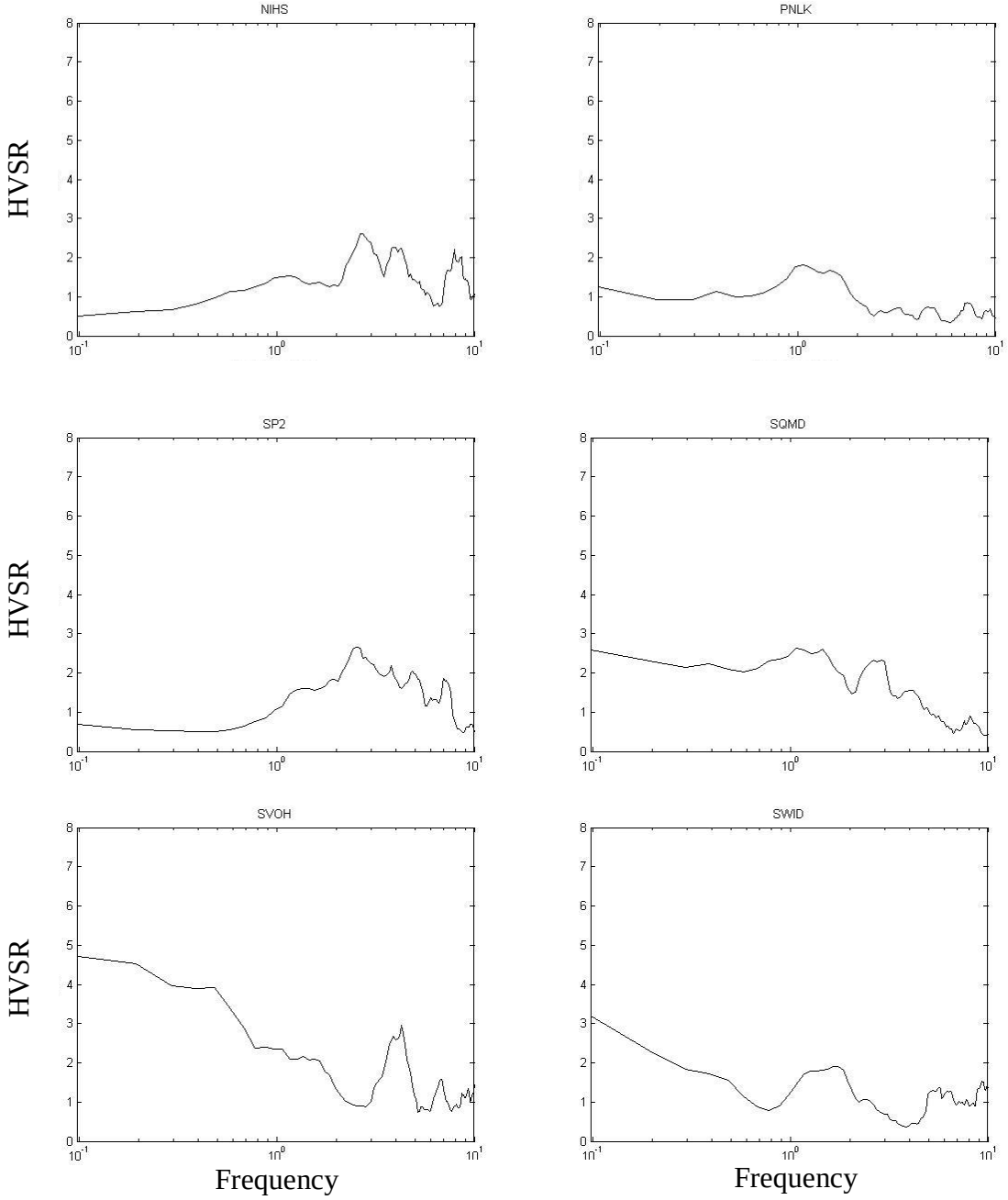

(a) Paleogene and Neogene volcanic rock

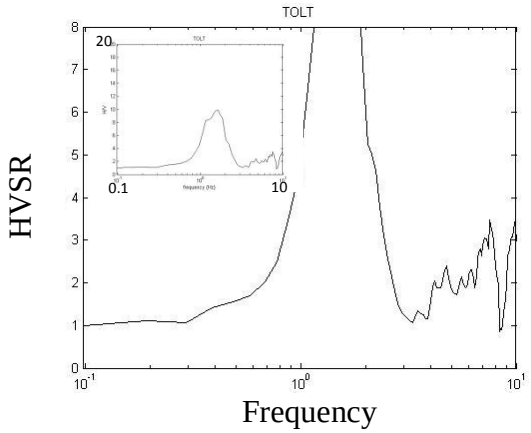

(b) Pleistocene and Holocene alluvium

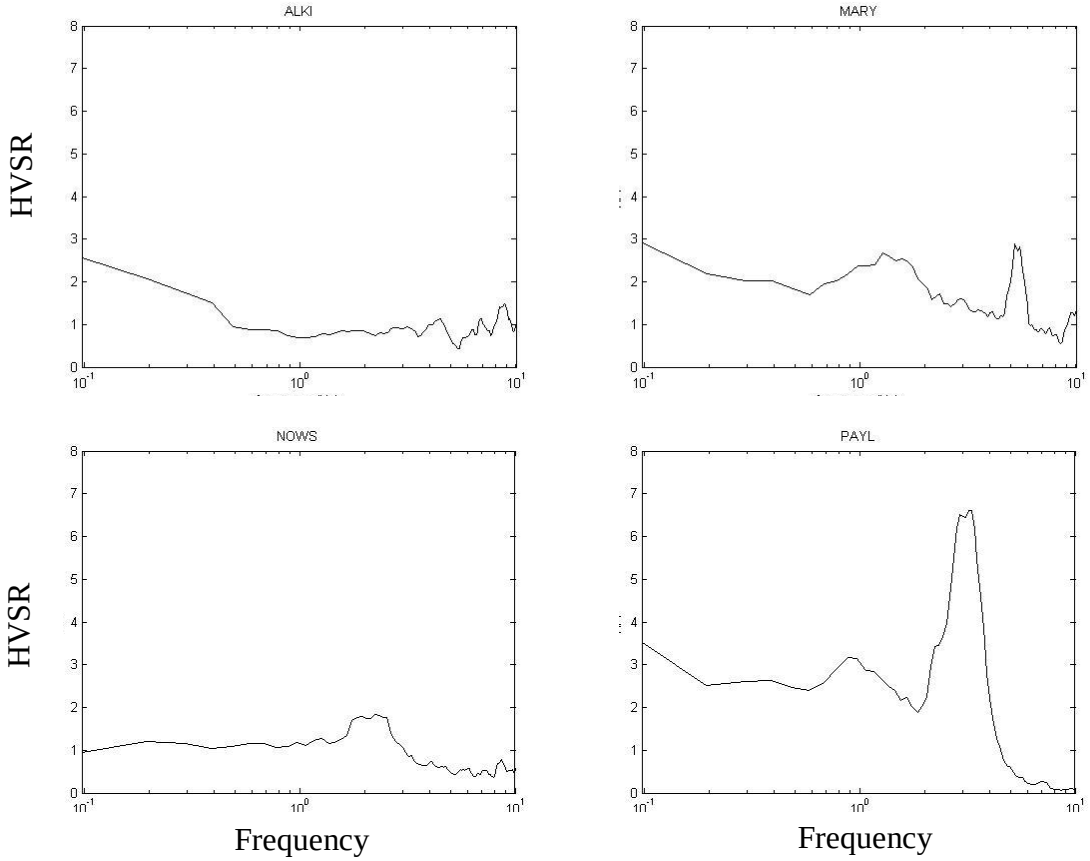

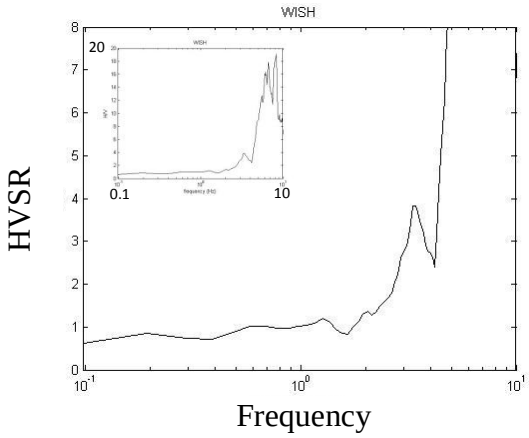

(c) Paleogene and Neogene fragmental volcanic rock

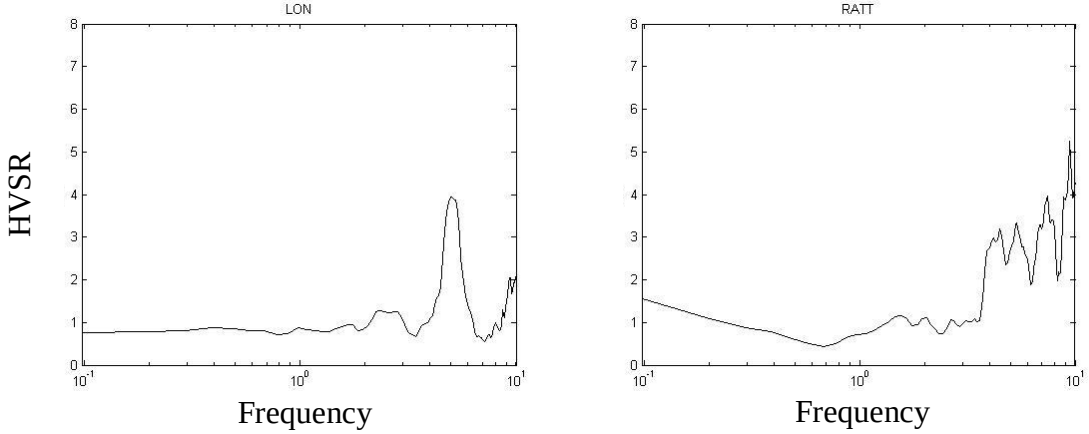

(d) Paleocene to Miocene marine sedimentary rock

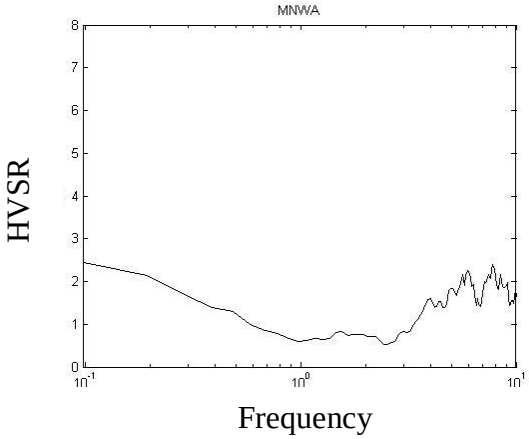

(e) Paleogene and Neogene intrusive rock

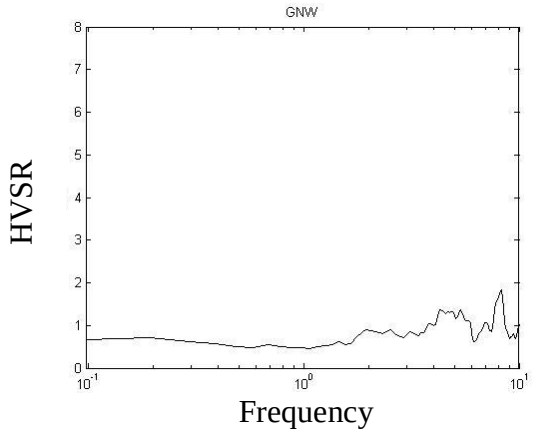

Fig. 18. HVSR results from the 2012 Queen Charlotte earthquake strong motion data. Results are displayed with respect to underlying geology, as determined from Washington Department of Natural Resources (http://www.dnr.wa.gov/BusinessPermits/Pages/PubMaps.aspx) last accessed on 8/8/2014. (a) Pleistocene continental glacial drift, (b) Paleogene and Neogene volcanic rock, (c) Pleistocene and Holocene alluvium, (d) Paleogene and Neogene fragmental volcanic rock, (e) Paleocene to Miocene marine sedimentary rock, (f) Paleogene and Neogene intrusive rock. Refer to Fig. 12 and Table 2 for station locations.

Four out of five stations located on Pleistocene and Holocene alluvium show different HVSR peaks in comparison to the SSR results for the same earthquake, except for PAYL, which shows the same peaks at 1 and 3 Hz. The peak frequencies include 1, 1.5, 2, 3, 3.5, 5, and 6 Hz. Large peaks at 3.5 and 6 Hz are observed on the WISH HVSR plot, which is different with its flat response on SSR plot. LON and MNWA, which are located on Paleogene and Neogene fragmental volcanic rocks and Paleocene to Miocene marine sedimentary rock, respectively, show the same peak frequencies as seen on the SSR plots.

2. The 2014 Vancouver Island earthquake

Fig. 19 shows the HVSR plots from strong motion data from the 2014 Vancouver Island earthquake organized by site geology at the station location.

(a) Pleistocene continental glacial drift

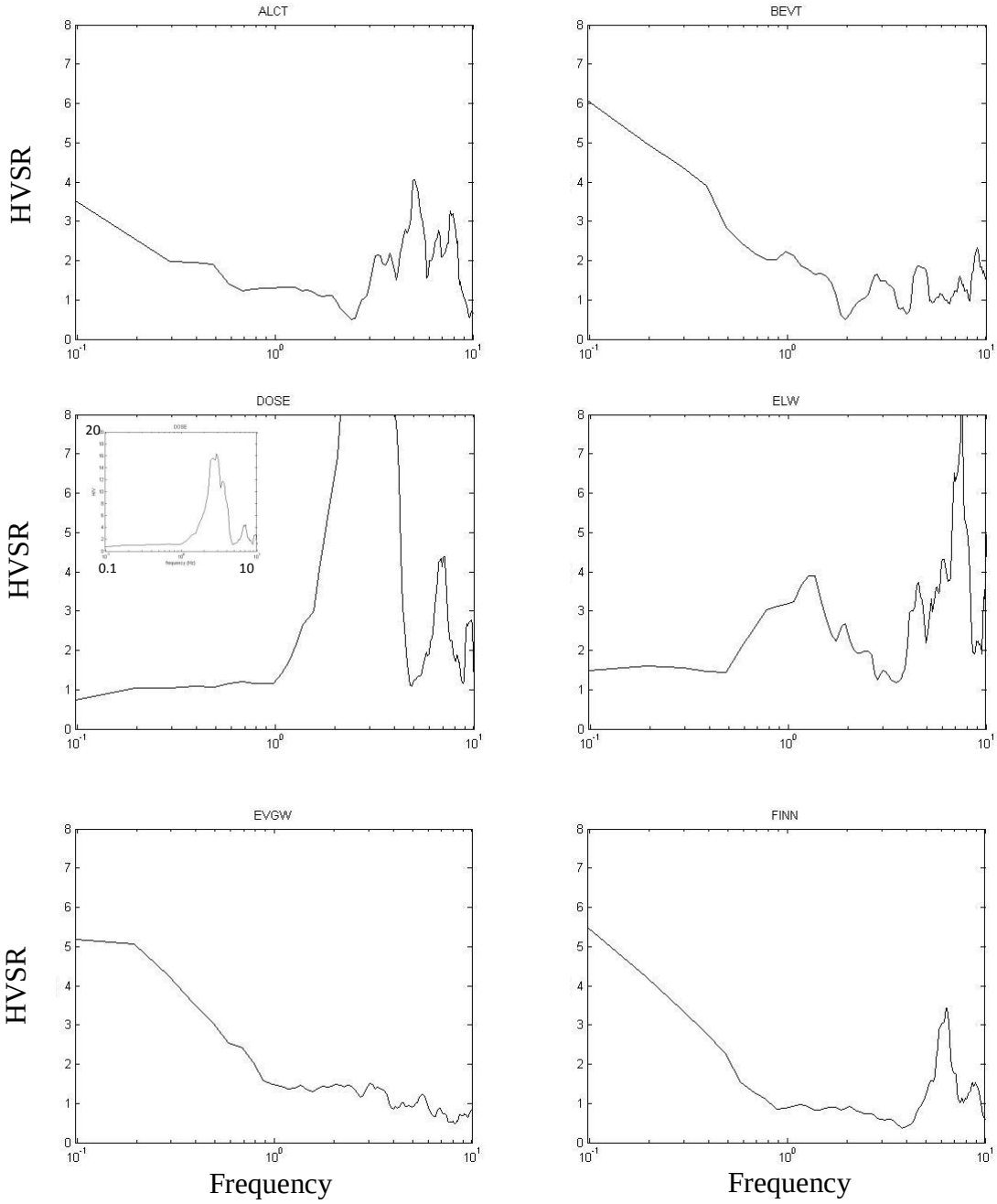

Pleistocene continental glacial drift (continued)

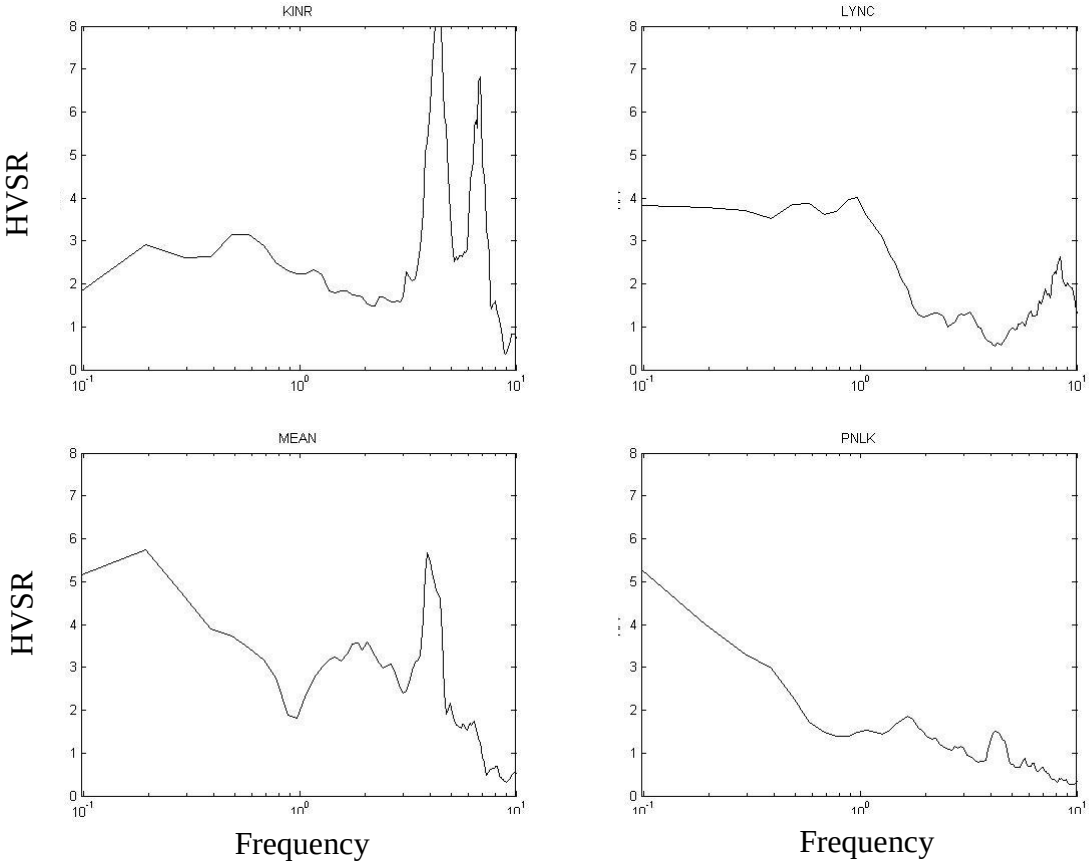

(b) Paleogene and Neogene volcanic rock

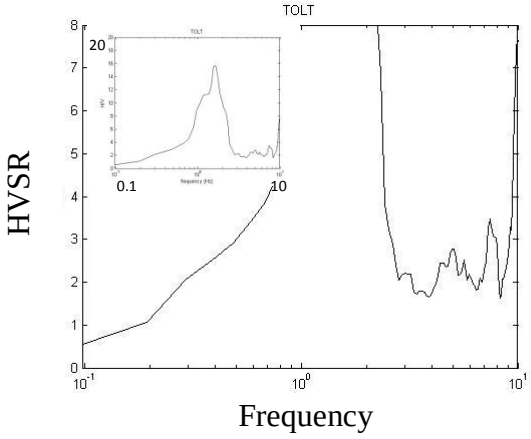

(c) Pleistocene and Holocene alluvium

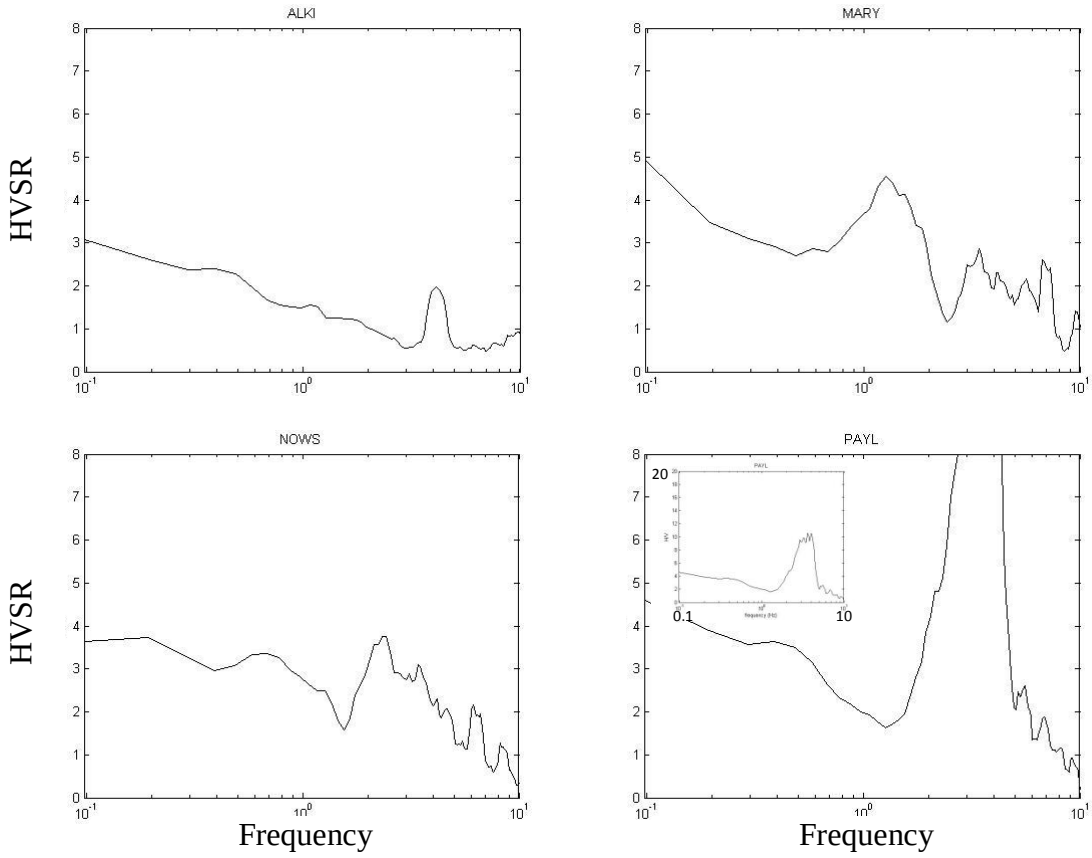

(d) Paleogene and Neogene intrusive rock

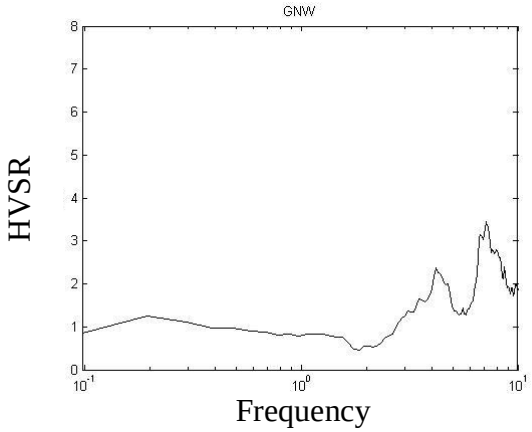

Fig. 19. HVSR results from the 2014 Vancouver Island earthquake strong motion data. Results are displayed with respect to underlying geology, as determined from Washington Department of Natural Resources (http://www.dnr.wa.gov/BusinessPermits/Pages/PubMaps.aspx) last accessed on 8/8/2014. (a) Pleistocene continental glacial drift, (b) Paleogene and Neogene volcanic rock, (c) Pleistocene and Holocene alluvium, (d) Paleogene and Neogene intrusive rock. Refer to Fig. 12 and Table 3 for station locations. The insets show the extent of larger.

Peaks at 7 Hz are observed at stations ALCT, BEVT, ELW, FINN, LYNC, and KINR. Other stations have peaks at 1, 2, 4, 5, and 9 Hz. TOLT shows consistent peaks relative to the previous event (2012 Queen Charlotte earthquake) with peaks at 1, 5, and 7 Hz.

Stations located on Pleistocene and Holocene alluvium show rather different results compared to the SSRs. Three of the stations share peaks at 2 to 3 Hz; two of them repeat the peak at 6 Hz.

3. The 2012 Vancouver Island earthquake

Fig. 20 shows the HVSR plots from broadband data from the 2012 Vancouver Island earthquake broadband data organized by site geology at the station location.

(a) Pleistocene continental glacial drift

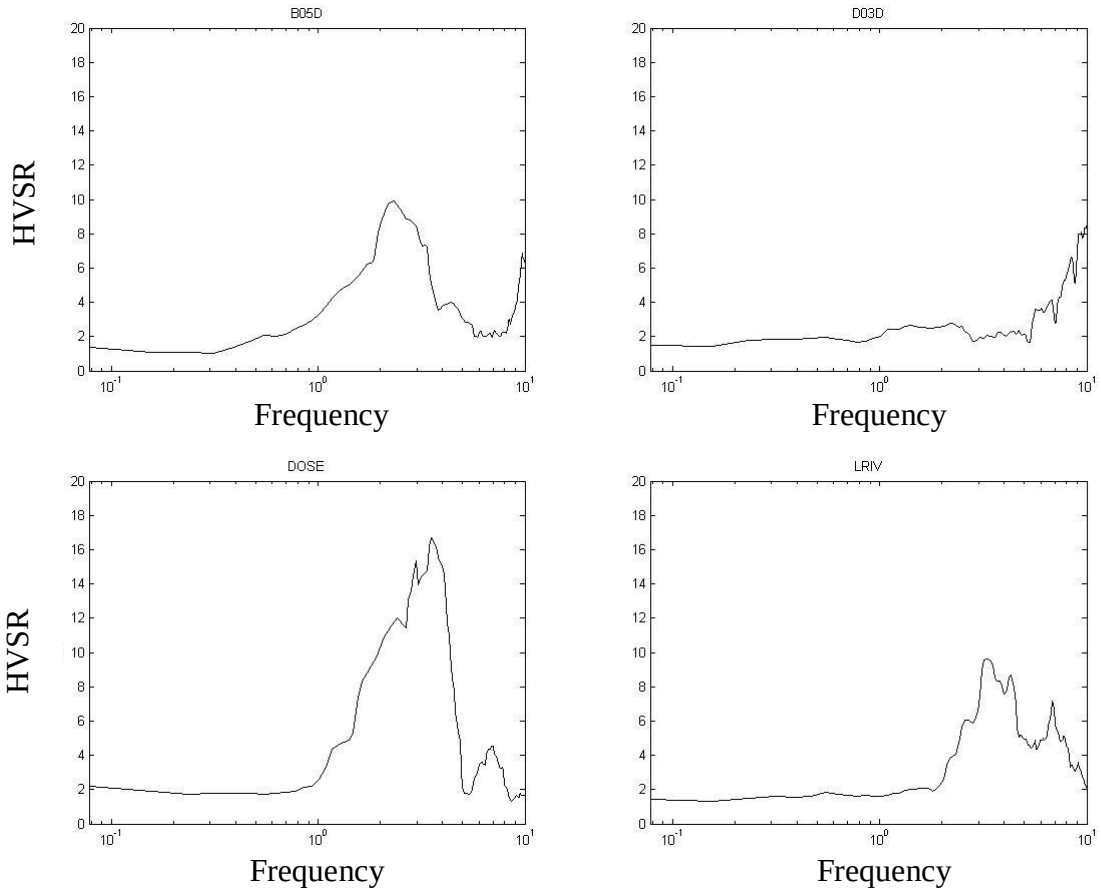

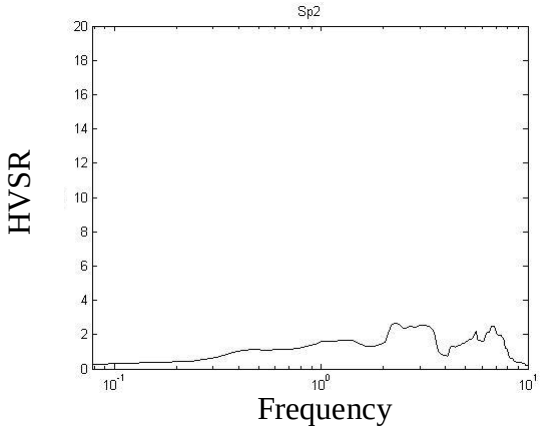

(b) Paleogene and Neogene volcanic rock

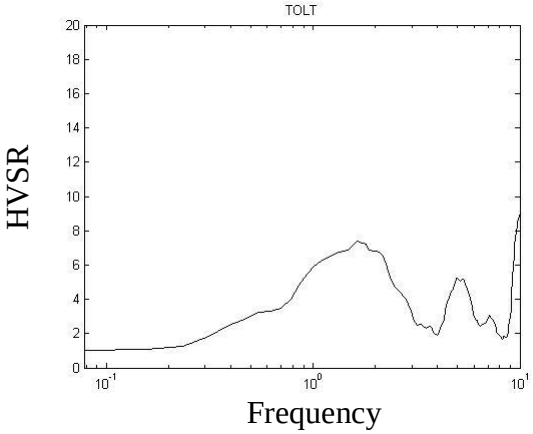

(c) Pleistocene and Holocene alluvium

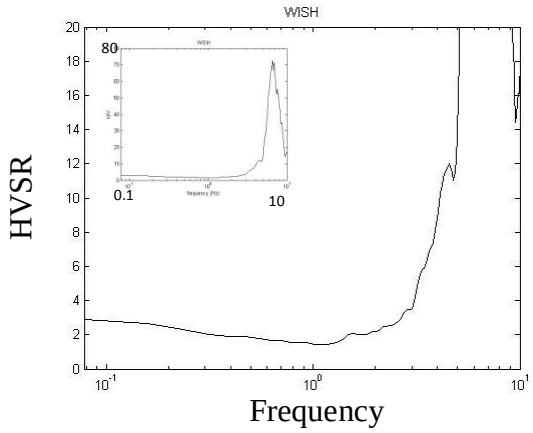

(d) Paleogene and Neogene intrusive rock

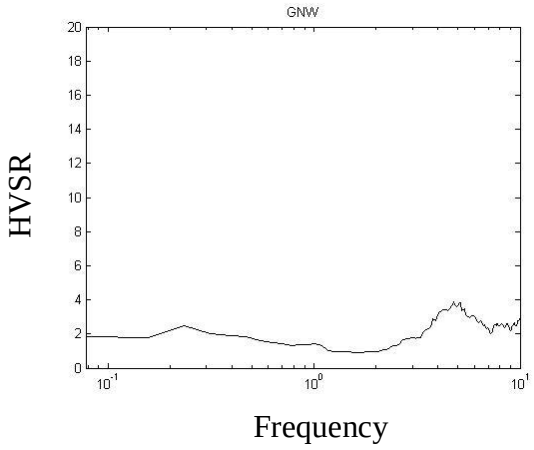

(e) Paleogene and Neogene fragmental volcanic rock

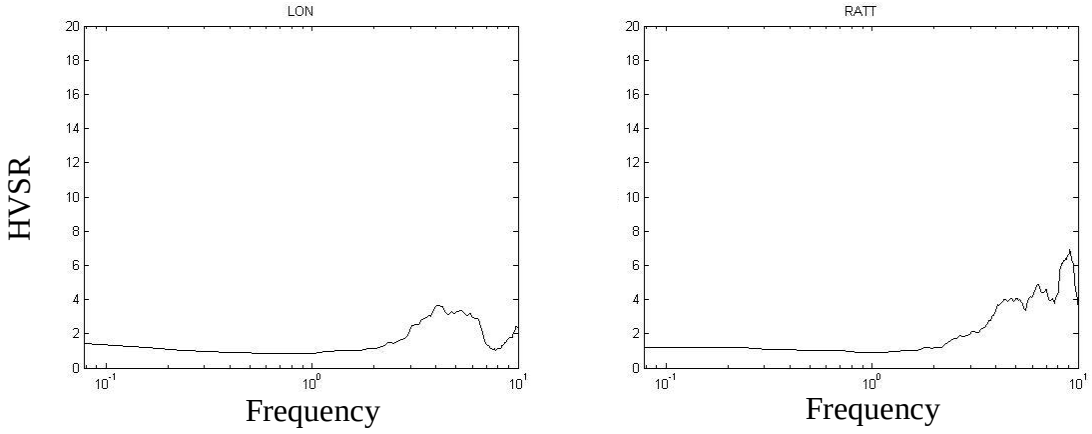

Fig. 20. HVSR results from the 2012 Vancouver Island earthquake broadband data. Results are displayed with respect to underlying geology, as determined from Washington Department of Natural Resources (http://www.dnr.wa.gov/BusinessPermits/Pages/PubMaps.aspx) last accessed on 8/8/2014. (a) Pleistocene continental glacial drift, (b) Paleogene and Neogene volcanic rock, (c) Pleistocene and Holocene alluvium, (d) Paleogene and Neogene intrusive rock, (e) Paleogene and Neogene fragmental volcanic rock. Refer to Fig. 11 and Table 1 for station locations. The insets show the extent of larger.

The HVSR plots from 2012 Vancouver Island are almost identical to their SSR plots at the stations located on Pleistocene continental glacial drift. The peaks are very consistent at 2-3 Hz. There are also peaks observed at higher frequencies (7, 8, and 10 Hz) that are also seen on the SSR plots. TOLT also shows a relatively similar result with peaks at 1.5, 5, and 10 Hz. WISH, which is located on Pleistocene and Holocene alluvium, shows a large peak at 8 Hz. GNW, indicates a flat response with a small peak at 5 Hz. The two stations, LON and RATT, that are located on Paleogene and Neogene fragmental volcanic rock show very similar results to their SSRs. Peaks are observed at 4 Hz for LON, and 5, 7, and 9 Hz for RATT.

To gain a better understanding of the site characteristics for each station, the frequencies observed were categorized in 5 groups, each representing a range of frequencies: 1 Hz (0-2 Hz), 3 Hz (2-4 Hz), 5 Hz (4-6 Hz), 7 Hz (6-8 Hz), and 9 Hz (8-10 Hz),as shown in Figures 21 to 35 and Tables 5 to 7. The tables list the maximum amplitude observed from SSR and HVSR analysis for each group at each station for each of the three earthquakes. At each peak frequency, low, moderate, and high relative amplification is shown in Figs. 21-24, with dot sizes proportional to the degree of amplification for a given earthquake. Fig. 21 shows the relative amplification from the 2012 Queen Charlotte earthquake at 1 Hz from HVSR and SSR data. The HVSR results suggest low to moderate amplification at most sites while the SSRs show moderate to high amplification at 1 Hz for the same geologic units. Stations ALCT, MARY, and MEAN, which show relatively high amplification, are located close to Seattle on the Pleistocene continental glacial drift.

Table 5. The maximum values (relative amplification) of SSR and HVSR from the 2012 Queen Charlotte earthquake at each station for different frequencies.

Station Name	1 Hz SSR	3 Hz SSR	5 Hz SSR	7 Hz SSR	9 Hz SSR	1 Hz HVSR	3 Hz HVSR	5 Hz HVSR	7 Hz HVSR	9 Hz HVSR
ALCT	80	15	9	9	40	2	1	2	1.3	1.6
ALKI	25	5	1	3	5	2.5	1	1.1	1.1	1.5
BABE	60	20	5	12	20	1.7	1.8	2.1	1.2	1.5
DOSE	20	180	30	20	5	3	20	5	2.2	1.5
EARN	32	18	5	4	4	2.2	1.8	1.9	1.4	1.2
ERW	33	18	2	3	4	2.7	3	2.2	1.5	2.3
EVCC	56	53	20	23	27	1.8	1.2	1	1.5	1.4
EVGW	48	20	5	5	9	3.7	1.3	1.1	1.1	1.1
FINN	20	17	10	5	7	1.9	1.2	2	2	1
LON	3	3	5	5	5	0.8	1.2	4	1.3	2
LRIV	5	10	9	3	2	1.6	3.6	7	2.6	2.1
LYNC	16	15	3	3	7	1.1	1.2	1.1	1	1.1
Mary	115	60	18	5	15	2.9	1.5	2.8	1	1.2
MEAN	95	65	18	30	90	4	2.9	1.3	1.3	0.9
MNWA	7	2	1	2	2	2.5	1.6	2.2	2.3	2
NIHS	44	49	22	20	23	1.5	2.6	2.2	2.1	2
NOWS	40	52	30	8	2	1.6	1.6	0.8	0.6	0.8
PAYL	90	90	30	8	10	3.5	6.5	2	0.2	0.1
PNLK	25	10	5	5	9	1.7	0.9	0.7	0.8	0.7
SP2	40	117	15	5	2	1.7	2.7	2.1	1.8	0.6
SQMD	45	40	12	5	2	2.6	2.2	1.6	0.8	0.9
SVOH	145	105	25	5	15	4.8	2.7	1.5	1.3	1.2

SWID	50	35	7	5	5	3.1	1.2	1.3	1.2	1.5
TOLT	52	53	20	10	6	10	4.5	2.2	3.3	3.3
WISH	3	2	3	6	7	1.1	4	12.5	19	12
GNW	-	-	-	-	-	0.9	1	1.4	1.5	1.7
RATT	-	-	-	-	-	1.5	3	3.2	4	5.2

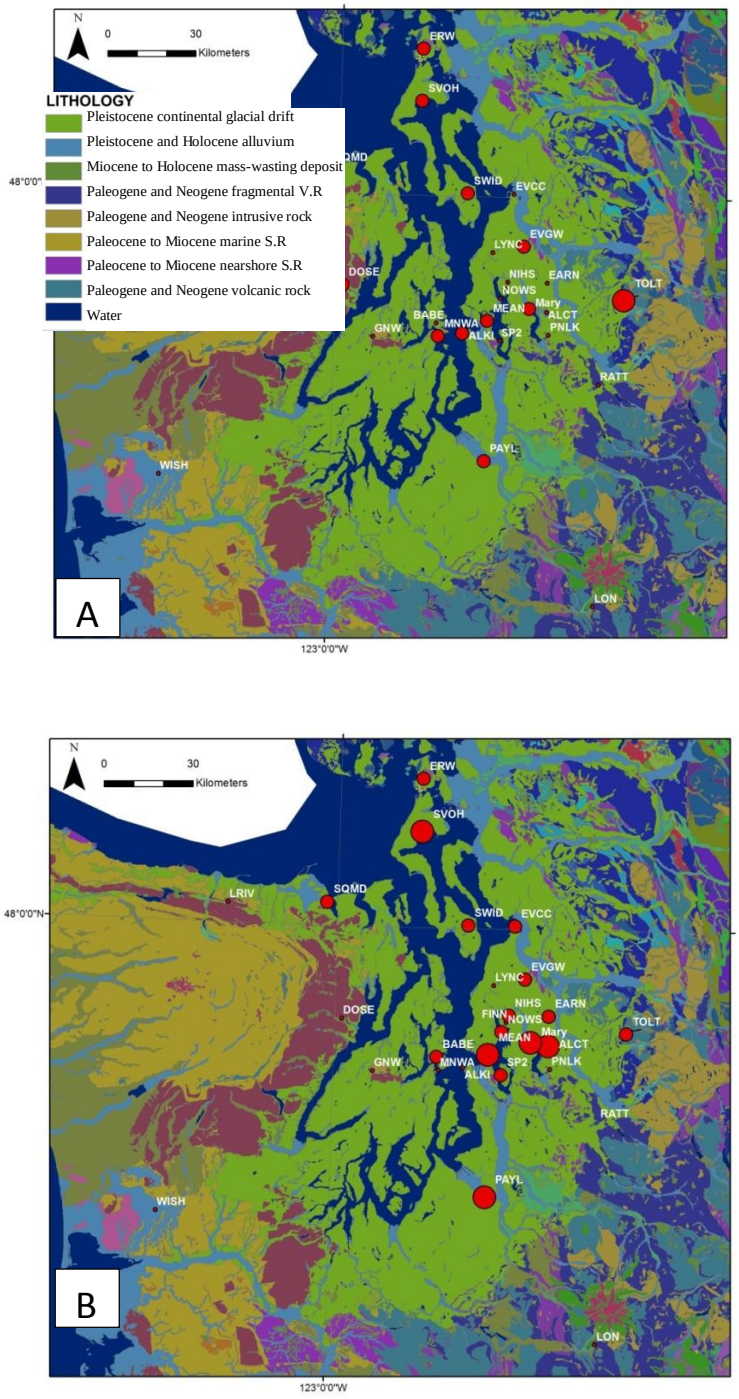

Fig. 21. Relative amplification in the 2012 Queen Charlotte earthquake (strong motion data) at 1 Hz from (A) HVSR and (B) SSR analyses overlain on geology map (from Washington Department of Natural Resources website [www.dnr.wa.gov] accessed 7/28/2014). Red dots are proportional to degree of amplification at the site (V.R and S.R represent volcanic and sedimentary rock, respectively).

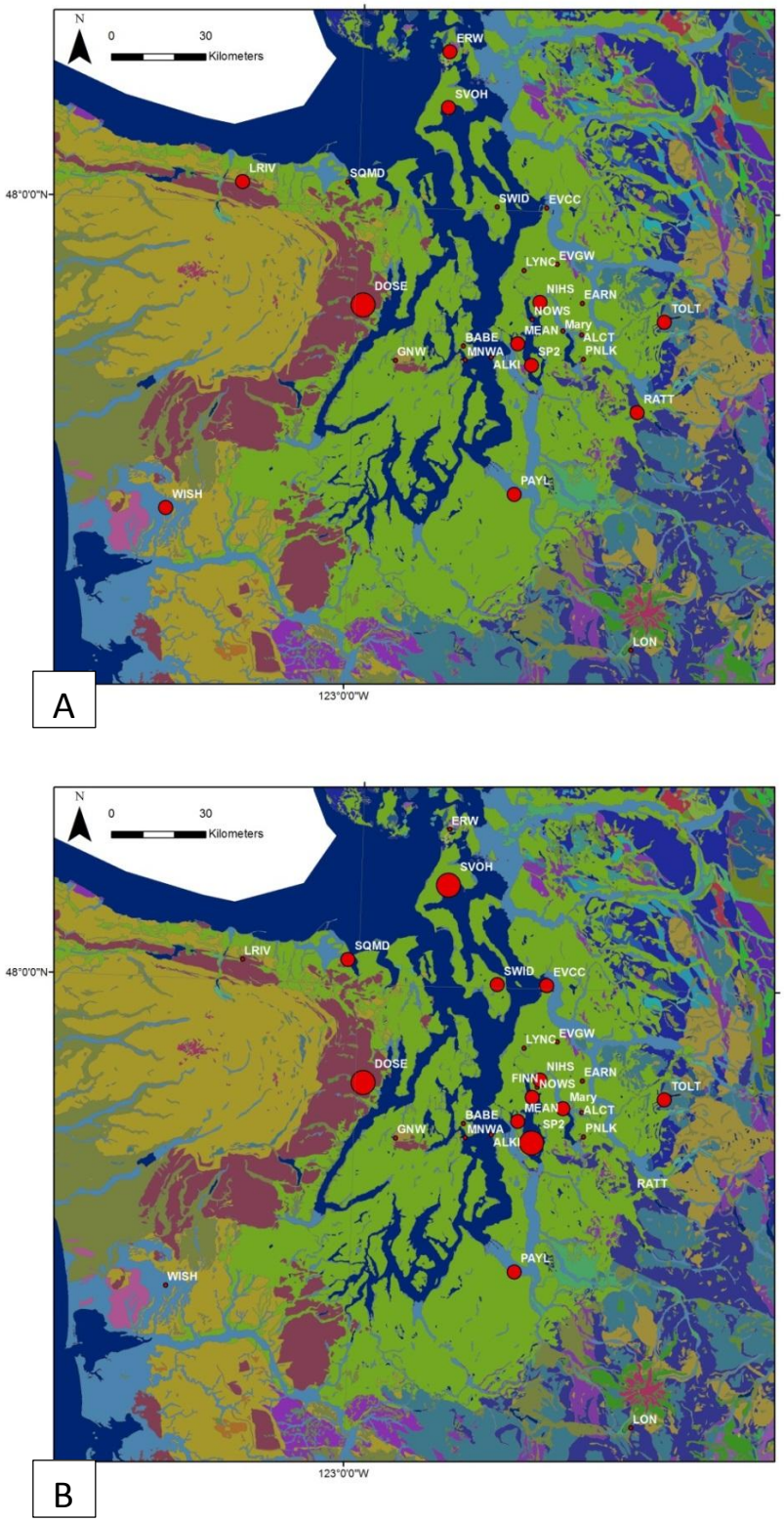

Fig. 22. Relative amplification in the 2012 Queen Charlotte earthquake (strong motion data) at 3 Hz from (A) HVSR and (B) SSR analyses overlain on geology map. Refer to Fig 21 for legend.

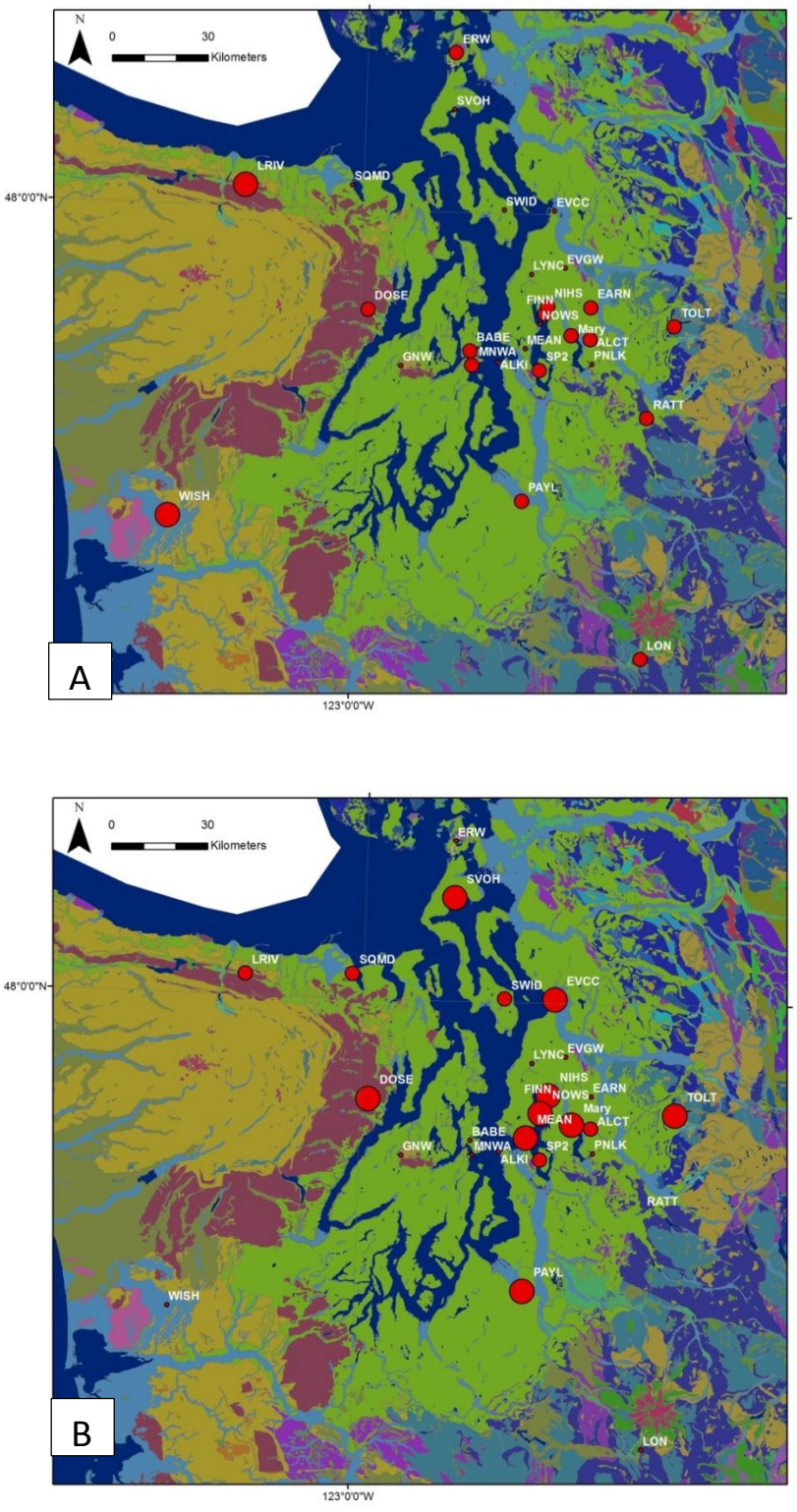

Fig. 23. Relative amplification in the 2012 Queen Charlotte earthquake (strong motion data) at 5 Hz from (A) HVSR and (B) SSR analyses overlain on geology map. Refer to Fig 21 for legend.

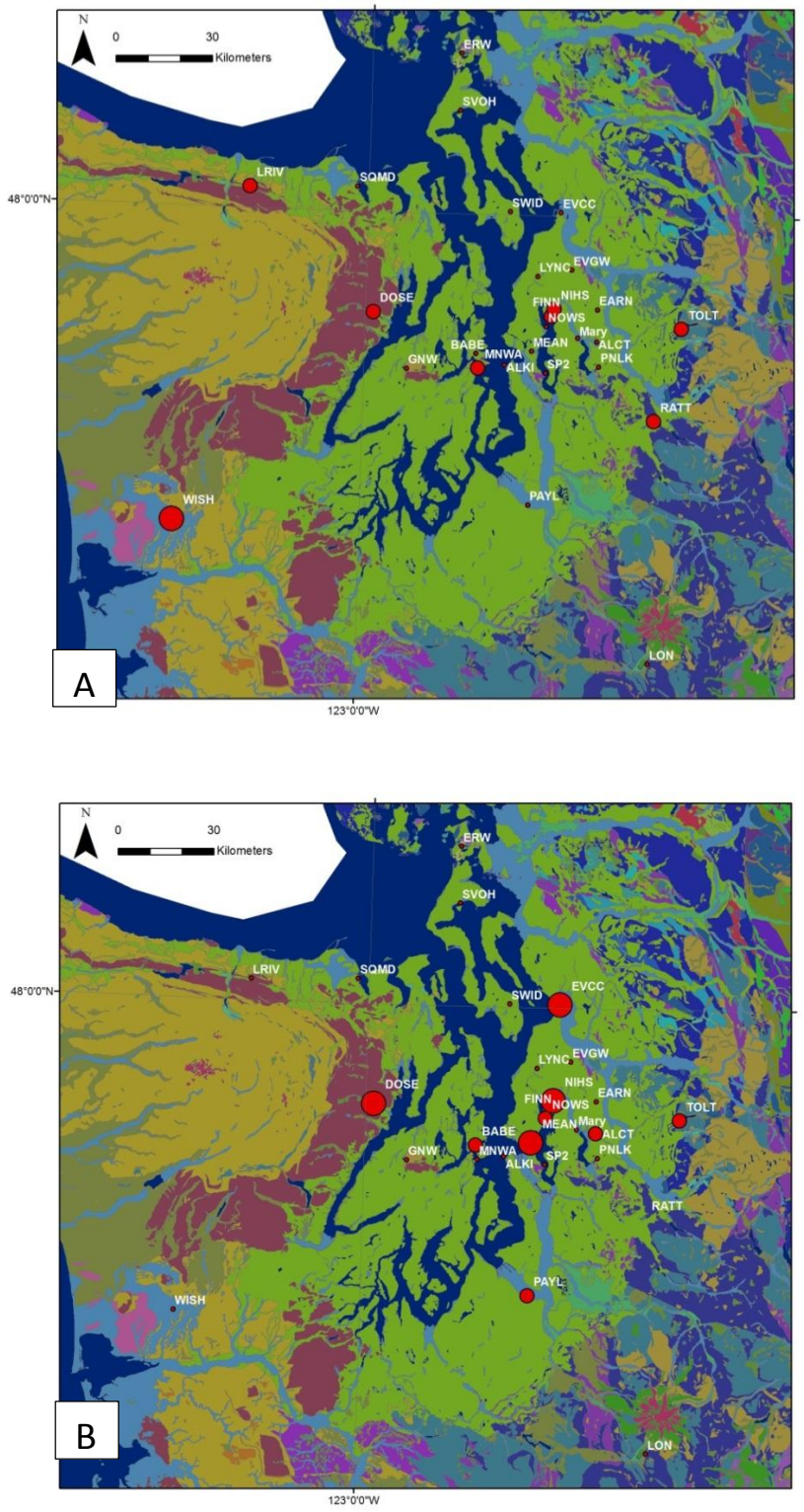

Fig.24. Relative amplification in the 2012 Queen Charlotte earthquake (strong motion data) at 7 Hz from (A) HVSR and (B) SSR analyses overlain on geology map. Refer to Fig 21 for legend.

According to the SSR results from the 2012 Queen Charlotte earthquake (Figs. 21-25), most of the stations located on Pleistocene continental glacial drift and the Pleistocene and Holocene alluvium have high amplification at low frequencies (0.5-3 Hz) and show a drop in amplification with increasing the frequency (> 5 Hz). Stations located on the Paleocene to Miocene marine sedimentary rock and the Paleogene and Neogene fragmental volcanic rock have low amplification at all frequencies.

The results from the 2012 Queen Charlotte earthquake HVSR data suggests high to moderate amplification at 1-5 Hz and low amplification at higher frequencies (> 6 Hz) at stations located on Pleistocene continental glacial drift. The analysis suggests similar results for the stations located on the Pleistocene and Holocene alluvium, with moderate amplification at 1-6 Hz and low amplification at higher frequencies (> 7 Hz). One of the stations however, shows high amplification at frequencies higher than 7 Hz. Stations on the Paleogene and Neogene fragmental volcanic rock have low amplification at 1-4 Hz and moderate to high amplification in higher frequencies (> 5 Hz). Relatively flat responses were observed at stations located on the Paleocene to Miocene marine sedimentary rock and the Paleogene and Neogene intrusive rock.

Despite the fact that there are a few stations with similar SSR and HVSR results, there are many inconsistencies between the two methods for the same stations.

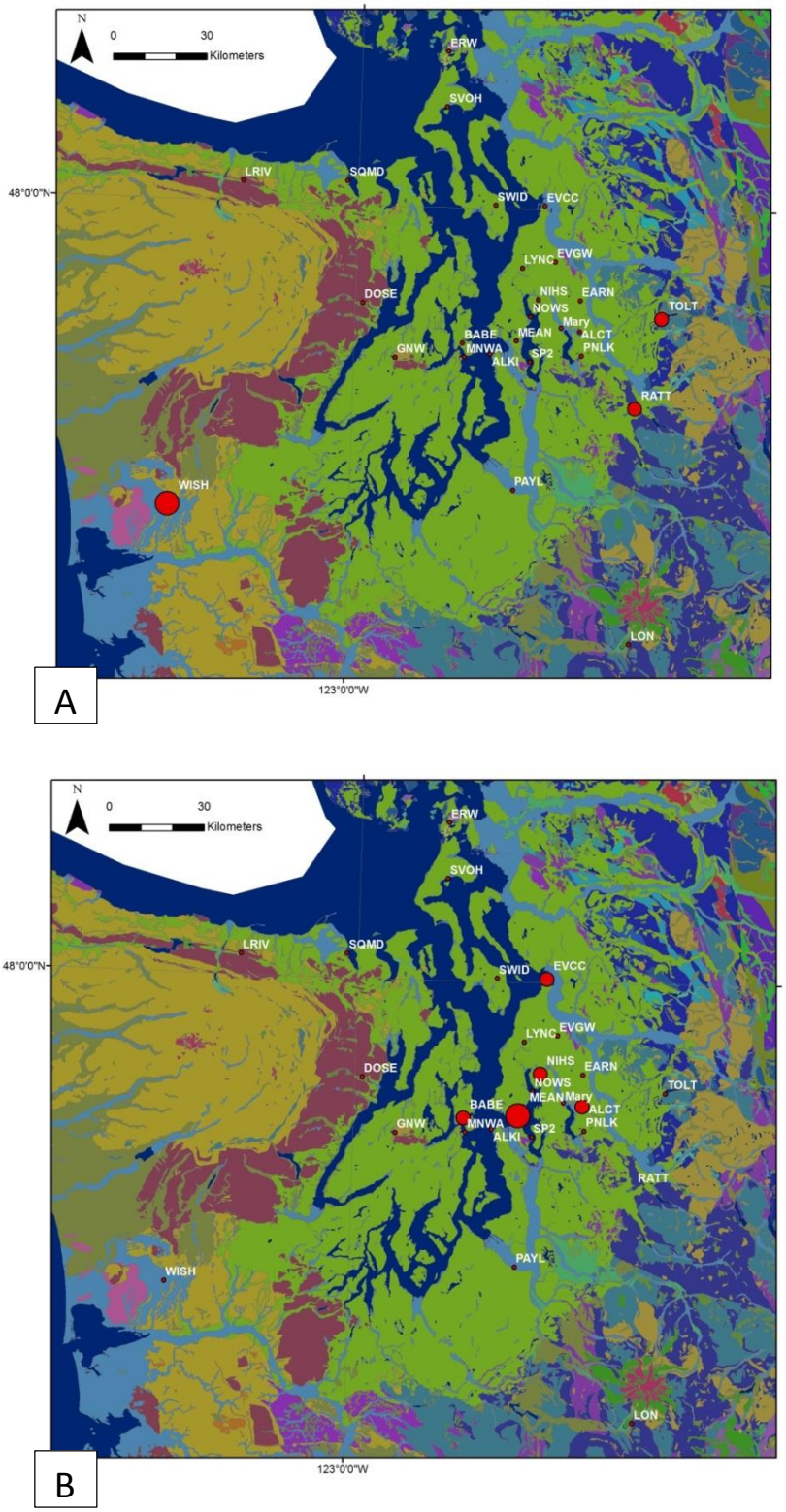

Fig.25. Relative amplification in the 2012 Queen Charlotte earthquake (strong motion data) at 9 Hz from (A) HVSR and (B) SSR analyses overlain on geology map. Refer to Fig. 21 for legend.

Table 6. The maximum values of SSR and HVSR from the 2012 Vancouver Island earthquake at each station in different frequencies.

Station	1 Hz SSR	3 Hz SSR	5 Hz SSR	7 Hz SSR	9 Hz SSR	1 Hz HVSR	3 Hz HVSR	5 Hz HVSR	7 Hz HVSR	9 Hz HVSR
B05D	30	67	35	12	8	7.5	10	4	2	6.8
D03D	2	3	2	2	3	2.5	2.5	3.5	5	8.5
DOSE	120	170	115	40	22	10	16.5	14	4.5	2
LON	1	1	2	1	2	1.5	3.5	3.7	3.2	2.3
LRIV	10	21	22	10	9	2	9.5	8.5	7	3.5
RATT	1	2	3	14	16	1.3	3	4	5	7
SP2	17	32	22	8	2	1.6	2.5	2.4	2.2	0.5
WISH	25	15	30	52	46	3	12	66	70	35
TOLT	122	130	175	100	135	7	7	5	3	9
GNW	-	-	-	-	-	2.5	2	4	3	3

According to the SSR results from the 2012 Vancouver Island earthquake, stations located on the Pleistocene continental glacial drift have high amplification at 2-3 Hz. Moderate to low amplification is observed on the high and low frequency ends at most of the stations. The station on the Pleistocene and Holocene alluvium shows high amplification at high frequencies (> 6 Hz) and moderate to low amplification at 1-5 Hz. High amplification is observed at 2-10 Hz on the Paleogene and Neogene volcanic rock. Stations located on the Paleogene and Neogene fragmental volcanic rock have moderate amplification at 8-10 Hz and low amplification in lower frequencies (< 7 Hz).

The HVSR results show high amplification at 2-4 Hz and moderate amplification at 7-10 Hz on the Pleistocene continental glacial drift (Figs. 26-30). The station located

on the Paleogene and Neogene volcanic rock has high amplification at 1-3 Hz and 9-10 Hz. High amplification is also observed at 6-10 Hz on the Pleistocene and Holocene alluvium. Stations located on the Paleogene and Neogene intrusive rock and Paleogene and Neogene fragmental volcanic rock have relatively low amplification in all frequencies. Generally, a comparison of the results from the HVSR and the SSR analyses show that they are very consistent for the 2012 Vancouver Island earthquake.

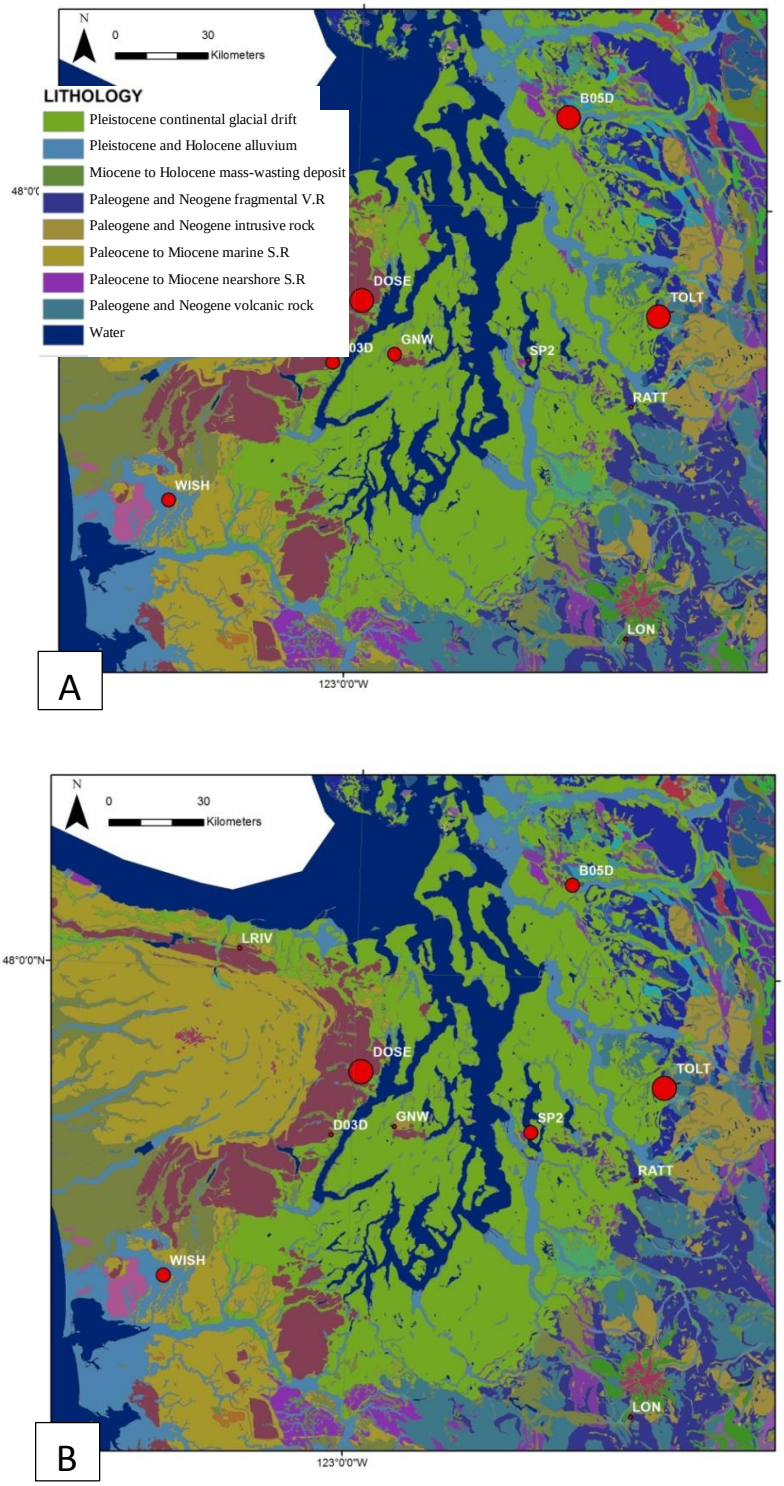

Fig. 26. Relative amplification in the 2012 Vancouver Island earthquake at 1Hz from (A) HVSR and (B) SSR analyses overlain on geology map(V.R and S.R represent volcanic and sedimentary rock, respectively).

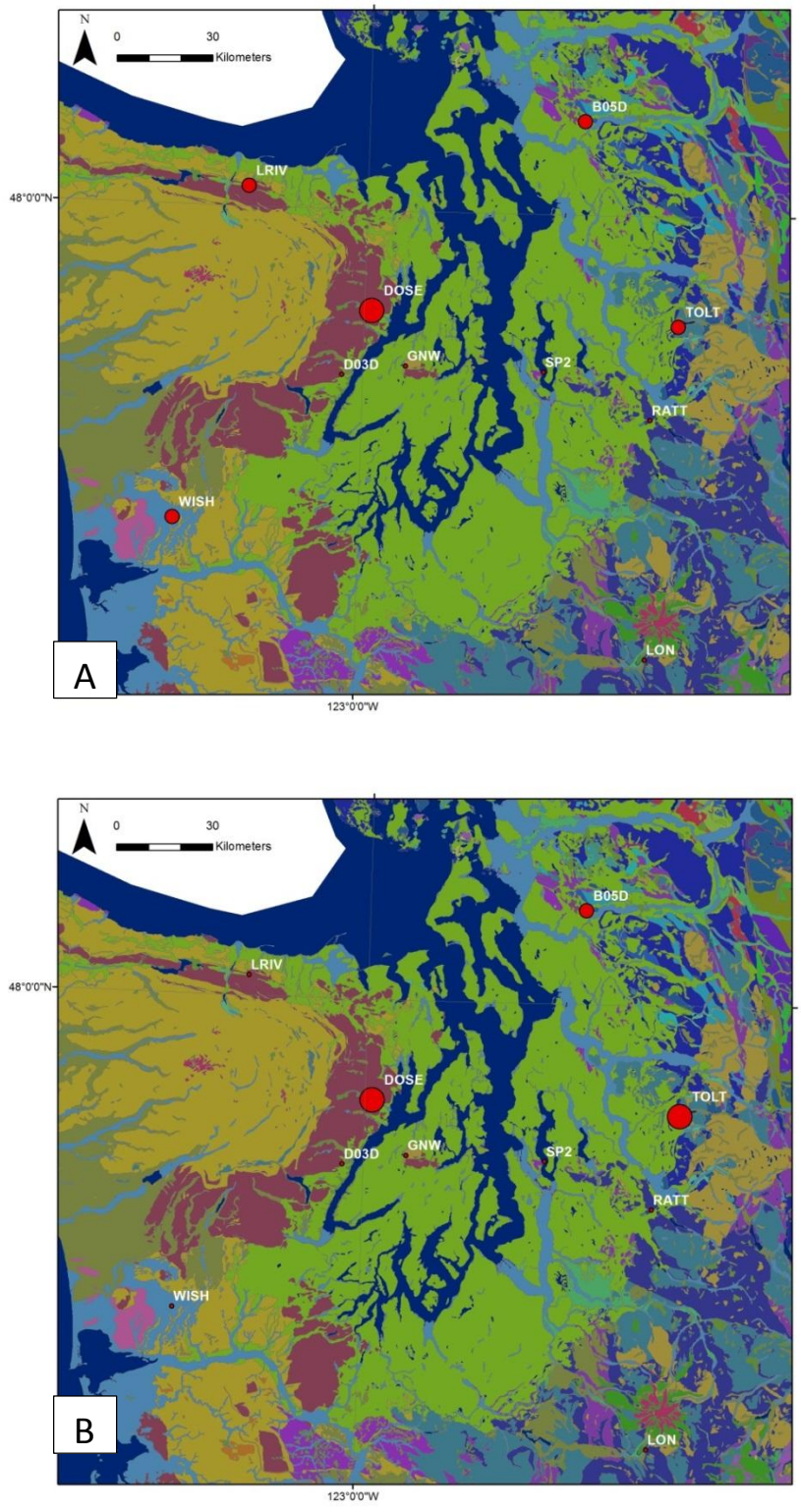

Fig. 27. Relative amplification in the 2012 Vancouver Island earthquake (broadband data) at 3 Hz from (A) HVSR and (B) SSR analyses overlain on geology map. Refer to Fig. 26 for legend.

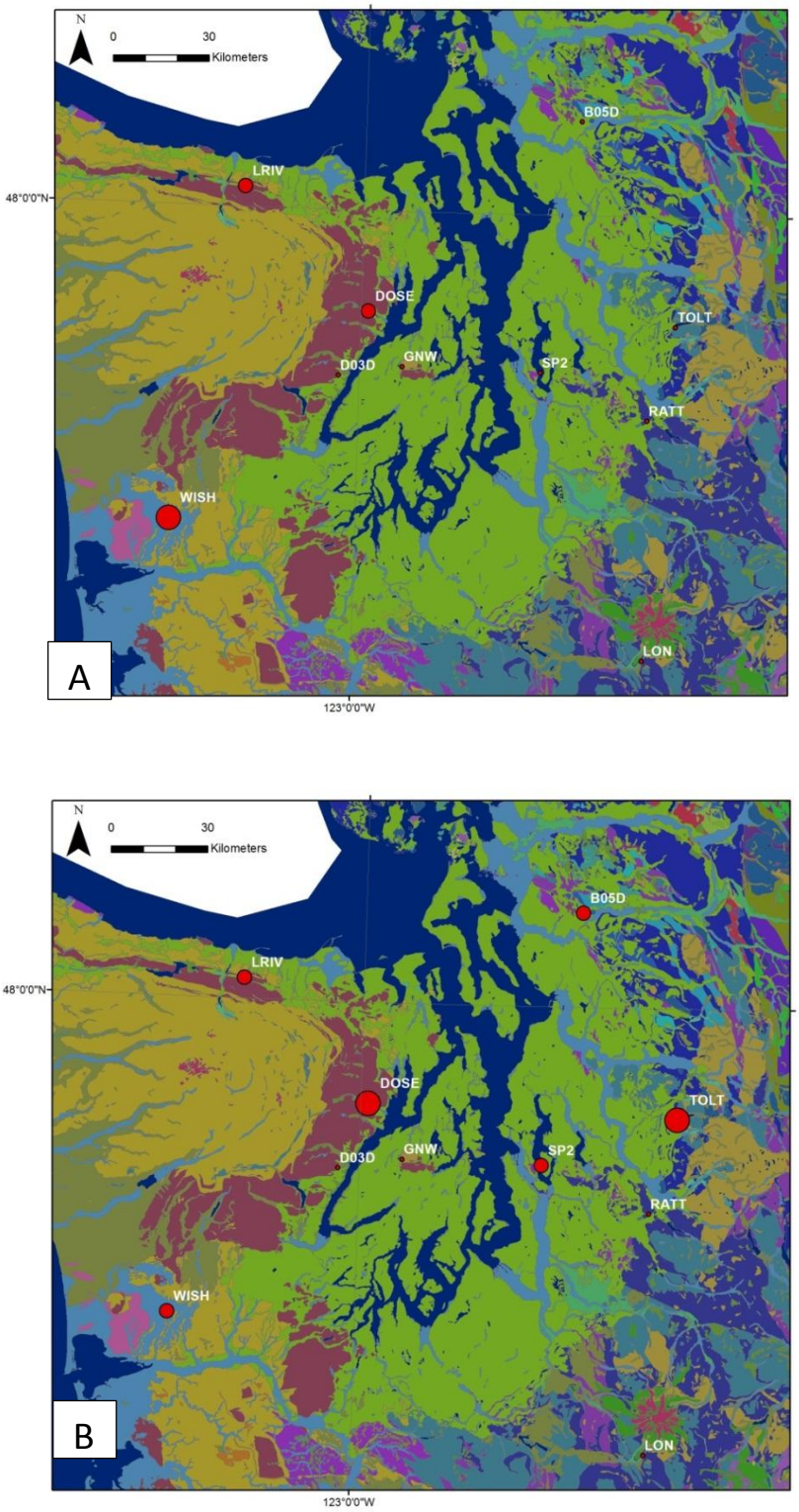

Fig. 28. Relative amplification in the 2012 Vancouver Island earthquake (broadband data) at 5 Hz from (A) HVSR and (B) SSR analyses overlain on geology map. Refer to Fig. 26 for legend.

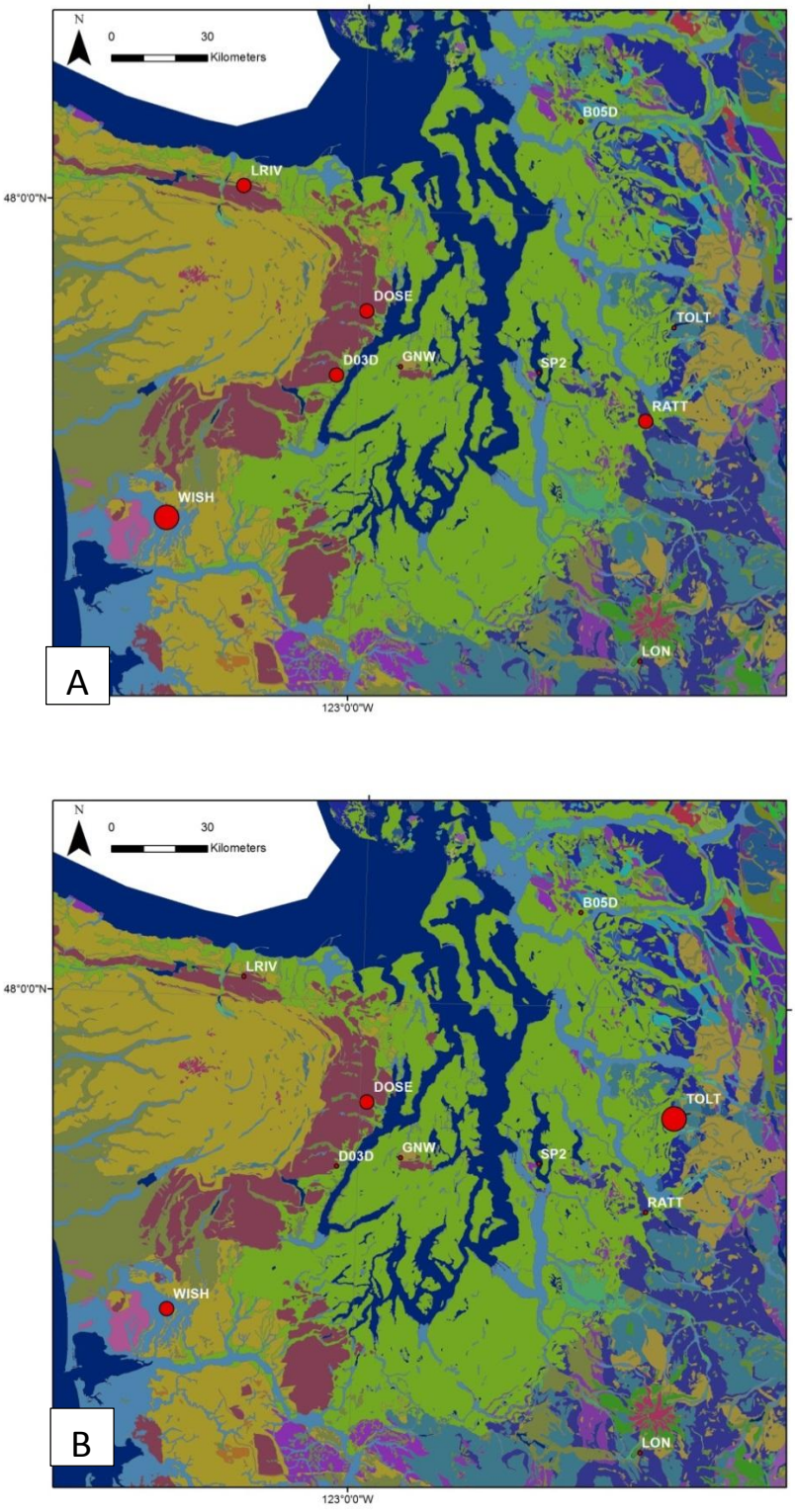

Fig. 29. Relative amplification in the 2012 Vancouver Island earthquake (broadband data) at 7 Hz from (A) HVSR and (B) SSR analyses overlain on geology map. Refer to Fig. 26 for legend.

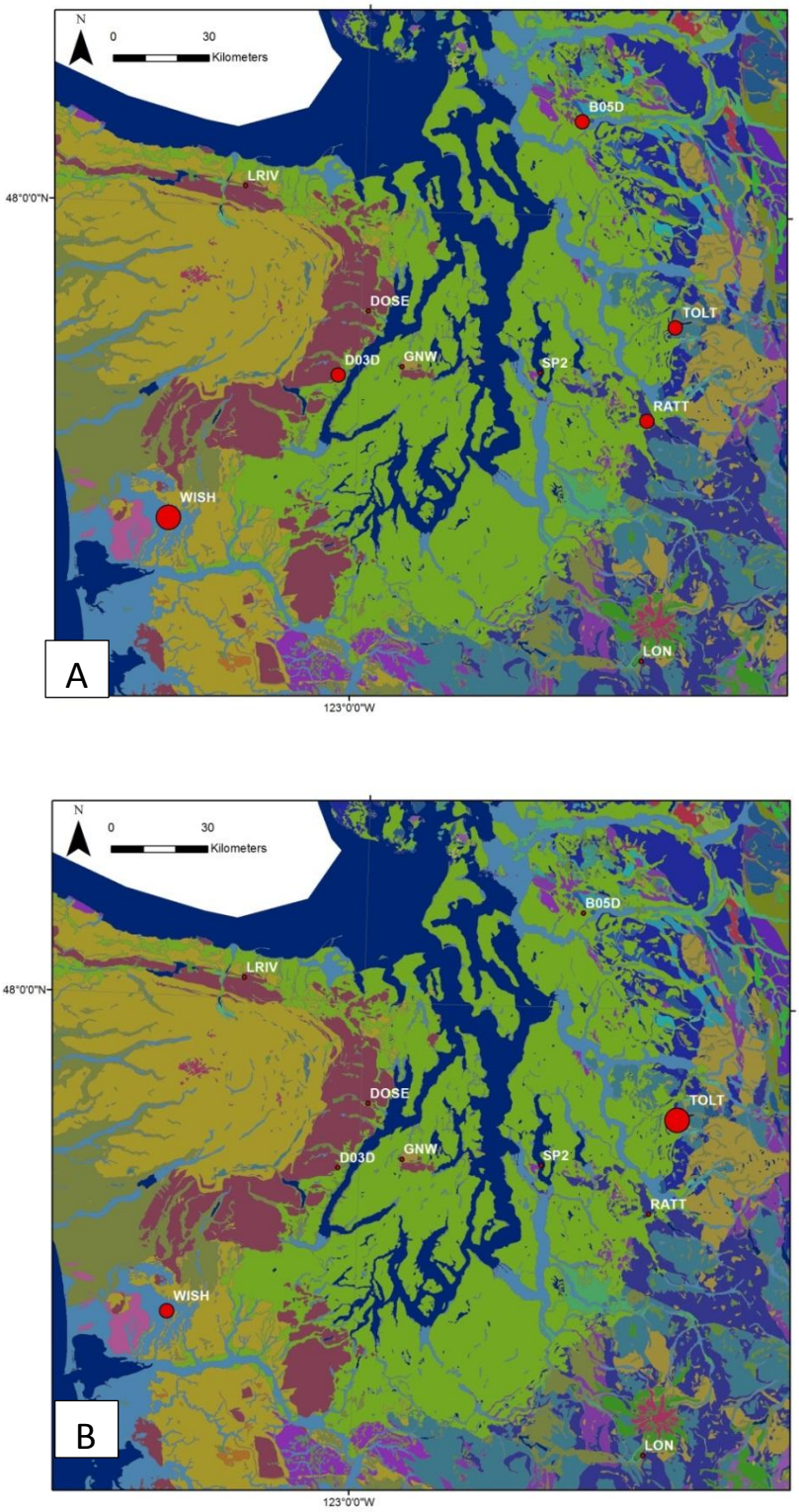

Fig. 30. Relative amplification in the 2012 Vancouver Island earthquake (broadband data) at 9 Hz from (A) HVSR and (B) SSR analyses overlain on geology map. Refer to Fig. 26 for legend.

According to the SSR results from the 2014 Vancouver Island earthquake (Figs. 31-35), the stations located on the Pleistocene continental glacial drift have high amplification at 0-1.5 Hz and moderate amplification at 6-8 Hz. However, 3 out of 11 stations show low amplification at 0-1 Hz. High to moderate amplification at 1.5-10 Hz is observed on the Paleogene and Neogene volcanic rock. Stations located on the Pleistocene and Holocene alluvium have high amplification at 0.6-1.5 Hz and moderate to low at 5-10 Hz.

Table 7. The maximum values of SSR and HVSR from the 2014 Vancouver Island earthquake at each station in different frequencies.

Station Name	1 Hz SSR	3 Hz SSR	5 Hz SSR	7 Hz SSR	9 Hz SSR	1 Hz HVSR	3 Hz HVSR	5 Hz HVSR	7 Hz HVSR	9 Hz HVSR
ALCT	22	13	17	14	8	3.5	2	4	3.3	2
ALKI	20	5	2	1	2	3	2	2	0.5	0.9
BEVT	65	14	13	8	16	6	1.7	1.9	1.6	2.3
DOSE	35	270	170	150	42	6.5	16.5	12	4.2	2.2
ELW	6	12	21	25	23	4	2	3.7	8	4
EVGW	220	60	42	30	20	5.1	1.5	1.2	0.8	0.8
FINN	18	13	18	4	2	5.5	1	3	3.5	1.5
KINR	45	53	75	30	18	3	6	8.5	6.8	1.5
LYNC	50	12	4	6	5	4	1.5	1.2	2	2.6
MARY	115	50	30	12	22	4.9	2.8	2	2.5	1.3
MEAN	60	50	35	12	165	5.7	5.5	5.5	1.7	0.7
NOWS	50	40	16	4	2	3.8	3.8	2	2.1	1.2

PAYL	51	57	36	43	30	4.5	10.5	10.5	1.8	1.1
PNLK	460	165	205	150	210	5.2	1.3	1.4	0.7	0.3
TOLT	62	38	40	47	44	16	10	2.6	3.5	7.5
CDMR	5	21	15	19	10	1.2	1.2	1.2	1.5	1.3
GNW	-	-	-	-	-	1.2	1.5	2.2	3.4	2.5

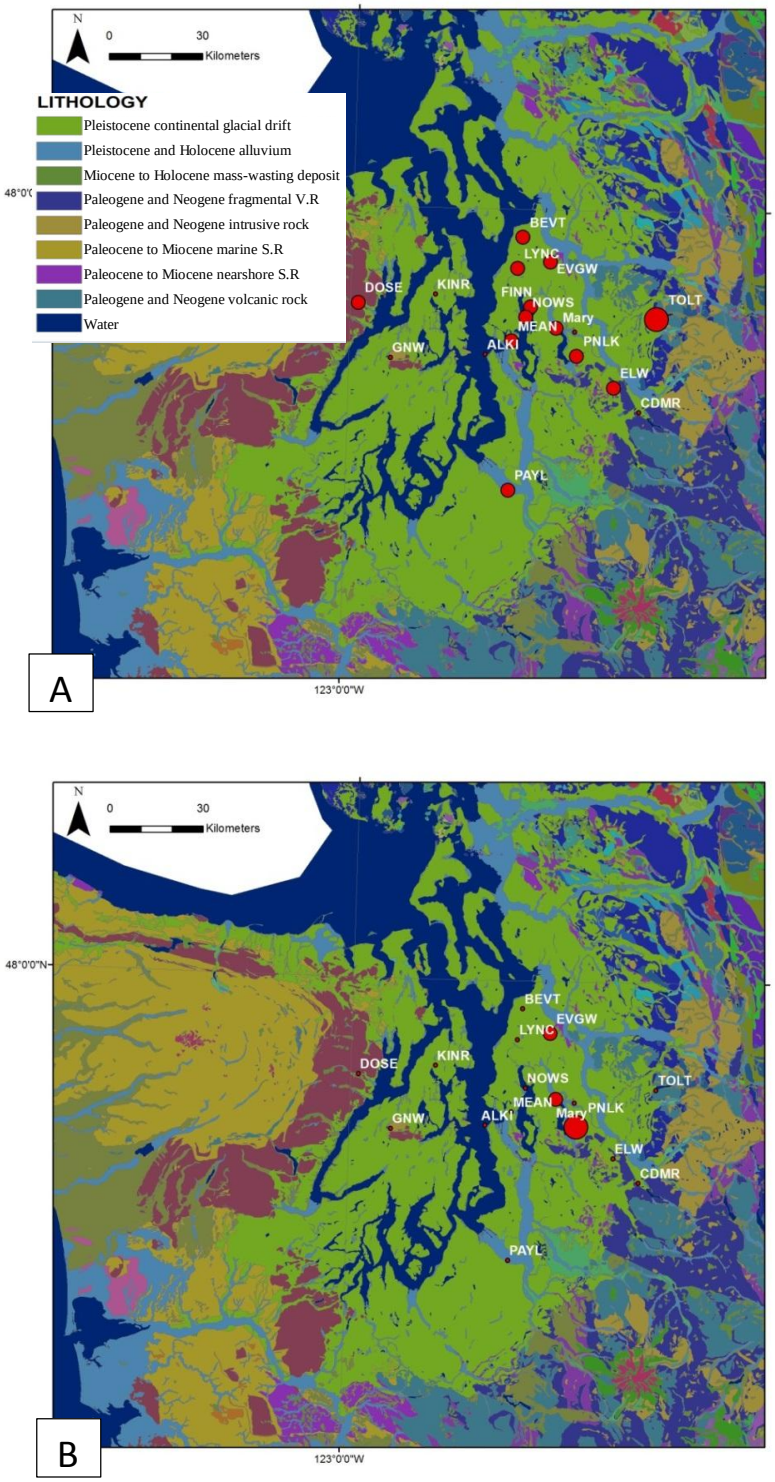

Fig. 31. Relative amplification in the 2014 Vancouver Island earthquake at 1Hz from (A) HVSR and (B) SSR analyses overlain on geology map(V.R and S.R represent volcanic and sedimentary rock, respectively).

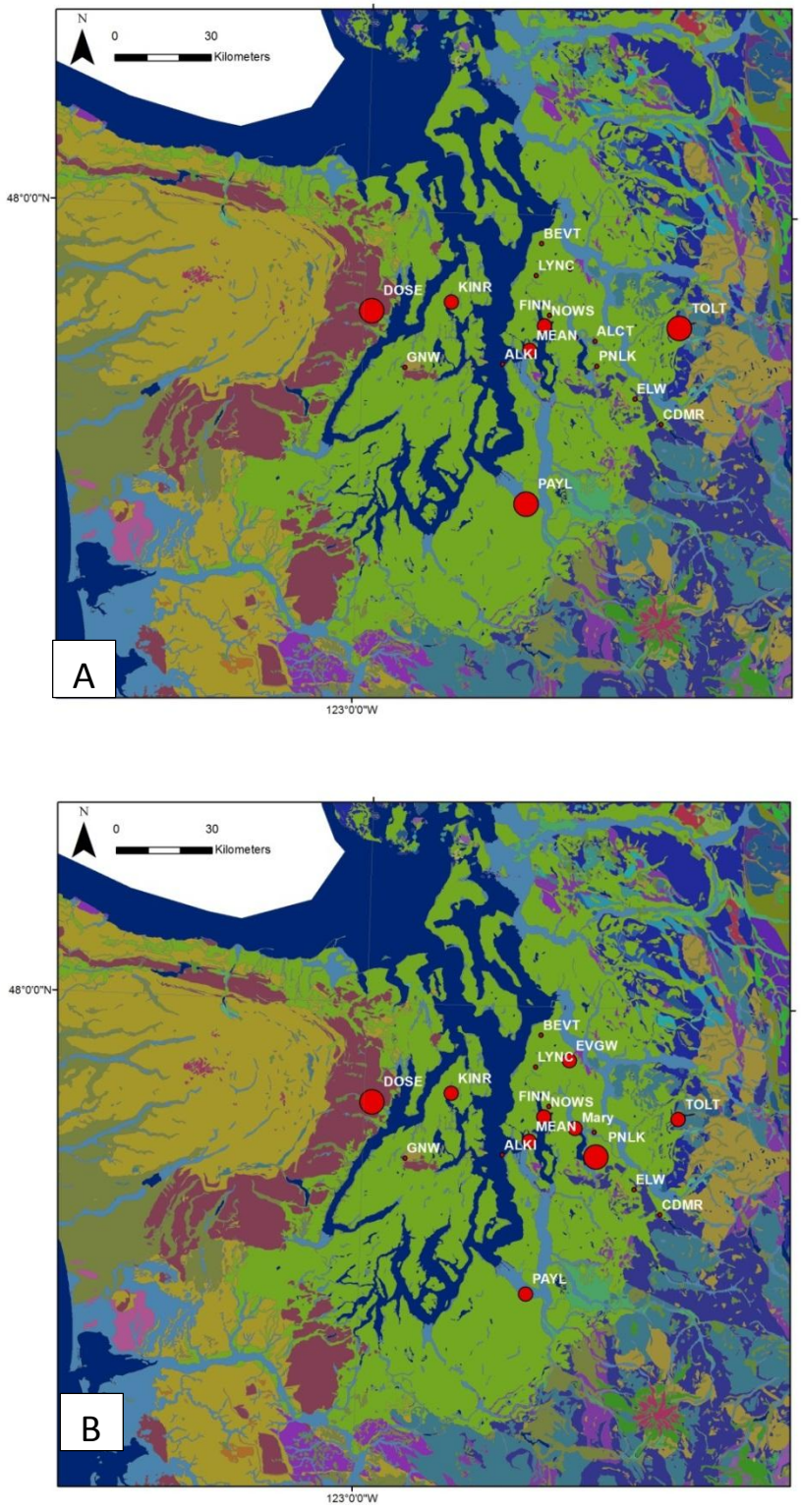

Fig. 32. Relative amplification in the 2014 Vancouver Island earthquake (strong motion data) at 3 Hz from (A) HVSR and (B) SSR analyses overlain on geology map. Refer to Fig. 31 for legend.

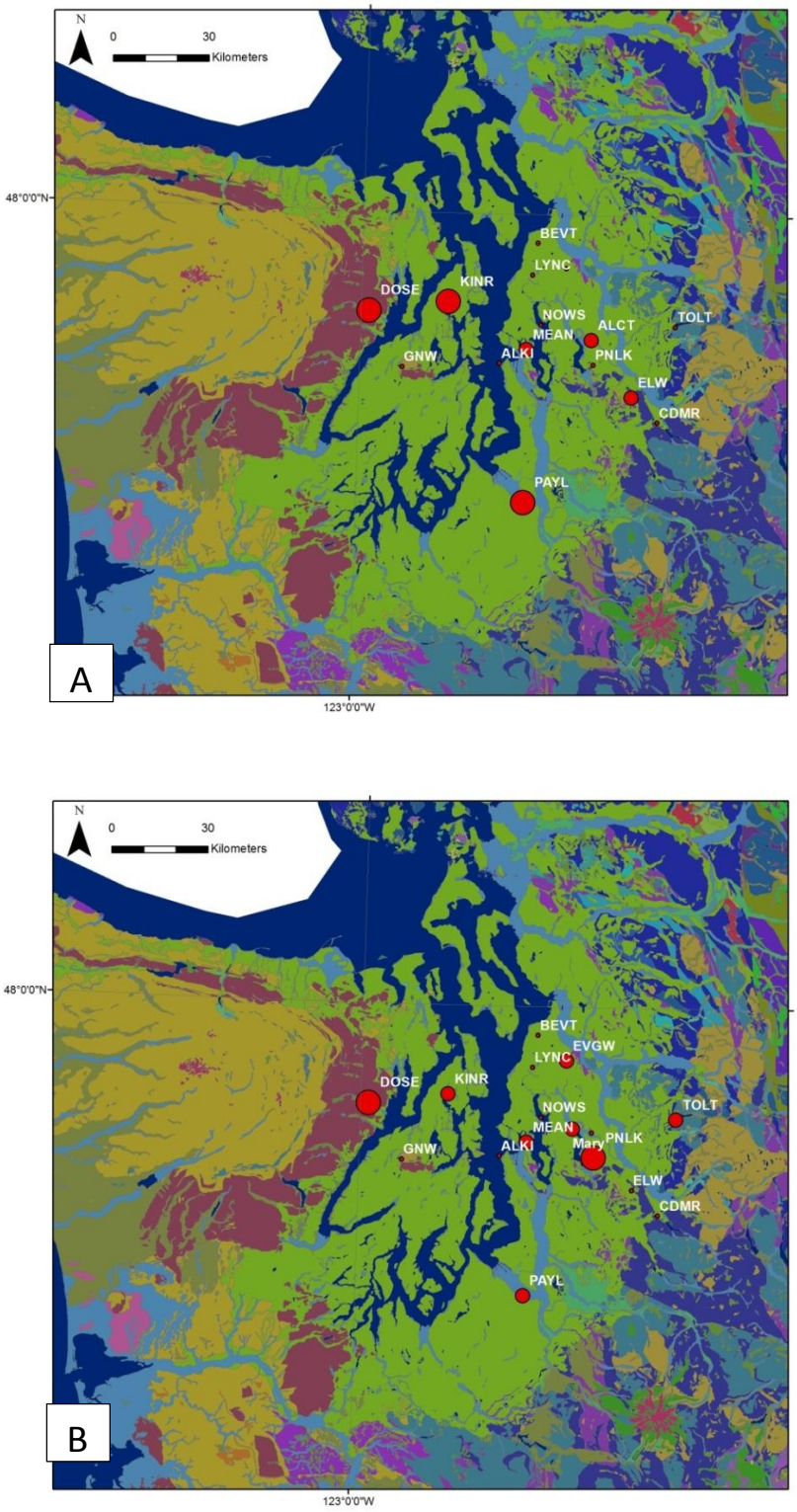

Fig. 33. Relative amplification in the 2014 Vancouver Island earthquake (strong motion data) at 5 Hz from (A) HVSR and (B) SSR analyses overlain on geology map. Refer to Fig. 31 for legend.

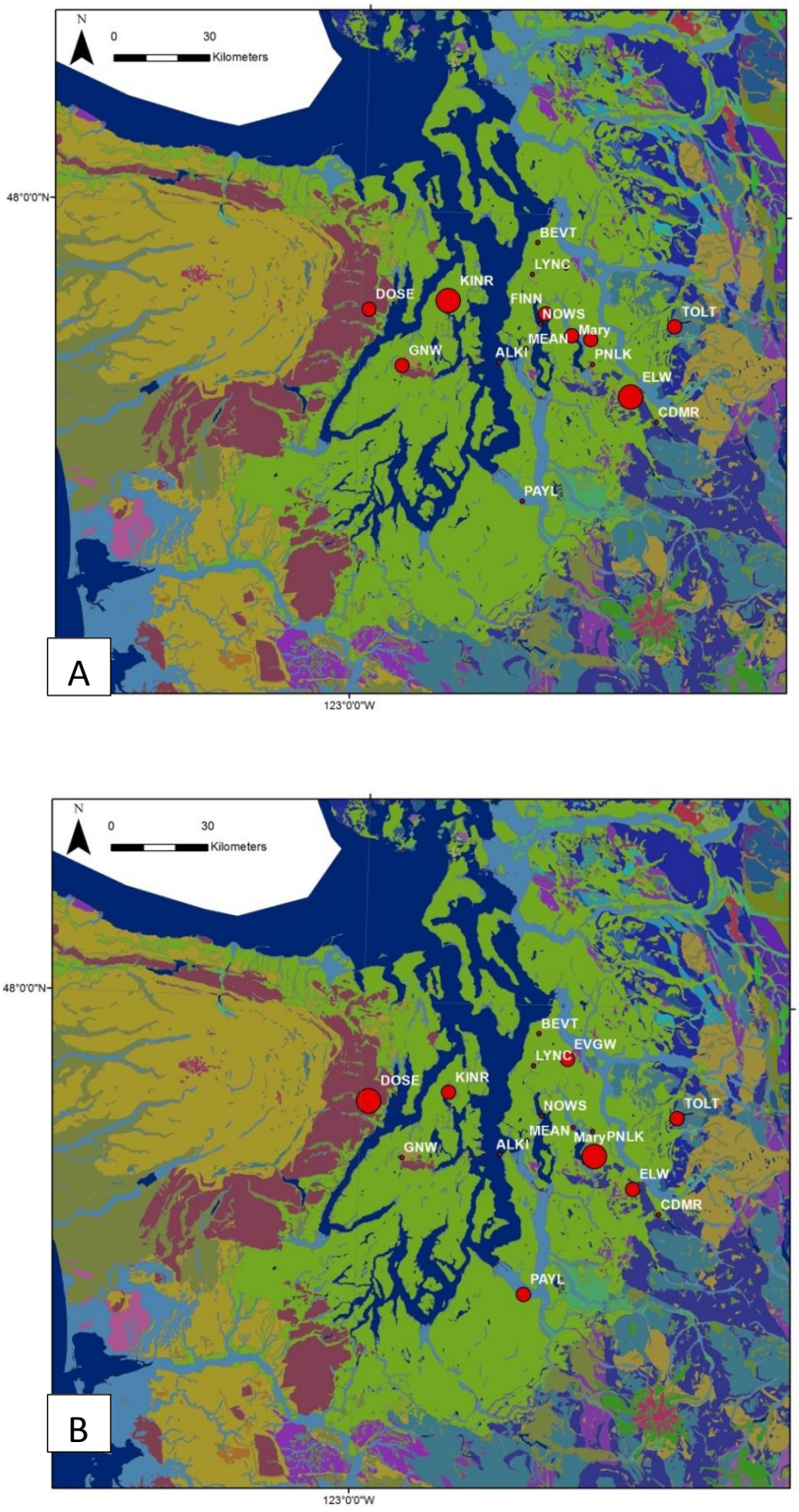

Fig. 34. Relative amplification in the 2014 Vancouver Island earthquake (strong motion data) at 7 Hz from (A) HVSR and (B) SSR analyses overlain on geology map. Refer to Fig. 31 for legend.

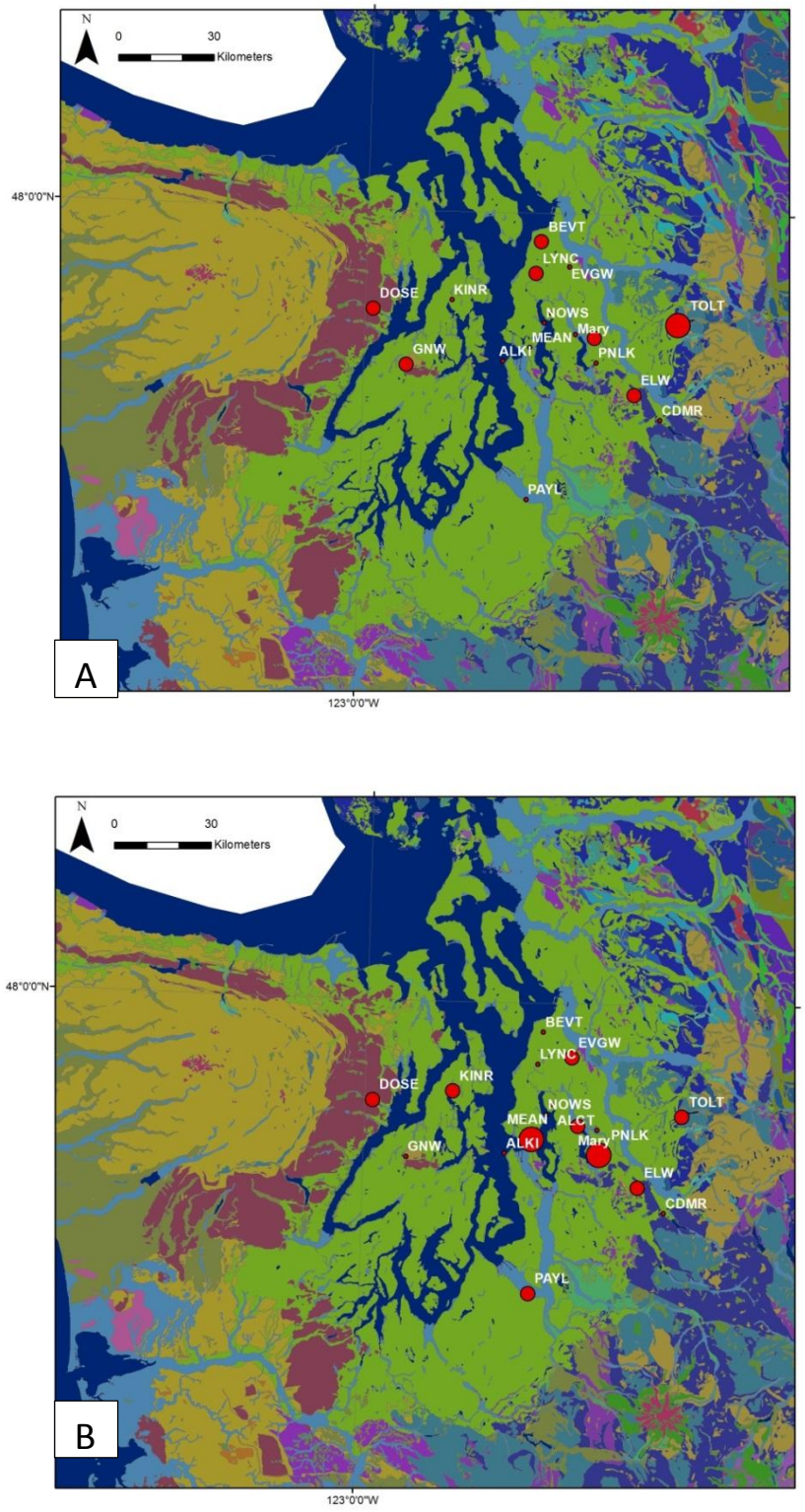

Fig. 35. Relative amplification in the 2014 Vancouver Island earthquake (strong motion data) at 9 Hz from (A) HVSR and (B) SSR analyses overlain on geology map. Refer to Fig. 31 for legend.

For the 2014 earthquake, 6 out of 9 stations located on the Pleistocene continental glacial drift show relatively similar HVSR responses compared to the ones from SSRs. They have high amplification at 0-1.5 Hz and 5-8 Hz. Likewise, the station on the Paleogene and Neogene volcanic rock, has identical HVSR results compared to the SSR, showing high amplification at 1-2 Hz and moderate at 3-10 Hz. Only half of the stations on the Pleistocene and Holocene alluvium have similar HVSR and SSR results. In spite of some inconsistencies between the results, they all agree on high amplification at 0-1 Hz and moderate to low amplification at 5-10 Hz. The station located on the Paleogene and Neogene intrusive rock has relatively low amplification at 0-3 Hz and moderate at 4-8 Hz. In general, 8 out of 16 stations have similar HVSR and SSR results in the 2014 Vancouver Island earthquake. 12 out of 24 in the 2012 Queen Charlotte earthquake, and 7 out of 8 in the 2012 Vancouver Island earthquake show similar results. Totally, 27 out of 48 (56%) of the stations have similar HVSR and SSR results for this earthquake.

Seattle Liquefaction Array (SLA)

SLA is a strong motion station that includes 4 accelerometers at different depths from the surface (0 m, 5.4 m, 44.9 m, and 56.4 m). Shear-wave velocities at the site linearly increase from ~100 m/s at the surface to ~250 m/s at a depth of 51 m. The deepest accelerometer (56.4 m) is in material with Vs of approximately 400 m/s, which is in Pleistocene and Holocene Pre-Vashon Deposits, with a transition zone above (51 m - 54 m) to material with Vs of 250 m/s (written communication, Jamison Steidl). The P wave velocity at the depth of 2.5 km is estimated to be 2.5-3.5 km/s based on the

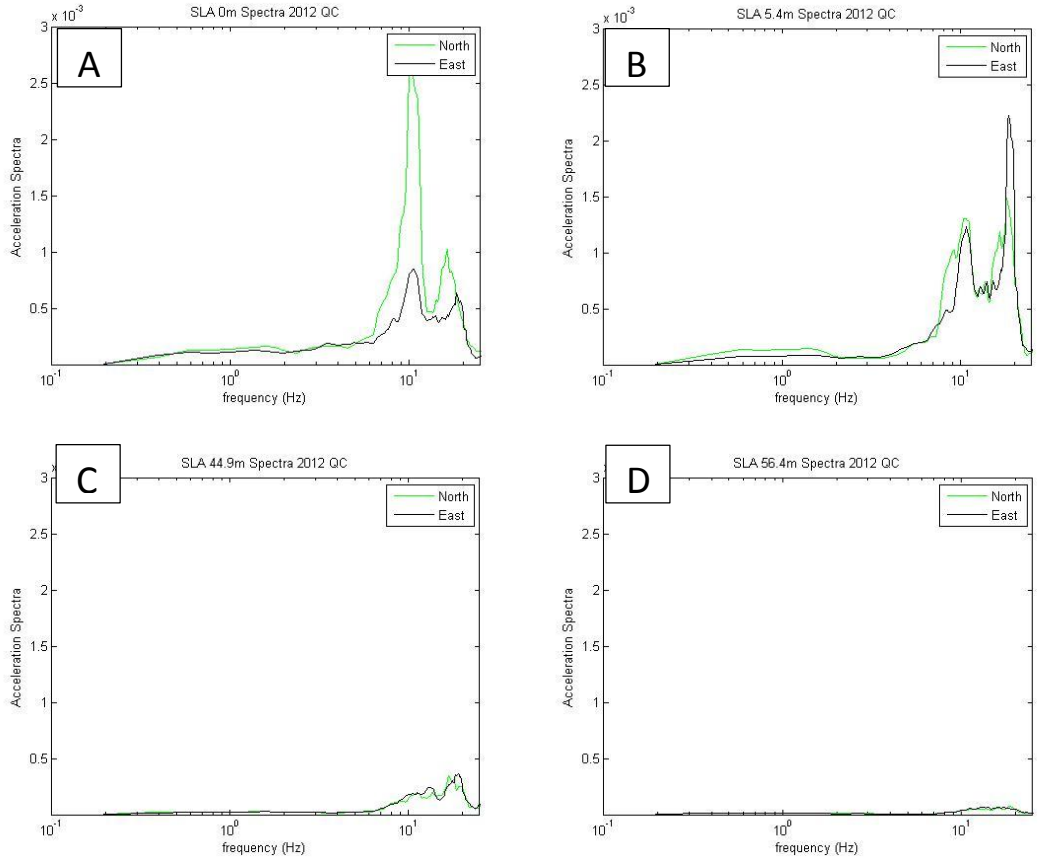

Fig. 36. Acceleration spectra of north and east components versus frequency at SLA from the 2012 Queen Charlotte earthquake (strong motion data).The receivers are located at (A) 0 m (surface), (B) 5.4 m, (C) 44.9 m, and (D) 56.4 m. Notice that (A) and (B) show high amplifications while (C) and (D) are relatively flat.

tomographic inversion of Van Wagoner et al. (2002). Due to the stiffness of the material at the deepest accelerometer, the seismic recording at this depth was used as the reference for the SSR calculations at this site. Figs. 36 and 37 show the spectra of the north and the east components at different depths for the 2012 Queen Charlotte earthquake and the 2014 Vancouver Island earthquake, respectively. The spectra from the 2012 Queen Charlotte earthquake are flat in the lower frequencies but show peaks at higher frequencies (>7). The peaks are larger at shallower depths and weaker at deeper receiver

loations. The spectra from the 2014 Vancouver Island earthquake at shallow receivers indicate peaks at low (0.5 to 1 Hz) and high (10 Hz) frequencies. The deeper receivers however, show smaller peaks at the same frequencies.

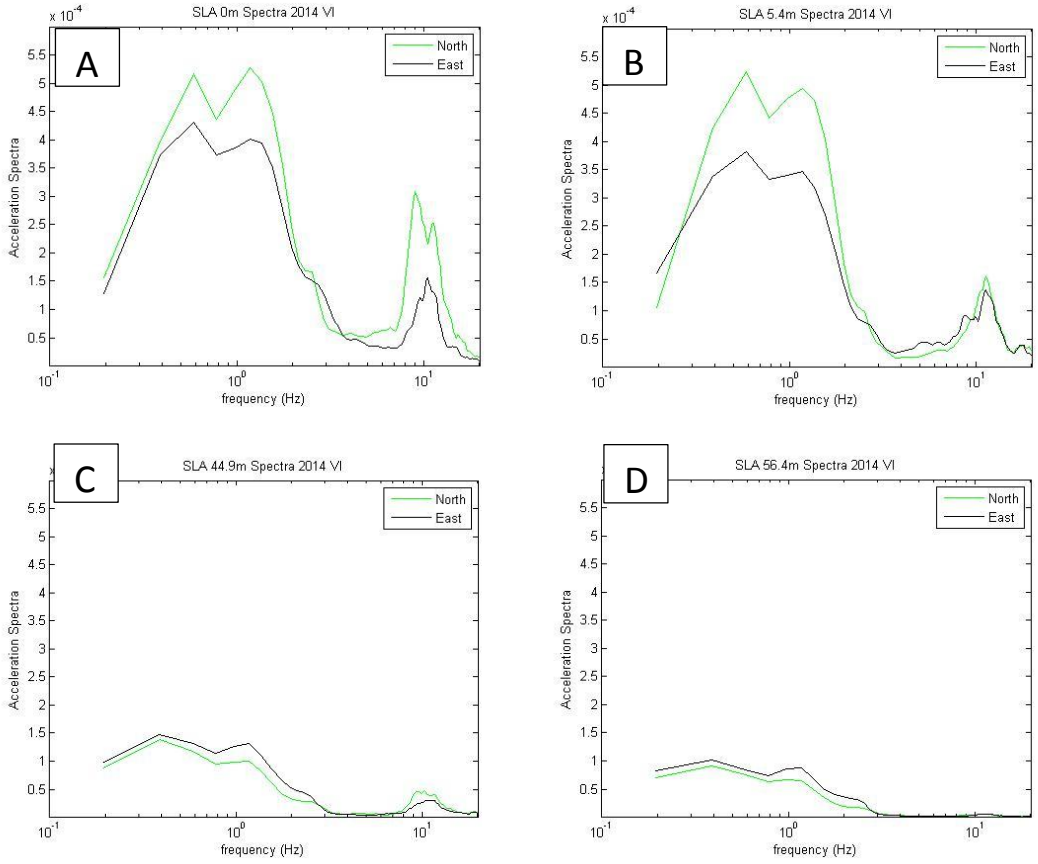

Fig. 37. Acceleration spectra of north and east components versus frequency at SLA station from the 2014 Vancouver Island earthquake (strong motion data).The receivers are located as indicated in Fig. 36.

DISCUSSION

Previous studies have suggested that the age and the type of the geologic units and the depth of the sediments to the bedrock are two major factors that determine the peak frequencies and relative amplification observed in both SSR and the HVSR analyses (Frankel, 1999; 2002; and 2009; Molnar et al. 2004; Pratt et al. 2006; Ghasemi et al. 2009; Koçkar and Akgün 2012). These two factors are investigated in this discussion. In addition, results from the Seattle liquefaction array are used to explore the validity of the SSR and HVSR methods.

Age and type of the geologic units

As reflected by the results shown in Figs 21-35, the SSRs from the three earthquakes used in this study agree on high amplification at 1-1.5 Hz in areas underlain by Pleistocene continental glacial drift. The HVSRs indicate a similar response for this type of geology, with high amplification at 1-1.5 Hz.

The SSR results from the three earthquakes also show high amplification at 0.5-1 Hz for the stations located on the Pleistocene and Holocene alluvium. The HVSRs agree with the SSRs to some extents. They suggest high to moderate amplification at 0-6 Hz.

These results agree with the results from Frankel et al. (2002) in which the highest amplification was observed at 1 Hz on artificial fill and young alluvium.

All the HVSR and the SSR results for the station located at Paleocene to Miocene marine sedimentary rock agree on low amplification at all frequencies. The same results are observed for the single station located on the Paleogene and Neogene intrusive rock.

The SSRs agree on low amplification at 0-7 Hz and moderate at 7-10 Hz for the stations located on the Paleogene and Neogene fragmental volcanic rock. The station on the Paleogene and Neogene volcanic rock shows high amplification at 2-10 Hz according to the SSRs. The HVSRs for this station suggests high amplification at 1-2 Hz. On the average, the stations located on the Pleistocene and Holocene alluvium show the highest amplification according to the HVSR results while the SSR results suggest Pleistocene continental glacial drift as the type of geology with the highest amplification observed. Overall there is a correlation between the observed peak frequencies and the type/age of the geologic units.

Depth to the basement

Using results from the tomographic velocity inversion of Van Wagoner et al., 2002 (Fig. 38) as a proxy for depth to basement, the correlation between the SSR and the HVSR results and the depth to the basement is investigated for a few of the stations, along with the correlation of SSR and HVSR results with the liquefaction susceptibility at the sites. Figure 38 shows station locations used in this study overlain on a map of p-wave velocities at a depth slice of 2.5 km. Basement is defined by the 4.25 km/s contour.

Areas having velocities less than 4.25 km at this depth are assumed to be above the basin-basement interface.

MEAN is located in an urban area approximately at the center of the Seattle basin on an area with the P wave velocity of 2.5-3 km/s at the depth of 2.5 km. The low P wave velocity implies that this site is located in section of the basin that is deep and would likely show amplification on the HVSR and the SSR results. However, very low liquefaction susceptibility is suggested at this station according to the liquefaction susceptibility map.

Moderate to high liquefaction susceptibility for NOWS is well justified by its low P wave velocity (2.5-3 km/s) (located at the center of the basin) and the high amplification at 1-3 Hz, as suggested by the HVSR and the SSR results. Located on the Pleistocene and Holocene alluvium close to a river in a wide valley is consistent with MARY's designation of moderate to high liquefaction susceptibility and the high amplification suggested by the SSR and the HVSR results at this station.

The station DOSE is located on the center of the valley on Pleistocene continental glacial drift and consistently shows high amplification at 3-4 Hz in both the HVSR and the SSR results from all the three events (Fig.38).In this regard, the SSR and HVSR results are consistent with the assumption that both the type of geology and the depth to basement are important factors governing the observed amplification at this site.

The relatively flat response on the SSR results for station FINN is consistent with its very low liquefaction susceptibility for FINN. However, this station overlays thick sediments, according to the velocity map (Fig. 38), near the center of the Seattle basin.

This might be caused by a rise or ridge in the subsurface structure in this part of the basin that is too small to be resolved by the tomographic velocity inversion.

Located on basement rock, RATT and LON have consistently flat responses in their SSR and HVSR results. The P wave velocity at the depth of 2.5 km is 5-6 km/s for RATT, which is likely representative of igneous rock. Likewise, GNW and MNWA, located on the Paleogene and Neogene intrusive rock and Paleocene to Miocene marine sedimentary rock, respectively, have P wave velocities of 4.5-6 km/s and show no amplification at any frequency.

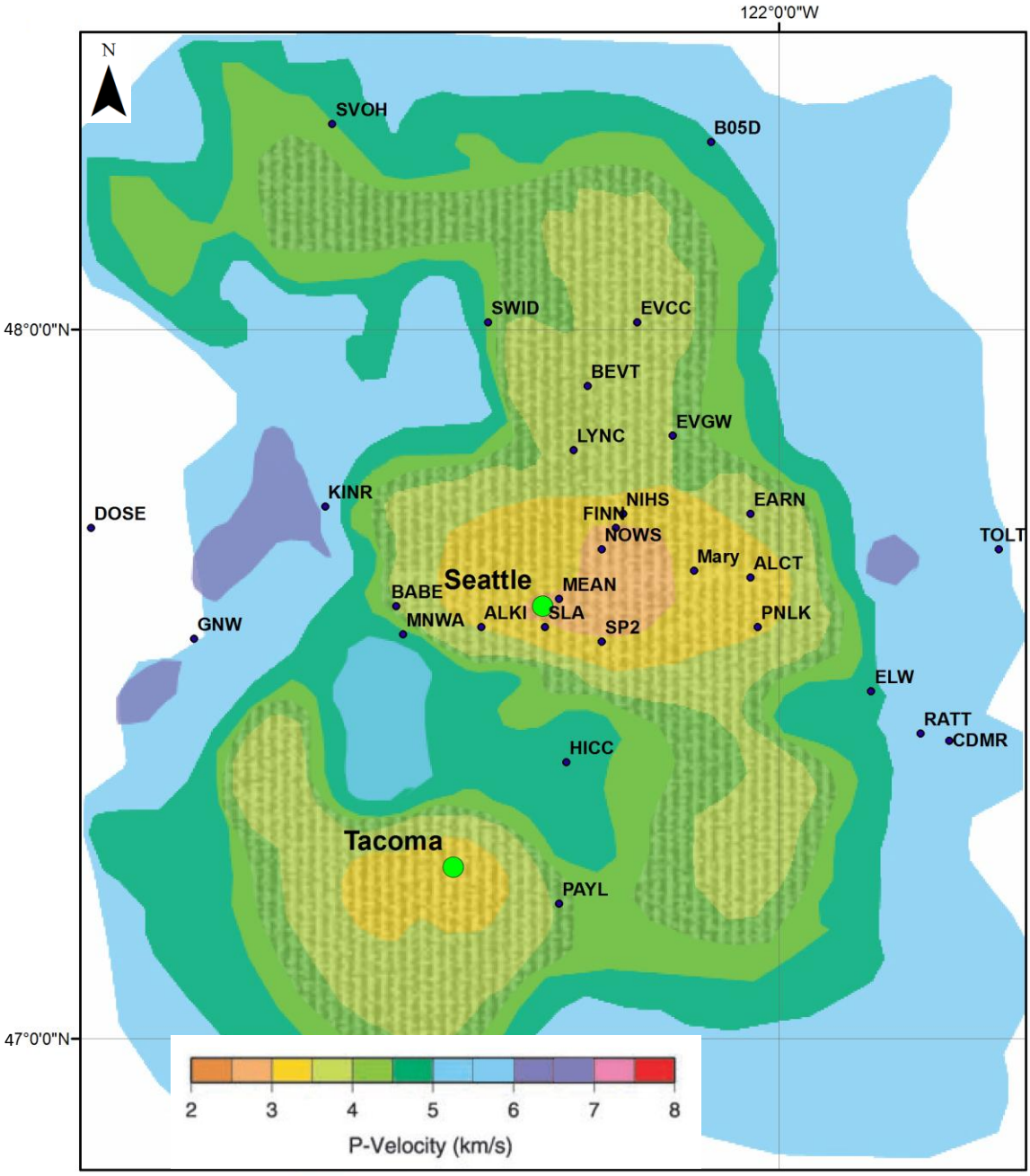

Fig. 38. Horizontal depth slice showing P wave velocity in the depth of 2.5 km overlain with strong motion station locations (modified from Van Wagoner et al., 2002). The shaded area is the 4.25 km/s contour line, which is assumed to mark the basins' boundaries and presence of basement rock.

TOLT, on the other hand, is located on the Paleogene and Neogene volcanic rock and has a P wave velocity of 5-6 km/s, which suggests basement rock. However, it shows consistent peaks at 1-2 Hz in its HVSR and SSR results. The possible reason that might explain this inconsistency is the fact that this station is located on the flank of a steep alluvial valley, which can reflect a complexity of structure or unconsolidated surface deposit that could give rise to near-surface amplification.

Fig. 39 shows the calculated SSRs using the two shallowest accelerometers (0 m and 5.4 m) referenced to the deepest one (56.4 m) for both the 2012 Queen Charlotte (A and B) and 2014 Vancouver Island (C and D) earthquakes. The results show a flat response at lower frequencies and relatively consistent peaks at 7 to 10 Hz. Notice (B) and (D), which are the deeper receivers, have smaller peaks in comparison to those from the receivers on the surface. This clearly indicates the increase in amplification in shallower depths.

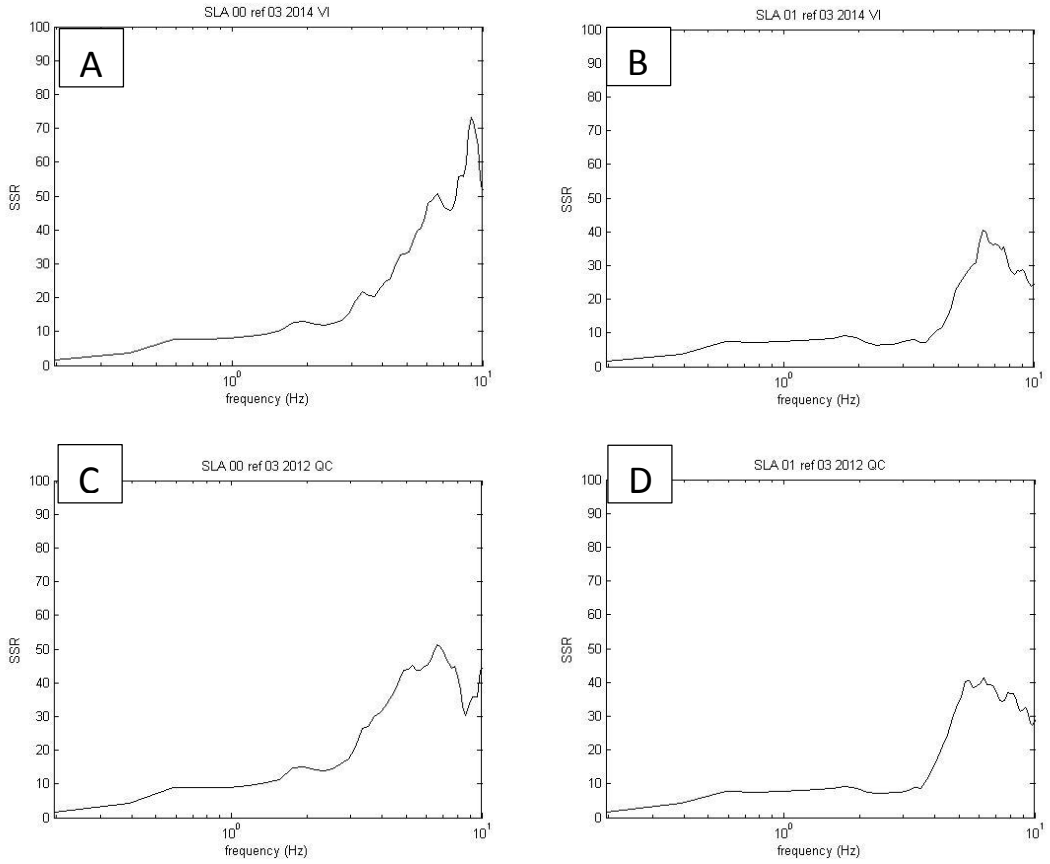

Fig. 39. SSR against frequency at SLA station referenced to the accelerometer located at the depth of 56.4m. (A) 0 m (surface) and (B) 5.4 m from the 2014 Vancouver Island earthquake. (C) 0 m (surface) and (D) 5.4 m from the 2012 Queen Charlotte earthquake. Notice that (A) and (C) have higher peaks in comparison to (B) and (D).

A similar comparison of the SSR results from the 2014 Vancouver earthquake and the 2012 Queen Charlotte earthquake is shown in Fig. 39. Here, GNW is used as the reference station used for the calculation. This station was chosen as a reference because its acceleration spectra are flat across most frequencies (Fig. 40). As with the results shown in Fig. 39, the SSRs from SLA calculated with GNW as a reference show increased amplification with shallow depth (Fig. 40).

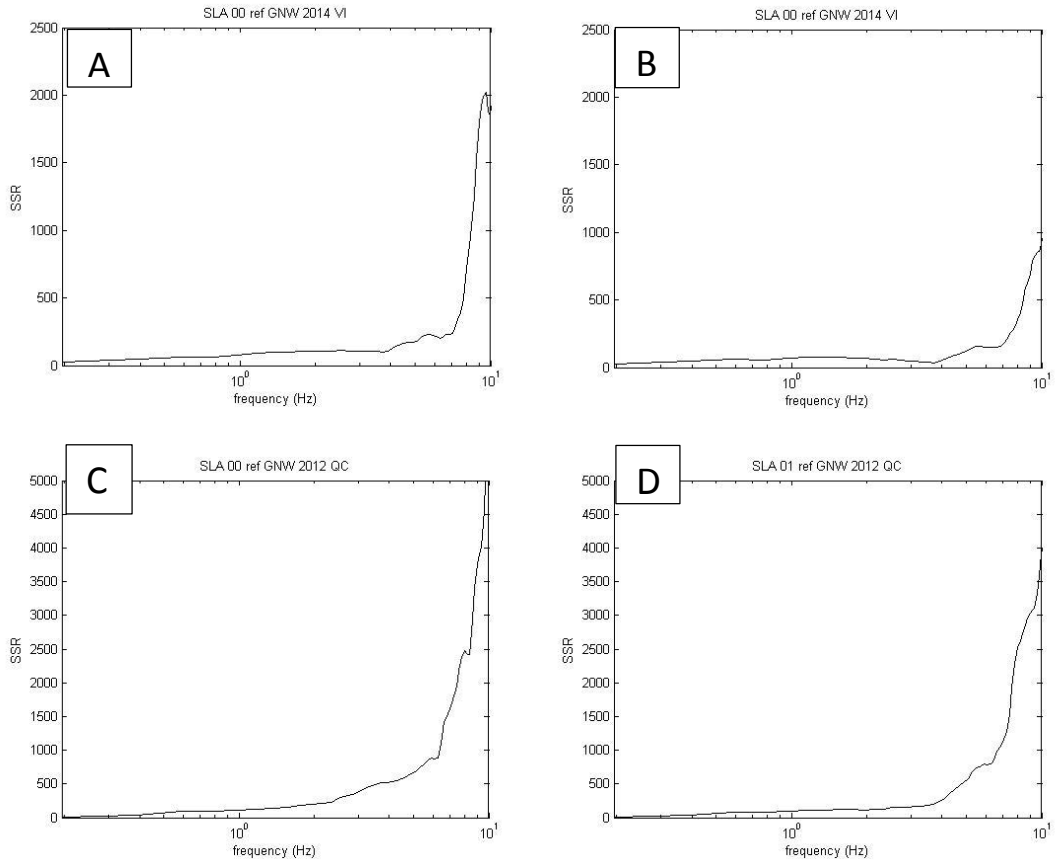

Fig. 40. SSR against frequency at SLA station referenced to GNW. (A) 0 m (surface) and (B) 5.4 m from the 2014 Vancouver Island earthquake. (C) 0 m (surface) and (D) 5.4 m from the 2012 Queen Charlotte earthquake.

Despite the slightly different peak frequencies in the spectra from the 2012 Queen Charlotte earthquake and the 2014 Vancouver Island earthquake, which is possibly due to the effect of source, the SSR peak frequencies are very consistent between the two earthquakes and the results shows the method has successfully eliminated the effect of the source.

The SSRs referenced to GNW also indicate higher amplification in the near surface compared to deeper strata. The frequency peaks are somewhat consistent between the two events. Although this result confirms the assumption that a different station can be used as a reference site for the SSR calculation, the result is not fully consistent with the results referenced to the deepest receiver at SLA. The fact that the deepest receiver at SLA is still in stiff soil (and not bedrock) could be one reason for the inconsistency of the SSR peak frequencies.

CONCLUSIONS

This study uses earthquake data to determine site effects, such as wave amplification and frequency characteristics of ground motions, at several locations in western Washington. It compares two common methodologies, SSR and HVSR, for broadband and strong motion stations located in a variety of geologic settings.

The SSR and HVSR both show that the stations located on the Pleistocene continental glacial drift show high amplification at 1-1.5 Hz.. Stations located on Pleistocene and Holocene alluvium show relatively high amplification at 0.5-1 Hz.Stations on the Paleogene and Neogene intrusive rock and the Paleocene to Miocene marine sedimentary rock show low amplification at all frequencies. Low amplification at 1-4 Hz a was observed for the only station located on the Paleogene and Neogene fragmental volcanic rock.

Acquiring data from multiple depths (liquefaction array) is a practical approach to study amplification characteristics that occur as a result of energy propagating through near-surface basin sediments. The results from the liquefaction array show the degree and frequency characteristics of near-surface wavesas energy travels through shallow layers, and the consistency of the results when compared among multiple earthquakes supports the validity of the technique.

In slightly more than half of the stations (56%), the HVSR and the SSR results show relatively similar peaks. the HVSR method shows some inconsistencies with the SSR and might not be a suitable method to estimate wave amplification in deep sedimentary basins with complicated underlying structure. The SSR, on the other hand, shows relatively more consistency, both within this study and with previous work done in this area, suggesting that this is a useful method in evaluating areas susceptible to liquefaction. However, it is suggested that the SSR method be used in conjunction with other geophysical and geotechnical studies.

REFERENCES

Atkinson, G.M., 1995. Attenuation and source parameters of earthquakes in the Cascadia region. Bulletin of the Seismological Society of America 85, 1327–1342.

Atwater, B.F., Musumi-Rokkaku, S., Satake, K., Tsuji, Y., Ueda, K., Yamaguchi, D.K., 2005. The orphan tsunami of 1700; Japanese clues to a parent earthquake in North America. U. S. Geological Survey Professional Paper 133.

Barnett, E.A., Weaver, C.S., Meagher, K.L., Haugerud, R.A., Wang, Z., Madin, I.P., Wang, Y., Wells, R.E., Blakely, R.J., Ballantyne, D.B., Darienzo, M., 2009a. Earthquake hazards and lifelines in the Interstate 5 urban corridor; Woodburn, Oregon, to Centralia, Washington. Scientific Investigations Map 1 sheet.

Barnett, E.A., Weaver, C.S., Meagher, K.L., Haugerud, R.A., Wang, Z., Madin, I.P., Wang, Y., Wells, R.E., Blakely, R.J., Ballantyne, D.B., Darienzo, M., 2009b. Earthquake hazards and lifelines in the Interstate 5 urban corridor; Woodburn, Oregon, to Centralia, Washington. Scientific Investigations Map 1 sheet.

Booth, D.B., 1994. Glaciofluvial infilling and scour of the Puget Lowland, Washington, during ice-sheet glaciation. Geology (Boulder) 22, 695–698. doi:http://dx.doi.org/10.1130/0091-7613(1994)022

Brocher, T.M., Parsons, T.E., Blakely, R.J., Christensen, N.I., Fisher, M.A., Wells, R.E., ten Brink, U.S., Pratt, T.L., Crosson, R.S., Creager, K.C., Symons, N.P., Preston, L.A., Van Wagoner, T., Miller, K.C., Snelson, C.M., Trehu, A.M., Langenheim, V.E., Spence, G.D., Ramachandran, K., Hyndman, R.D., Mosher, D.C., Zelt, B.C., Weaver, C.S., 2001. Upper crustal structure in Puget Lowland, Washington; results from the 1998 seismic

hazards investigation in Puget Sound. Journal of Geophysical Research 106, 13,541–13,564.

Brocher, T.M., Parsons, T.E., Creager, K.C., Crosson, R.S., Symons, N.P., Spence, G.D., Zelt, B.C., Hammer, P.T., Hyndman, R.D., Mosher, D.C., Trehu, A.M., Miller, K.C., ten Brink, U.S., Fisher, M.A., Pratt, T.L., Alvarez, M.G., Beaudoin, B.C., Louden, K.E., Weaver, C.S., 1999. Wide-angle seismic recordings from the 1998 Seismic Hazards Investigation of Puget Sound (SHIPS), western Washington and British Columbia. Open-File Report - U. S. Geological Survey 110.

Fernandez, L.M., Brandt, M.B.C., 2000. The reference spectral noise ratio method to evaluate the seismic response of a site. Soil Dynamics and Earthquake Engineering 20, 381–388. doi:10.1016/S0267-7261(00)00086-5

Frankel, A., Stephenson, W., Carver, D., 2009. Sedimentary basin effects in Seattle, Washington; ground-motion observations and 3D simulations. Bulletin of the Seismological Society of America 99, 1579–1611. doi:http://dx.doi.org/10.1785/0120080203

Frankel, A.D., Carver, D.L., Cranswick, E., Meremonte, M.E., Bice, T., Overturf, D.E., 1999. Site response for Seattle and source parameters of earthquakes in the Puget Sound region. Bulletin of the Seismological Society of America 89, 468–483.

Frankel, A.D., Carver, D.L., Williams, R.A., 2002. Nonlinear and linear site response and basin effects in Seattle for the M 6.8 Nisqually, Washington, earthquake. Bulletin of the Seismological Society of America 92, 2090–2109.

Garcia-Fernandez, M., Jimenez, M.J., 2012. Site characterization in the Vega Baja, SE Spain, using ambient-noise H/V analysis. Bulletin of Earthquake Engineering 10, 1163–1191. doi:http://dx.doi.org/10.1007/s10518-012-9351-1

Ghasemi, H., Zare, M., Fukushima, Y., Sinaeian, F., 2009. Applying empirical methods in site classification, using response spectral ratio (H/V): A case study on Iranian strong motion network (ISMN). Soil Dynamics and Earthquake Engineering 29, 121–132. doi:http://dx.doi.org/10.1016/j.soildyn.2008.01.007

Johnson, S.Y., Potter, C.J., Armentrout, J.M., 1994. Origin and evolution of the Seattle Fault and Seattle Basin, Washington. Geology (Boulder) 22, 71–74. doi:http://dx.doi.org/10.1130/0091-7613(1994)022

Johnson, S.Y., Potter, C.J., Armentrout, J.M., Miller, J.J., Finn, C.A., Weaver, C.S., 1996. The southern Whidbey Island Fault; an active structure in the Puget Lowland, Washington. Geological Society of America Bulletin 108, 334–354. doi:http://dx.doi.org/10.1130/0016-7606(1996)108

Jones, M.A., 1996. Thickness of unconsolidated deposits in the Puget Sound Lowland, Washington and British Columbia. Water-Resources Investigations - U. S. Geological Survey 1 sheet.

Khazaradze, G., Qamar, A., Dragert, H., 1999. Tectonic deformation in western Washington from continuous GPS measurements. Geophysical Research Letters 26, 3153–3156. doi:http://dx.doi.org/10.1029/1999GL010458

Koçkar, M.K., Akgün, H., 2012. Evaluation of the site effects of the Ankara basin, Turkey. Journal of Applied Geophysics 83, 120–134. doi:10.1016/j.jappgeo.2012.05.007

Mahajan, A.K., Mundepi, A.K., Chauhan, N., Jasrotia, A.S., Rai, N., Gachhayat, T.K., 2012. Active seismic and passive microtremor HVSR for assessing site effects in Jammu city, NW Himalaya, India—A case study. Journal of Applied Geophysics 77, 51–62. doi:10.1016/j.jappgeo.2011.11.005

Microtremor measurements in the northern coast of İzmir Bay, Turkey to evaluate site-specific characteristics and fundamental periods by H/V spectral ratio method - Springer, n.d.

Molnar, S., Cassidy, J.F., Dosso, S.E., 2004. Site response in Victoria, British Columbia from spectral ratios and 1D modeling. Bulletin of the Seismological Society of America 94, 1109–1124.

Palmer, S., Magsino, S., Bilderback, E., Poelstra, J., Folger, D., Niggemann, R., 2004. Liquefaction Susceptibility and Site Class Maps of Washington State, by County.

Pratt, T.L., 2006. Site response, basin effects, and attenuation in the Puget Lowland, Washington State, U. S. Bulletin of the Earthquake Research Institute = Tokyo Daigaku Jishin Kenkyusho Iho 81, 283–289.

Pratt, T.L., Brocher, T.M., Anonymous, 2003. Basin attenuation and the characteristics of simple spectral ratio and H/V site response estimates. Eos, Transactions, American Geophysical Union 84, F1041.

Pratt, T.L., Brocher, T.M., Weaver, C.S., Miller, K.C., Trehu, A.M., Creager, K.C., Crosson, R.S., Anonymous, 2000. Amplification of seismic waves by the Seattle Basin, Washington State. Eos, Transactions, American Geophysical Union 81, 827.

Snelson, C.M., Brocher, T.M., Miller, K.C., Pratt, T.L., Trehu, A.M., 2007. Seismic amplification within the Seattle Basin, Washington State; insights from SHIPS seismic

tomography experiments. Bulletin of the Seismological Society of America 97, 1432–1448. doi:http://dx.doi.org/10.1785/0120050204

Troost, K.G., Booth, D.B., 2008. Geology of Seattle and the Seattle area, Washington. Reviews in Engineering Geology 20, 1–35. doi:http://dx.doi.org/10.1130/2008.4020(01

Van Wagoner, T.M., Crosson, R.S., Creager, K.C., Medema, G.F., Preston, L.A., Symons, N.P., Brocher, T.M., 2002. Crustal structure and relocated earthquakes in the Puget Lowland, Washington, from high-resolution seismic tomography. Journal of Geophysical Research 107, 23. doi:http://dx.doi.org/10.1029/2001JB000710

APPENDICES

Appendix A

The north, east, and vertical components of spectra for strong motion data from 2014 Vancouver Island earthquake relative to the surface geology at the station locations.

1) Pleistocene continental glacial drift

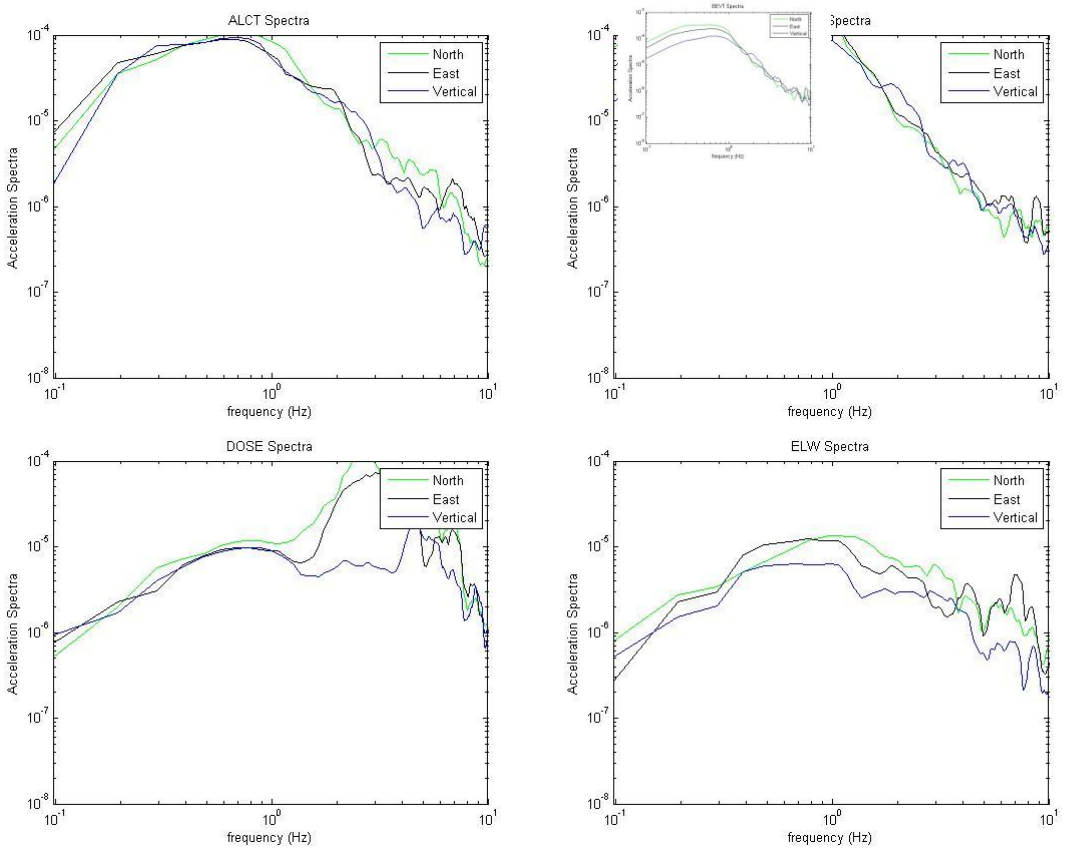

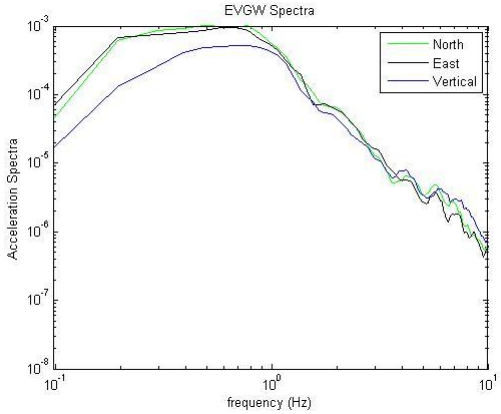
EVGW Spectra
North
East
Vertical
Acceleration Spectra
frequency (Hz)

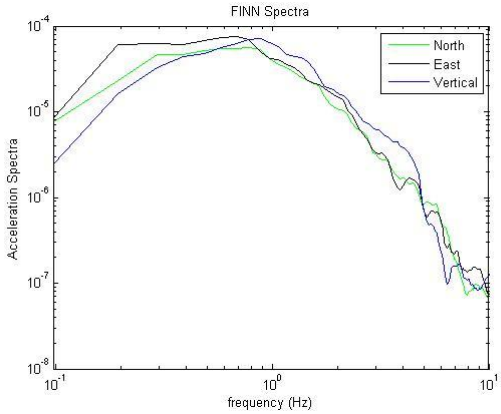
FINN Spectra
North
East
Vertical
Acceleration Spectra
frequency (Hz)

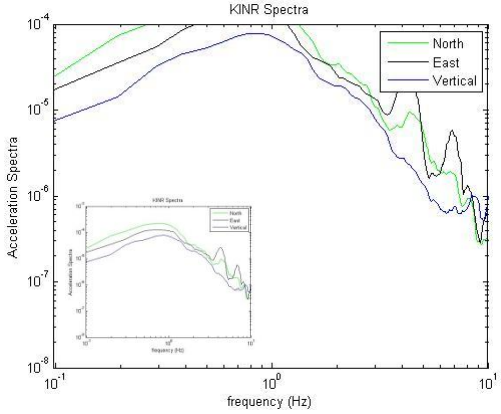
KINR Spectra
North
East
Vertical
Acceleration Spectra
frequency (Hz)

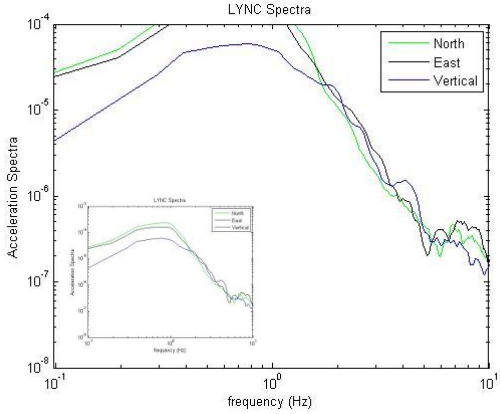
LYNC Spectra
North
East
Vertical
Acceleration Spectra
frequency (Hz)

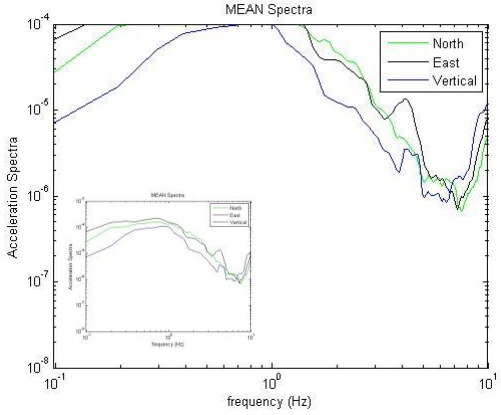
MEAN Spectra
North
East
Vertical
Acceleration Spectra
frequency (Hz)

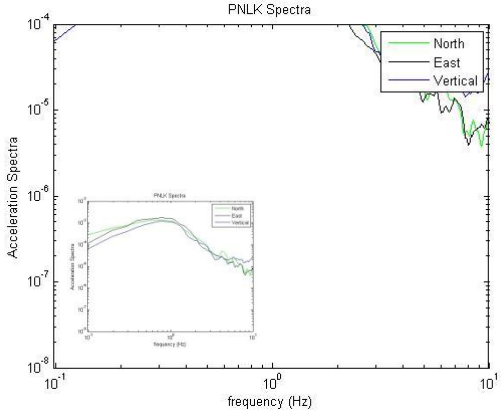
PNLK Spectra
North
East
Vertical
Acceleration Spectra
frequency (Hz)

2) Paleogene and Neogene volcanic rock

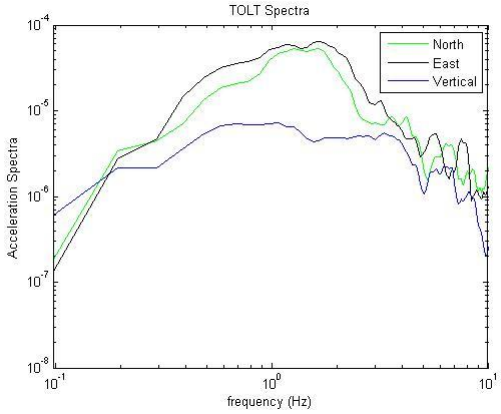

3) Pleistocene and Holocene alluvium

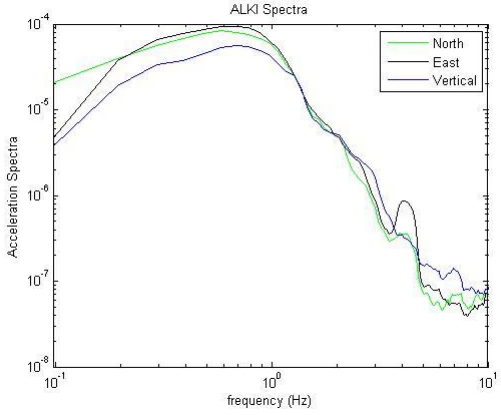

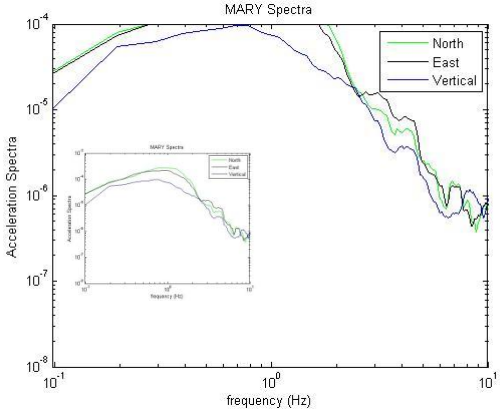

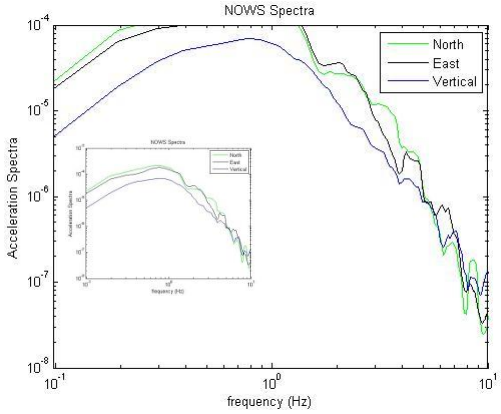

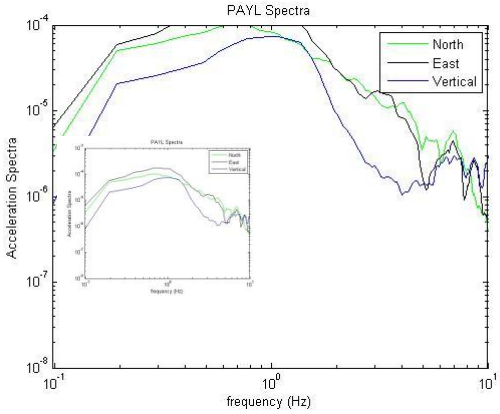

4) Paleogene and Neogene intrusive rock

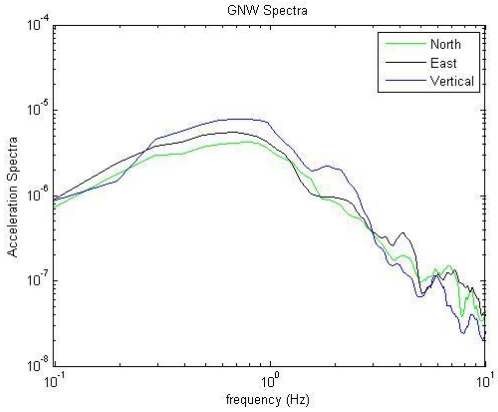

Appendix B

The north, east, and vertical components of spectra for broadband data from 2012 Vancouver Island earthquake relative to the surface geology at the station locations.

1) Pleistocene continental glacial drift

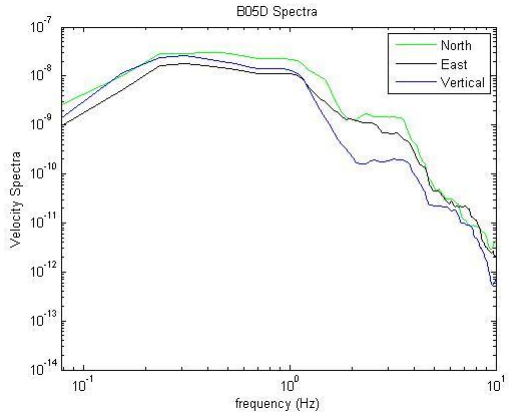

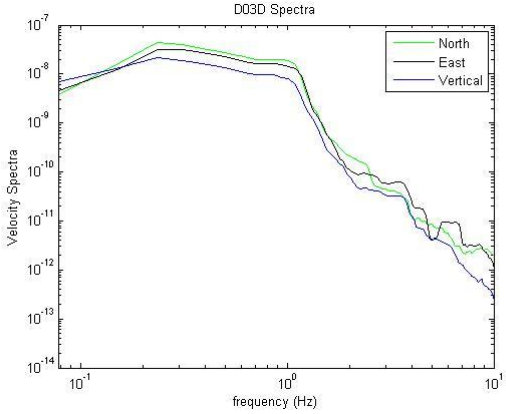

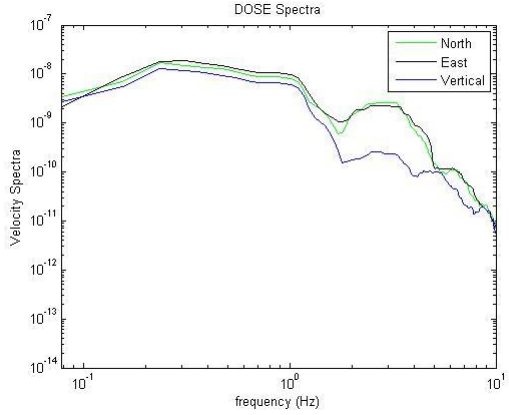

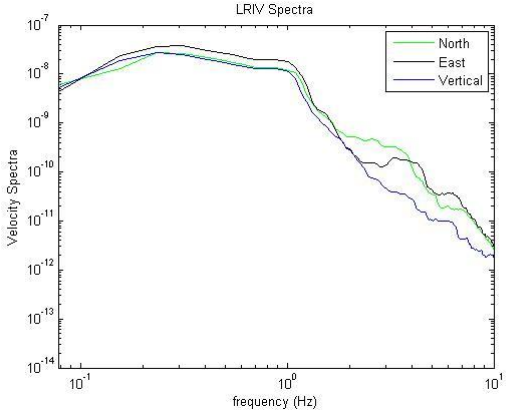

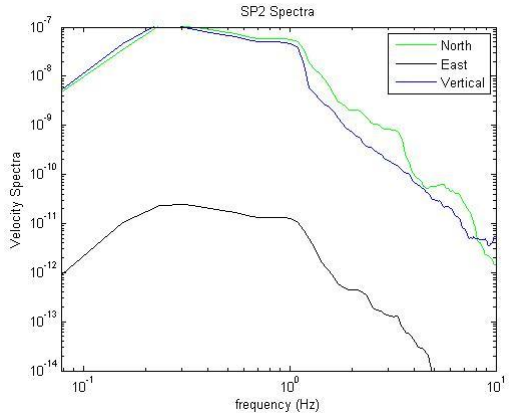

1) Paleogene and Neogene volcanic rock

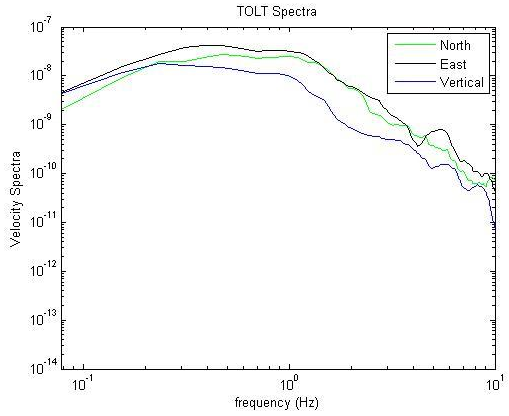

2) Pleistocene and Holocene alluvium

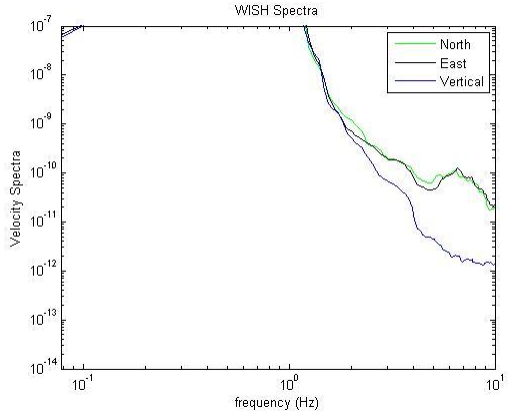

3) Paleogene and Neogene intrusive rock

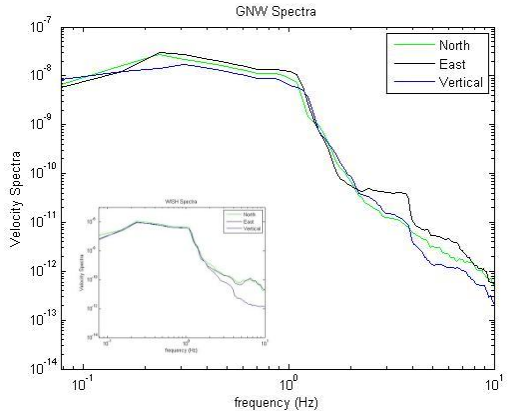

4) Paleogene and Neogene fragmental volcanic rock

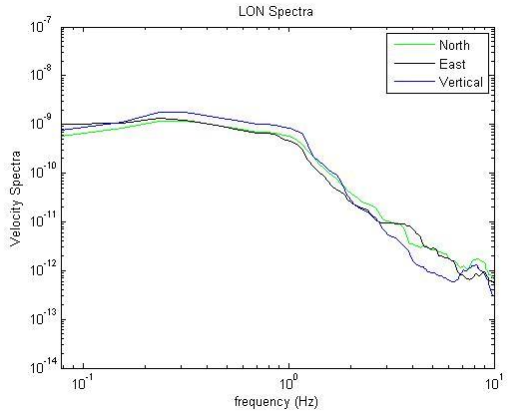

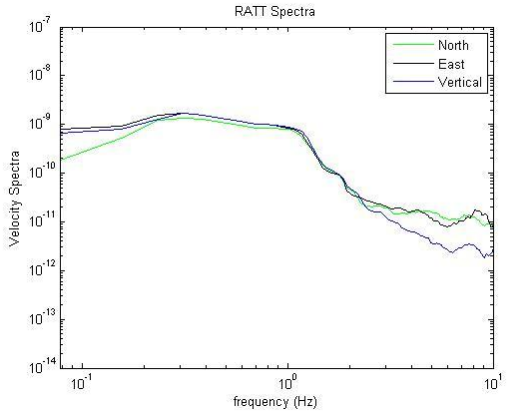

Appendix C

The north, east, and vertical components of spectra for strong motion data from 2012 Queen Charlotte earthquake relative to the surface geology at the station locations.

1) Pleistocene continental glacial drift

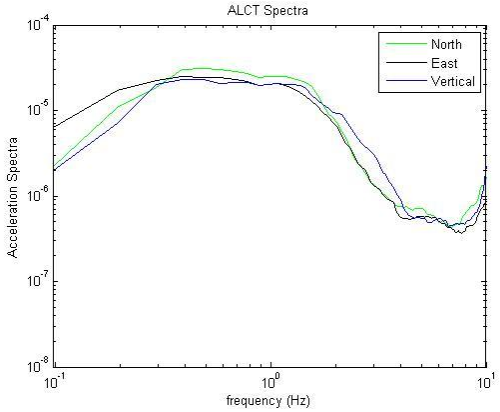

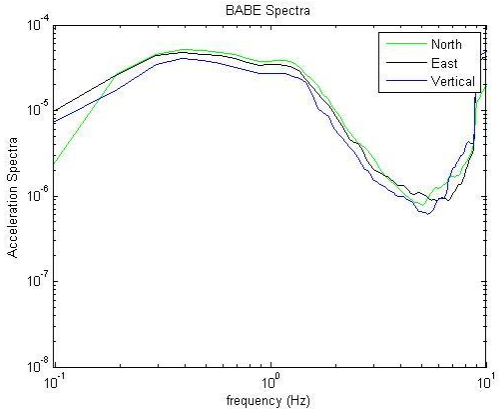

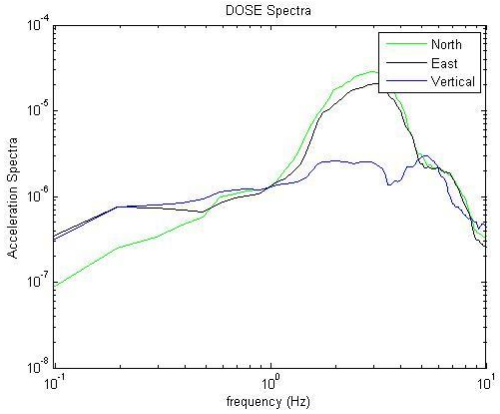
DOSE Spectra
North
East
Vertical
Acceleration Spectra
frequency (Hz)

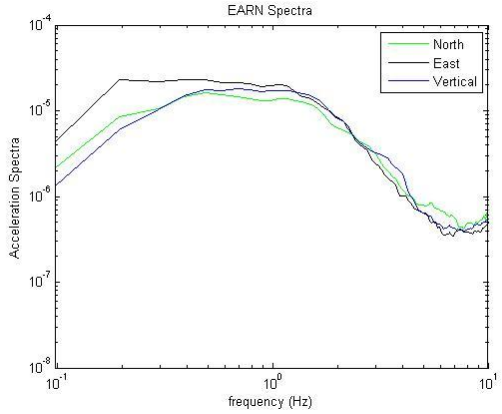
EARN Spectra
North
East
Vertical
Acceleration Spectra
frequency (Hz)

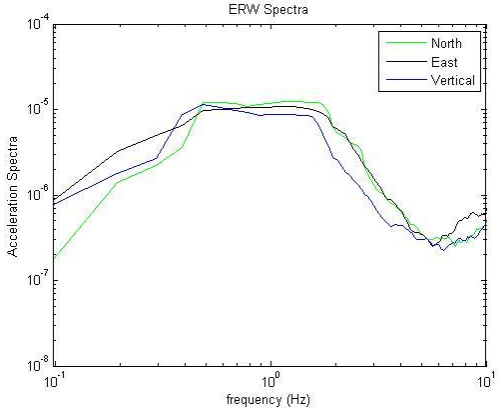
ERW Spectra
North
East
Vertical
Acceleration Spectra
frequency (Hz)

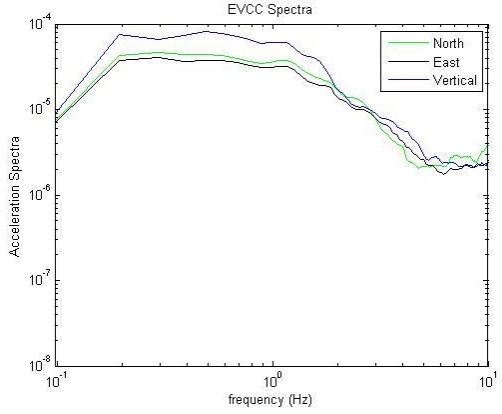
EVCC Spectra
North
East
Vertical
Acceleration Spectra
frequency (Hz)

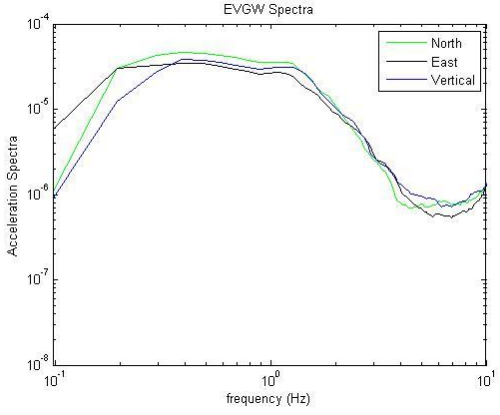
EVGW Spectra
North
East
Vertical
Acceleration Spectra
frequency (Hz)

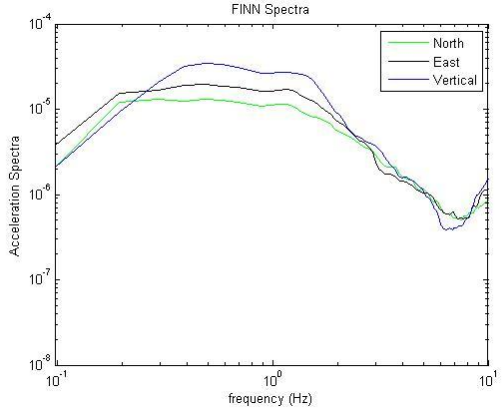
FINN Spectra
North
East
Vertical
Acceleration Spectra
frequency (Hz)

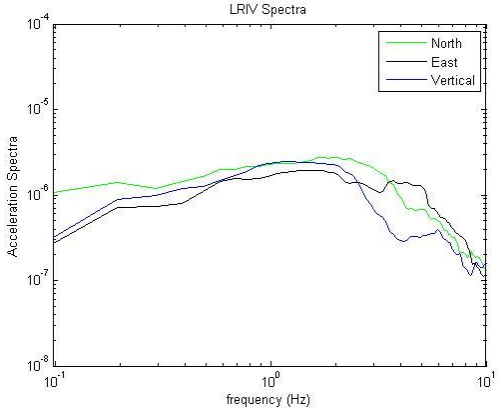
LRIV Spectra
North
East
Vertical
Acceleration Spectra
frequency (Hz)

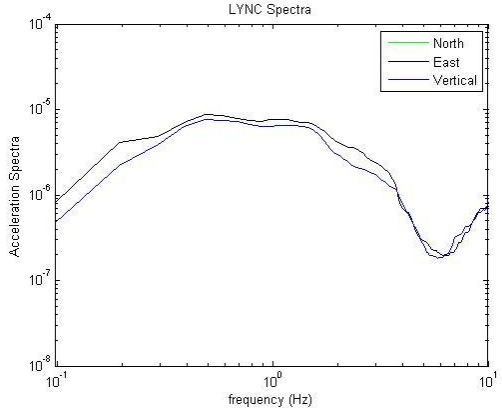
LYNC Spectra
North
East
Vertical
Acceleration Spectra
frequency (Hz)

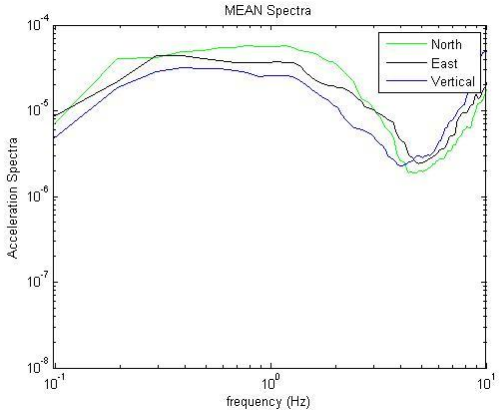
MEAN Spectra
North
East
Vertical
Acceleration Spectra
frequency (Hz)

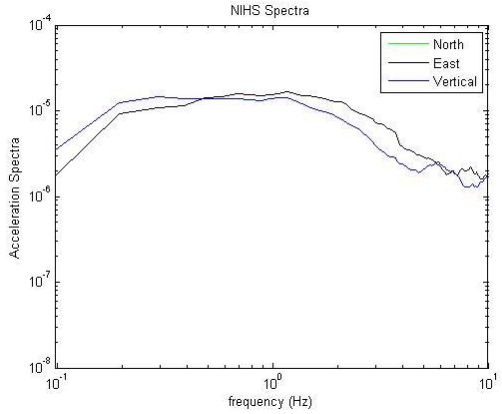
NIHS Spectra
North
East
Vertical
Acceleration Spectra
frequency (Hz)

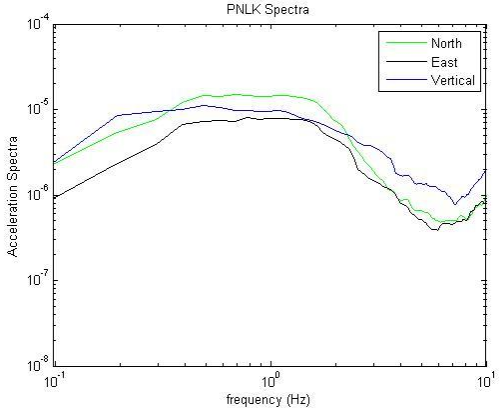
PNLK Spectra
North
East
Vertical
Acceleration Spectra
frequency (Hz)

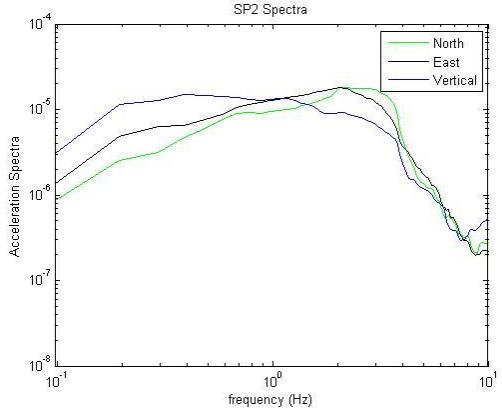
SP2 Spectra
North
East
Vertical
Acceleration Spectra
frequency (Hz)

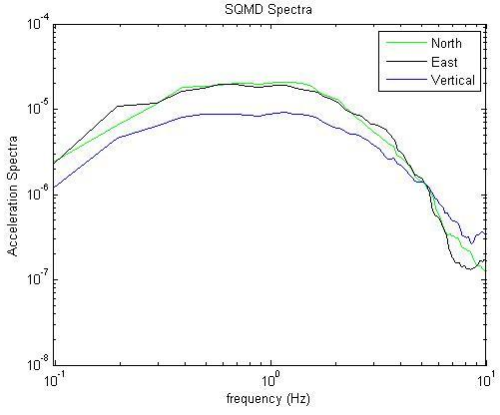
SQMD Spectra
North
East
Vertical
Acceleration Spectra
frequency (Hz)

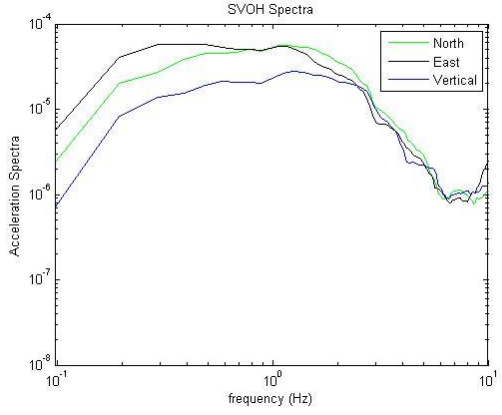
SVOH Spectra
North
East
Vertical
Acceleration Spectra
frequency (Hz)

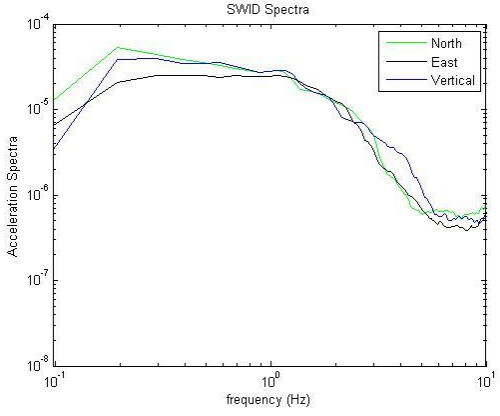
SWID Spectra
North
East
Vertical
Acceleration Spectra
frequency (Hz)

2) Paleogene and Neogene volcanic rock

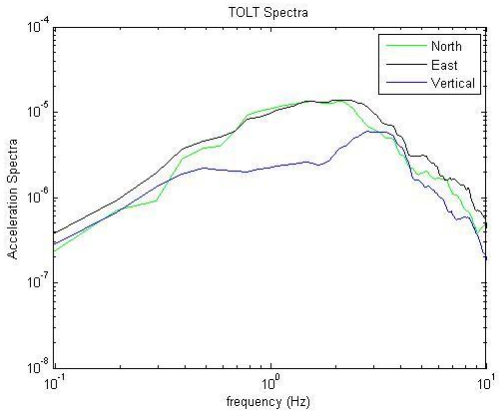

3) Pleistocene and Holocene alluvium

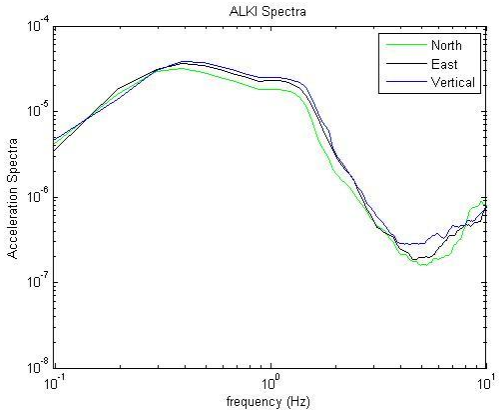

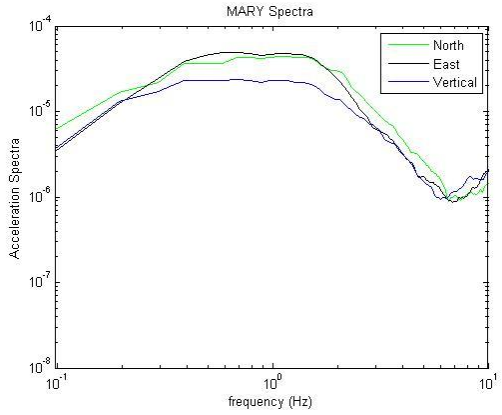

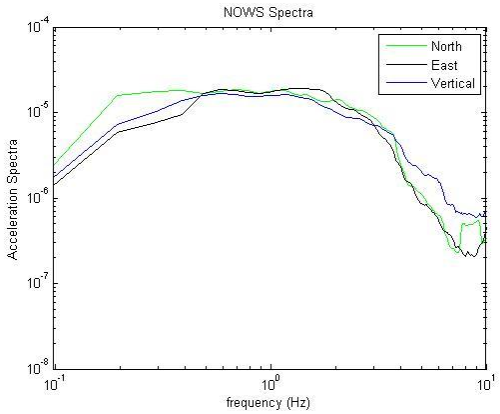

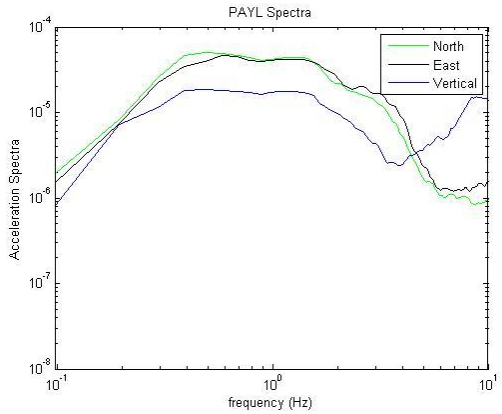

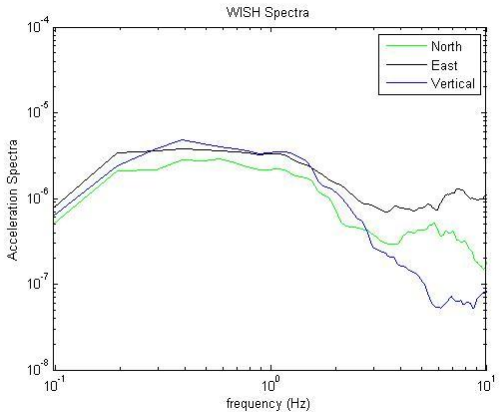

4) Paleogene and Neogene fragmental volcanic rock

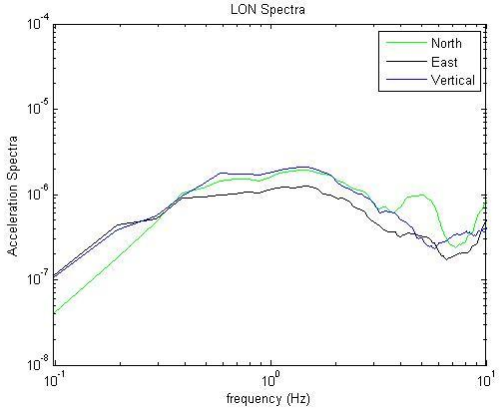

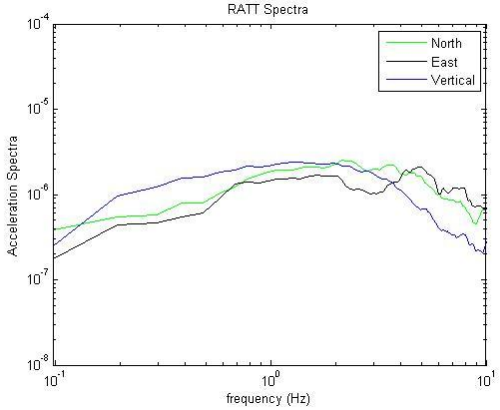

5) Paleocene to Miocene marine sedimentary rock

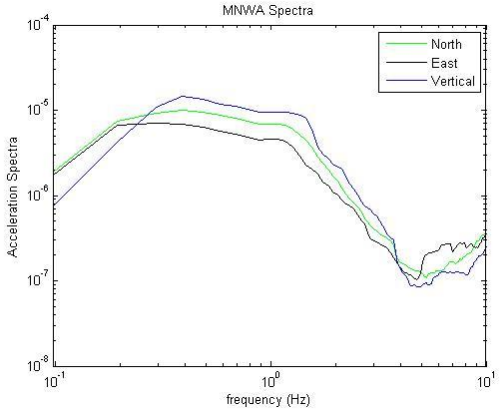

6) Paleogene and Neogene intrusive rock

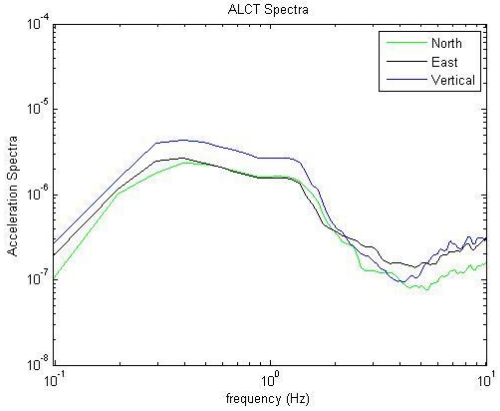

Appendix D

MATLAB codes used to calculate the HVSRs for 2014 Vancouver Island Earthquake strong motion data.

```
% Script to calculate and plot the HVSR for 2014 Vancouver Island
% earthquake strong motion data

echo off
%

nfft=1024;
noverlap=nfft/2;
prob=.95;


%traveltime and radial distance
t=67.6;
r=465.2387224;


%Selecting a window that starts before S-wave and continues for 7001
%samples
LOCUT = 69000;
HICUT = 76000;


% load multicomponent sac files
[sachdrE,data2E] = load_sac('ALCT.UW..ENE.2014.114.03.00.00.000-
2014.114.03.39.59.999.scale-AUTO.sac');
[sachdrN,data2N] = load_sac('ALCT.UW..ENN.2014.114.03.00.00.000-
2014.114.03.39.59.999.scale-AUTO.sac');
[sachdrZ,data2Z] = load_sac('ALCT.UW..ENZ.2014.114.03.00.00.000-
2014.114.03.40.00.000.scale-AUTO.sac');


% Applying the filter
[data2Z]=bandpass(data2Z,0.2,25,7001,0.01);
[data2E]=bandpass(data2E,0.2,25,7001,0.01);
[data2N]=bandpass(data2N,0.2,25,7001,0.01);


%cut the data
data2E = data2E(LOCUT:HICUT);
```

```
data2N = data2N(LOCUT:HICUT);
data2Z = data2Z(LOCUT:HICUT);

% demean and detrend the time segment
data2E = detrend(data2E-mean(data2E));
data2N = detrend(data2N-mean(data2N));
data2Z = detrend(data2Z-mean(data2Z));

% create Hann taper the length of your data
w = hann(length(data2E));

% taper the data
data2E = data2E.*w;
data2N = data2N.*w;
data2Z = data2Z.*w;



%Calculating the Power Spectral Density

% Vertical Component
dt=1.0/sachdrZ.delta;
[Pmz,Fmz]=psd(data2Z,nfft,dt,[],noverlap,prob);

%East Component
dt=1.0/sachdrE.delta;
[Pme,Fmz]=psd(data2E,nfft,dt,[],noverlap,prob);

%North Component
dt=1.0/sachdrN.delta;
[Pmn,Fmz]=psd(data2N,nfft,dt,[],noverlap,prob);



%Attenuation Correction
Pmz_corr=Pmz.*(r^0.5).*exp(pi.*(Fmz.^0.61).*t/380);
Pmn_corr=Pmn.*(r^0.5).*exp(pi.*(Fmz.^0.61).*t/380);
Pme_corr=Pme.*(r^0.5).*exp(pi.*(Fmz.^0.61).*t/380);



% Calculating the HVSR
ratmiMT=(Pme_corr+Pmn_corr)./(2.0.*Pmz_corr);

%smoothing
ratmiMT1=smooth(ratmiMT,10);
```

```
%Plotting
semilogx(Fmz,ratmiMT1,'k')
title ('ALCT')
ylabel ('H/V')
xlabel ('frequency (Hz)')
set(gca,'xlim',[0,10],'ylim',[0,8])
```

MATLAB codes used to calculate the HVSRs for 2012 Vancouver Island Earthquake broadband data.

```
% Script to calculate and plot the HVSR for 2012 Vancouver Island
% earthquake broadband data


echo off
%

nfft=512;
noverlap=nfft/2;
prob=.95;

%traveltime and radial distance
t=64;
r=480.0804502;



%Selecting a window that starts before S-wave and continues for 3001
%samples

LOCUT = 31800;
HICUT = 34800;


% load multicomponent sac files
[sachdrE,data2E] = load_sac('B05D.TA..BHE.2012.313.01.50.00.000-
2012.313.02.30.00.000.scale-AUTO.sac');
[sachdrN,data2N] = load_sac('B05D.TA..BHN.2012.313.01.50.00.000-
2012.313.02.30.00.000.scale-AUTO.sac');
[sachdrZ,data2Z] = load_sac('B05D.TA..BHZ.2012.313.01.50.00.000-
2012.313.02.29.59.999.scale-AUTO.sac');
```

```
% Applying the filter
[data2Z]=bandpass(data2Z,0.2,15,3001,0.025);
[data2E]=bandpass(data2E,0.2,15,3001,0.025);
[data2N]=bandpass(data2N,0.2,15,3001,0.025);


%cut the data
data2E = data2E(LOCUT:HICUT);
data2N = data2N(LOCUT:HICUT);
data2Z = data2Z(LOCUT:HICUT);


% demean and detrend the time segment
data2E = detrend(data2E-mean(data2E));
data2N = detrend(data2N-mean(data2N));
data2Z = detrend(data2Z-mean(data2Z));


%create Hann taper the length of your data
w = hann(length(data2E));

% taper the data
data2E = data2E.*w;
data2N = data2N.*w;
data2Z = data2Z.*w;



%Calculating the Power Spectral Density

% Vertical Component
dt=1.0/sachdrZ.delta;
[Pmz,Fmz]=psd(data2Z,nfft,dt,[],noverlap,prob);

%East Component
dt=1.0/sachdrE.delta;
[Pme,Fmz]=psd(data2E,nfft,dt,[],noverlap,prob);

%North Component
dt=1.0/sachdrN.delta;
[Pmn,Fmz]=psd(data2N,nfft,dt,[],noverlap,prob);
```

```
%Attenuation Correction
Pmz_corr=Pmz.*(r.^0.5).*exp(pi.*(Fmz.^0.61).*t/380);
Pmn_corr=Pmn.*(r.^0.5).*exp(pi.*(Fmz.^0.61).*t/380);
Pme_corr=Pme.*(r.^0.5).*exp(pi.*(Fmz.^0.61).*t/380);



% Calculating the HVSR
ratmiMT=(Pme_corr+Pmn_corr)./(2.0*Pmz_corr);


%smoothing
ratmiMT1=smooth(ratmiMT,20);


%Plotting
semilogx(Fmz,ratmiMT1,'k')
title ('B05D')
ylabel ('H/V')
xlabel ('frequency (Hz)')
set(gca,'xlim',[0,10],'ylim',[0,20])
```

MATLAB codes used to calculate the HVSRs for 2012 Queen Charlotte Island Earthquake strong motion data.

```
% Script to calculate and plot the HVSR for 2012 Queen Charlotte Island
% earthquake strong motion data


echo off
%

nfft=1024;
noverlap=nfft/2;
prob=.95;


%traveltime and radial distance
t=135;
r=917.4316109;


%Selecting a window that starts before S-wave
```

```
LOCUT = 101000;
HICUT = 108000;

% load multicomponent sac files
[sachdrE,data2E] = load_sac('ALCT.UW..ENE.2012.302.02.50.00.000-
2012.302.03.30.00.000.scale-AUTO.sac');
[sachdrN,data2N] = load_sac('ALCT.UW..ENN.2012.302.02.50.00.000-
2012.302.03.30.00.000.scale-AUTO.sac');
[sachdrZ,data2Z] = load_sac('ALCT.UW..ENZ.2012.302.02.50.00.000-
2012.302.03.30.00.000.scale-AUTO.sac');



% Applying the filter
[data2Z]=bandpass(data2Z,0.2,25,7001,0.01);
[data2E]=bandpass(data2E,0.2,25,7001,0.01);
[data2N]=bandpass(data2N,0.2,25,7001,0.01);

%cut the data
data2E = data2E(LOCUT:HICUT);
data2N = data2N(LOCUT:HICUT);
data2Z = data2Z(LOCUT:HICUT);

% demean and detrend the time segment
data2E = detrend(data2E-mean(data2E));
data2N = detrend(data2N-mean(data2N));
data2Z = detrend(data2Z-mean(data2Z));


% create Hann taper the length of your data
w = hann(length(data2E));

% taper the data
data2E = data2E.*w;
data2N = data2N.*w;
data2Z = data2Z.*w;



%Calculating the Power Spectral Density

% Vertical Component
dt=1.0/sachdrZ.delta;
[Pmz,Fmz]=psd(data2Z,nfft,dt,[],noverlap,prob);

%East Component
```

```
dt=1.0/sachdrE.delta;
[Pme,Fmz]=psd(data2E,nfft,dt,[],noverlap,prob);

%North Component
dt=1.0/sachdrN.delta;
[Pmn,Fmz]=psd(data2N,nfft,dt,[],noverlap,prob);



%Attenuation Correction
Pmz_corr=Pmz.*(r^0.5).*exp(pi.*(Fmz.^0.61).*t/380);
Pmn_corr=Pmn.*(r^0.5).*exp(pi.*(Fmz.^0.61).*t/380);
Pme_corr=Pme.*(r^0.5).*exp(pi.*(Fmz.^0.61).*t/380);



% Calculating the HVSR
ratmiMT=(Pme_corr+Pmn_corr)./(2.0*Pmz_corr);


%smoothing
ratmiMT1=smooth(ratmiMT,10);


%Plotting
semilogx(Fmz,ratmiMT1,'k')
title ('ALCT')
ylabel ('H/V')
xlabel ('frequency (Hz)')
set(gca,'xlim',[0,10],'ylim',[0,8])
```

MATLAB codes used to calculate the SSRs for 2014 Vancouver Island Earthquake strong motion data.

```
% Script to calculate and plot the SSR for 2014 Vancouver Island
% earthquake strong motion data referenced to GNW and CDMR stations


echo off
%

nfft=1024;
noverlap=nfft/2;
prob=.95;
```

```
%traveltime and radial distance
t=67.6;
r=465.2387224;


%Selecting a window that starts before S-wave and continues for 7001
%samples
LOCUT = 69000;
HICUT = 76000;


% load multicomponent sac files
[sachdrE,data2E] = load_sac('ALCT.UW..ENE.2014.114.03.00.00.000-
2014.114.03.39.59.999.scale-AUTO.sac');
[sachdrN,data2N] = load_sac('ALCT.UW..ENN.2014.114.03.00.00.000-
2014.114.03.39.59.999.scale-AUTO.sac');

% Applying the filter
[data2E]=bandpass(data2E,0.2,25,7001,0.01);
[data2N]=bandpass(data2N,0.2,25,7001,0.01);


%cut the data
data2E = data2E(LOCUT:HICUT);
data2N = data2N(LOCUT:HICUT);


% demean and detrend the time segment
data2E = detrend(data2E-mean(data2E));
data2N = detrend(data2N-mean(data2N));


% create Hann taper the length of your data
w = hann(length(data2E));

% taper the data
data2E = data2E.*w;
data2N = data2N.*w;



%Calculating the Power Spectral Density

%East Component
```

```
dt=1.0/sachdrE.delta;
[Pme,Fmz]=psd(data2E,nfft,dt,[],noverlap,prob);

%North Component
dt=1.0/sachdrN.delta;
[Pmn,Fmz]=psd(data2N,nfft,dt,[],noverlap,prob);



%Attenuation Correction
Pmn_corr=Pmn.*(r^0.5).*exp(pi.*(Fmz.^0.61).*t/380);
Pme_corr=Pme.*(r^0.5).*exp(pi.*(Fmz.^0.61).*t/380);



% Calculating the average
ratmiMT=(Pme_corr+Pmn_corr)./(2.0);


%Calculating the reference site "GNW"

%traveltime and radial distance
t=56.3;
r=497.0186862;

%traveltime and radial distance
t=71.1;
r=404.0315121;


%Selecting a window that starts before S-wave
LOCUT = 67830;
HICUT = 74830;

% load multicomponent sac files
[sachdrE,data2E] = load_sac('GNW.UW..ENE.2014.114.03.00.00.005-
2014.114.03.39.59.995.bp-0.01-25.scale-AUTO.sac');
[sachdrN,data2N] = load_sac('GNW.UW..ENN.2014.114.03.00.00.005-
2014.114.03.39.59.994.bp-0.01-25.scale-AUTO.sac');


% Applying the filter
[data2E]=bandpass(data2E,0.2,25,7001,0.01);
[data2N]=bandpass(data2N,0.2,25,7001,0.01);
```

```
%cut the data
data2E = data2E(LOCUT:HICUT);
data2N = data2N(LOCUT:HICUT);


% demean and detrend the time segment
data2E = detrend(data2E-mean(data2E));
data2N = detrend(data2N-mean(data2N));



% create Hann taper the length of your data
w = hann(length(data2E));

% taper the data
data2E = data2E.*w;
data2N = data2N.*w;


%Calculating the Power Spectral Density

%East Component
dt=1.0/sachdrE.delta;
[Pme,Fmz]=psd(data2E,nfft,dt,[],noverlap,prob);

%North Component
dt=1.0/sachdrN.delta;
[Pmn,Fmz]=psd(data2N,nfft,dt,[],noverlap,prob);


%Attenuation Correction
Pmn_corr=Pmn.*(r^0.5).*exp(pi.*(Fmz.^0.61).*t/380);
Pme_corr=Pme.*(r^0.5).*exp(pi.*(Fmz.^0.61).*t/380);


% Calculating the average
ratmiMTGNW=(Pme_corr+Pmn_corr)./(2.0);

% Calculating the ratio
ratmiMT1=ratmiMT./ratmiMTGNW;

%smoothing
ratmiMT1GNW=smooth(ratmiMT1,10);

%Plotting
semilogx(Fmz,ratmiMT1GNW,'k')
```

```
title ('ALCT')
ylabel ('SSR')
xlabel ('frequency (Hz)')
set(gca,'xlim',[0,10],'ylim',[0,100])
```

MATLAB codes used to calculate the SSRs for 2012 Vancouver Island Earthquake broadband data.

```
% Script to calculate and plot the SSR for 2012 Vancouver Island
% earthquake broadband data

echo off
%

nfft=512;
noverlap=nfft/2;
prob=.95;

%traveltime and radial distance
t=64;
r=480.0804502;

%Selecting a window that starts before S-wave and continues for 3001
%samples

LOCUT = 31800;
HICUT = 34800;

% load multicomponent sac files
[sachdrE,data2E] = load_sac('B05D.TA..BHE.2012.313.01.50.00.000-
2012.313.02.30.00.000.scale-AUTO.sac');
[sachdrN,data2N] = load_sac('B05D.TA..BHN.2012.313.01.50.00.000-
2012.313.02.30.00.000.scale-AUTO.sac');


% Applying the filter
[data2E]=bandpass(data2E,0.2,15,3001,0.025);
[data2N]=bandpass(data2N,0.2,15,3001,0.025);


%cut the data
data2E = data2E(LOCUT:HICUT);
data2N = data2N(LOCUT:HICUT);
```

```
% demean and detrend the time segment
data2E = detrend(data2E-mean(data2E));
data2N = detrend(data2N-mean(data2N));


% create Hann taper the length of your data
w = hann(length(data2E));
% taper the data
data2E = data2E.*w;
data2N = data2N.*w;


%Calculating the Power Spectral Density

%East Component
dt=1.0/sachdrE.delta;
[Pme,Fmz]=psd(data2E,nfft,dt,[],noverlap,prob);

%North Component
dt=1.0/sachdrN.delta;
[Pmn,Fmz]=psd(data2N,nfft,dt,[],noverlap,prob);


%Attenuation Correction
Pmn_corr=Pmn.*(r.^0.5).*exp(pi.*(Fmz.^0.61).*t/380);
Pme_corr=Pme.*(r.^0.5).*exp(pi.*(Fmz.^0.61).*t/380);



% Calculating the average
ratmiMT=(Pme_corr+Pmn_corr)./(2.0);

%traveltime and radial distance
t=60.75;
r=463.714543;

%Selecting a window that starts before S-wave
LOCUT = 31800;
HICUT = 34800;

% load multicomponent sac files
[sachdrE,data2E] = load_sac('GNW.UW..BHE.2012.313.01.50.00.015-
2012.313.02.29.59.990.scale-AUTO.sac');
[sachdrN,data2N] = load_sac('GNW.UW..BHN.2012.313.01.50.00.015-
2012.313.02.29.59.989.scale-AUTO.sac');
```

```
% Applying the filter
[data2E]=bandpass(data2E,0.2,15,3001,0.025);
[data2N]=bandpass(data2N,0.2,15,3001,0.025);


%cut the data
data2E = data2E(LOCUT:HICUT);
data2N = data2N(LOCUT:HICUT);

% demean and detrend the time segment
data2E = detrend(data2E-mean(data2E));
data2N = detrend(data2N-mean(data2N));

% create Hann taper the length of your data
w = hann(length(data2E));

% taper the data
data2E = data2E.*w;
data2N = data2N.*w;



%Calculating the Power Spectral Density

%East Component
dt=1.0/sachdrE.delta;
[Pme,Fmz]=psd(data2E,nfft,dt,[],noverlap,prob);

%North Component
dt=1.0/sachdrN.delta;
[Pmn,Fmz]=psd(data2N,nfft,dt,[],noverlap,prob);


%Attenuation Correction
Pmn_corr=Pmn.*(r^0.5).*exp(pi.*(Fmz.^0.61).*t/380);
Pme_corr=Pme.*(r^0.5).*exp(pi.*(Fmz.^0.61).*t/380);

% Calculating the average
ratmiMTGNW=(Pme_corr+Pmn_corr)./(2.0);

ratmiMT1=ratmiMT./ratmiMTGNW;


%smoothing
ratmiMT1=smooth(ratmiMT1,20);
```

```
%Plotting
semilogx(Fmz,ratmiMT1,'k')
title ('B05D')
ylabel ('SSR')
xlabel ('frequency (Hz)')
set(gca,'xlim',[0,10],'ylim',[0,100])
```

MATLAB codes used to calculate the SSRs for 2012 Queen Charlotte Island Earthquake strong motion data.

```
% Script to calculate and plot the SSR for 2012 Vancouver Island
% earthquake broadband data

echo off
%

nfft=512;
noverlap=nfft/2;
prob=.95;

%traveltime and radial distance
t=64;
r=480.0804502;

%Selecting a window that starts before S-wave and continues for 3001
%samples

LOCUT = 31800;
HICUT = 34800;

% load multicomponent sac files
[sachdrE,data2E] = load_sac('B05D.TA..BHE.2012.313.01.50.00.000-
2012.313.02.30.00.000.scale-AUTO.sac');
[sachdrN,data2N] = load_sac('B05D.TA..BHN.2012.313.01.50.00.000-
2012.313.02.30.00.000.scale-AUTO.sac');


% Applying the filter
[data2E]=bandpass(data2E,0.2,15,3001,0.025);
[data2N]=bandpass(data2N,0.2,15,3001,0.025);


%cut the data
```

```
data2E = data2E(LOCUT:HICUT);
data2N = data2N(LOCUT:HICUT);


% demean and detrend the time segment
data2E = detrend(data2E-mean(data2E));
data2N = detrend(data2N-mean(data2N));


% create Hann taper the length of your data
w = hann(length(data2E));
% taper the data
data2E = data2E.*w;
data2N = data2N.*w;


%Calculating the Power Spectral Density

%East Component
dt=1.0/sachdrE.delta;
[Pme,Fmz]=psd(data2E,nfft,dt,[],noverlap,prob);

%North Component
dt=1.0/sachdrN.delta;
[Pmn,Fmz]=psd(data2N,nfft,dt,[],noverlap,prob);


%Attenuation Correction
Pmn_corr=Pmn.*(r.^0.5).*exp(pi.*(Fmz.^0.61).*t/380);
Pme_corr=Pme.*(r.^0.5).*exp(pi.*(Fmz.^0.61).*t/380);



% Calculating the average
ratmiMT=(Pme_corr+Pmn_corr)./(2.0);

%traveltime and radial distance
t=60.75;
r=463.714543;

%Selecting a window that starts before S-wave
LOCUT = 31800;
HICUT = 34800;

% load multicomponent sac files
```

```
[sachdrE,data2E] = load_sac('GNW.UW..BHE.2012.313.01.50.00.015-
2012.313.02.29.59.990.scale-AUTO.sac');
[sachdrN,data2N] = load_sac('GNW.UW..BHN.2012.313.01.50.00.015-
2012.313.02.29.59.989.scale-AUTO.sac');

% Applying the filter
[data2E]=bandpass(data2E,0.2,15,3001,0.025);
[data2N]=bandpass(data2N,0.2,15,3001,0.025);


%cut the data
data2E = data2E(LOCUT:HICUT);
data2N = data2N(LOCUT:HICUT);

% demean and detrend the time segment
data2E = detrend(data2E-mean(data2E));
data2N = detrend(data2N-mean(data2N));

% create Hann taper the length of your data
w = hann(length(data2E));

% taper the data
data2E = data2E.*w;
data2N = data2N.*w;



%Calculating the Power Spectral Density

%East Component
dt=1.0/sachdrE.delta;
[Pme,Fmz]=psd(data2E,nfft,dt,[],noverlap,prob);

%North Component
dt=1.0/sachdrN.delta;
[Pmn,Fmz]=psd(data2N,nfft,dt,[],noverlap,prob);


%Attenuation Correction
Pmn_corr=Pmn.*(r^0.5).*exp(pi.*(Fmz.^0.61).*t/380);
Pme_corr=Pme.*(r^0.5).*exp(pi.*(Fmz.^0.61).*t/380);

% Calculating the average
ratmiMTGNW=(Pme_corr+Pmn_corr)./(2.0);

ratmiMT1=ratmiMT./ratmiMTGNW;
```

```
%smoothing
ratmiMT1=smooth(ratmiMT1,20);

%Plotting
semilogx(Fmz,ratmiMT1,'k')
title ('B05D')
ylabel ('SSR')
xlabel ('frequency (Hz)')
set(gca,'xlim',[0,10],'ylim',[0,100])
```

Appendix E

Geological Society of America (GSA) geologic time scale.